Shear Zones of the Maud Belt, Antarctica: Kinematics and Deformation Mechanisms

David McGibbon

a thesis submitted for the degree of
Master of Science
at the University of Cape Town, Cape Town,
South Africa.

2014

Plagarism declaration:

I know the meaning of plagarism and declare that all of the work in the document, save for that which is properly acknowledged, is my own.

David Colquhoun McGibbon

14 February 2014

Abstract

The rocks of the Maud Belt, western Dronning Maud Land, Antarctica, have experienced at least two deformation phases related to the Grenvillian and Pan-African orogenies. Deformation is heterogeneous and strain is commonly localized within shear zones.

The two study areas H.U. Sverdrupfjella and Neumayerskarvet mainly consist of paragneisses and orthogneisses and in places migmatites and granite intrusions. The orthogneisses and paragneisses mainly consist of coarse to medium grained quartz, feldspar and biotite and in places hornblende, garnet and epidote. The rock types only differ in the proportion of these minerals, the paragneisses having a higher proportion of biotite than the orthogneisses. Both study areas contain well developed lineations, defined by elongated quartz grains and in places hornblende and epidote, and a S_{1+2} foliation defined by biotite. The foliation is related to the shear zones in the region which are commonly sub-horizontal but locally sub-vertical in eastern Neumayerskarvet. In eastern Neumayerskarvet the paragneisses wrap around the competent orthogneiss units, resulting in sub-vertical strike-slip shear zones alongside the competent orthogniess units.

Two differently orientated lineations are found in the study areas, a weak, shallow plunging, E-trending lineation that occurs within the host rock and always alongside a well developed, shallow plunging, SE-trending lineation. Within the shear zones only the SE-trending lineation is found. The presence of only the SE-trending lineation in the shear zones implies that the SE-trending lineation is associated with a more recent deformation phase, D_2, and that the weak E-trending lineation is associated with an older deformation phase, D_1.

Two major collisional events affected the region, the Grenvillian ($\sim$1300 Ma to $\sim$900 Ma) and the Pan-African ($\sim$600 Ma to $\sim$450 Ma). D_2 is therefore likely associated with the Pan-African orogeny and D_1 with the older Grenvillian orogeny. Evidence for D_1 is distributed broadly within the host rock and is absent from the shear zones. If D_1 localized shear zones did exist, they have been overprinted by D_2. The presence of only D_2 in the shear zones implies that strain in D_2 was localized. The strain partitioning into narrow shear zones during the more recent deformation phase could be due to pre-existing fabrics from an earlier deformation phase. Superposition of later deformation into zones of pre-existing fabrics could be typical of areas that have experienced multiple deformation phases.

Acknowledgements

I would like to thank SANAP for funding both my field work in Antarctica and my R40 000 study grant in 2013. I would like to thank the NRF for my R20 000 incentive grant. Thank you to Ake Fagereng and Johann Dienar for guiding me through my thesis and always giving me constructive feedback promptly.

Contents

List of Tables

List of Figures

Chapter 1

Introduction

Strain in rocks is heterogeneous and during continental collisions strain is commonly partitioned into narrow zones (Boutonnet *et al.*, 2013). Shear zones are a manifestation of ductile strain localization (Ramsay, 1980). Deformation can be localized by a number of weakening mechanisms, such as grain size reduction (Rutter and Brodie, 1988; Platt and Behr, 2011), geometric softening (White *et al.*, 1980), fluid-related softening (Imber *et al.*, 1997) and preferred orientation of weaker minerals by retrogressive metamorphism (Imber *et al.*, 1997; Jefferies *et al.*, 2006; Fagereng and Diener, 2011). These weakening mechanisms are efficient at localizing strain initially but strain hardening usually follows (Berthe *et al.*, 1979; Holyoke and Tullis, 2006) and in order for a shear zone to exist it needs to remain weak. For a shear zone to be maintained, a combination of weakening mechanisms needs to continue the strain softening and prevent strain hardening (Handy *et al.*, 1999; Holyoke and Tullis, 2006; Berthe *et al.*, 1979).

Internal fabrics of the shear zones can provide information on the strain orientations and strain magnitudes experienced during deformation. Shear sense indicators within the shear zones fabric can give information on the kinematics experienced during deformation. The mineral assemblages found in the shear zone can describe the metamorphic facies conditions that they formed under and if any fluids were present.

There are still many questions about the formation and maintenance of shear zones that need to be fully answered and it is therefore worth further study. For instance, how is strain softening maintained and able to prevent strain hardening? Why is strain heterogeneous and partitioned into shear zones? How do pre-existing fabrics affect the partitioning of later deformation?

The Maud Belt of Antarctica has experienced at least two major orogenies, the Grenvillian (∼1000 Ma) and Pan-African (∼500 Ma) (Grantham *et al.*, 1995; Board, 2001). These deformation phases resulted in many shear zones forming. The shear zones provide the opportunity to study what affect pre-existing fabrics have on later strain localization. The Maud Belt contains a large amount of well exposed continuous outcrop that is in pristine condition because little to no weathering has taken place during and after exhumation, due to the cool and dry climatic conditions. This allows the shear zones of the Maud Belt to be studied in context.

Two areas, Neumayerskarvet and H.U. Sverdrupfjella, within the Maud Belt have well-exposed outcrop of representative Maud Belt structures (Fig. 3.3). Previous authors (Grantham *et al.*, 1995; Groenewald, 1995; Board, 2001; Harris, 1999) were unable to clearly separate deformation fabrics related to the two orogenies. They recognised several fabric generations but these could not be distinctly linked to the two deformation phases that affected the Maud Belt. Grantham (1995) suggested a top-to-the-NW transport direction for the Grenvillian orogeny and a top-to-the-SE transport direction for the Pan-African orogeny. The two study areas, which are separated by the Jutulstraumen Glacier, have been described as displaying different structural styles and geometries because Neumayerskarvet contains sub-vertical fabrics and H.U. Sverdrupfjella contains sub-horizontal fabrics (Grantham *et al.*, 1995). Neumayerskarvet and H.U. Sverdrupfjella are however interpreted as having similar deformational histories (Harris, 1999). The change in the structural style of Neumayerskarvet may reflect a deep seated lateral ramp (Jackson and Jacobs, 1995; Harris, 1999).

The aim of this report is to study the dynamics of the shear zones situated in the study areas, by observing the geometry, mineralogy, and microstructure of the deformation fabrics. The geometry of the fabrics can be used to separate the geological history of the area. The lineation along with kinematic indicators can be used to determine the transport direction of the rocks to compare these findings with Grantham's (1995) findings. The difference in strain in the rocks with different compositions can help in determining if there is a lithological control on strain partitioning. The strain rates in the shear zones and host rocks associated with the most recent deformation will be calculated using Shimizu's (2008) piezometer and Hirth et al.'s (2001) quartz flow law. Melt migration will be studied in order to determine

if it had an affect in strain partitioning or if the melts intruded into the already weakened shear zones. The affect of a pre-existing fabric on strain localization in a later deformation event will be studied. The two study areas are compared in order to determine if there is any structural and metamorphic correlation between them. The final aim of this report is to determine the regional significance of these shear zones in the assemblage of Queen Maud Land with possible relative timing associated to the Pan-African and Grenvillian orogenic events.

Chapter 2

Shear Zone Mechanics

2.1 Shear zone geometry

Deformation in rocks is heterogeneous and strain is commonly localized in tabular shear zones that accommodate relative movement of less strained host rocks. Shear zones can be related to a syn-tectonic process or the superposition of later deformation into a zone of pre-existing deformation (Worley and Wilson, 1996). Commonly the amount of strain is highest in the centre of the shear zone and gradually decreases outward into the wall rocks. There are a number of weakening mechanisms that could cause this deformation localization, including grain size reduction (Rutter and Brodie, 1988; Platt and Behr, 2011), geometric softening (White *et al.*, 1980), fluid-related softening (Imber *et al.*, 1997) and preferred orientation of weaker minerals by retrogressive metamorphism (Imber *et al.*, 1997; Jefferies *et al.*, 2006; Fagereng and Diener, 2011). These softening and localization mechanisms are, however, less significant at higher metamorphic grades and this results in wider shear zones forming at greater temperatures and depths (Hanmer *et al.*, 1995; Platt and Behr, 2011).

Shear zones are a common feature within the Earth's crust and for this reason there are a number of different types of shear zones which correspond to varying depths in the crust. Two broad types of shear zones exist, ductile and brittle shear zones, these occur at different depths in the crust depending on rock types, geothermal gradients, fluid content and pressures (Sibson, 1982). Above the brittle-ductile transition rocks deform by fracturing and below the transition rocks deform ductilely (Ramsay, 1980). This study concentrates on ductile shear zones where no discontinuity of layers in the rock is experienced, if layers exist

in the rock, then they are instead bent but not broken (Ramsay, 1980). Ductile shear zones form in rocks of the middle crust and deeper, such as gneiss, schist, marble, amphibolite, granulite, migmatite, large intrusions and deep level mafic and ultramafic rocks (Davis *et al.*, 2012). Shear zones have a variety of orientations ranging from horizontal to vertical and these can have a variety of transport directions. Shear zones that form during plate convergence and crustal shortening commonly have thrust displacements, which bring older, deeper rocks up against younger, higher level rocks (Ramsay, 1980). Examples of collisional zones that exhibit thrust shear zones are the Alpine-Zagros-Himalayan belt (Zeitler *et al.*, 2001; Henry *et al.*, 1997), New Zealand (Holm *et al.*, 1989) and the Maud Belt (Antarctica) (Grantham *et al.*, 1995; Groenewald, 1995; Board, 2001). Shear zones can be isolated or form in sets, such as duplex structures, which are arrays of thrust surfaces that anastomose upwards or downwards. The duplex is bounded by a higher, roof thrust and a lower, floor thrust (Fig. 2.1). The fault-bounded rock bodies in a duplex structure are referred to as horses (Butler, 1982; Schelling and Arita, 1991; McClay, 1991).

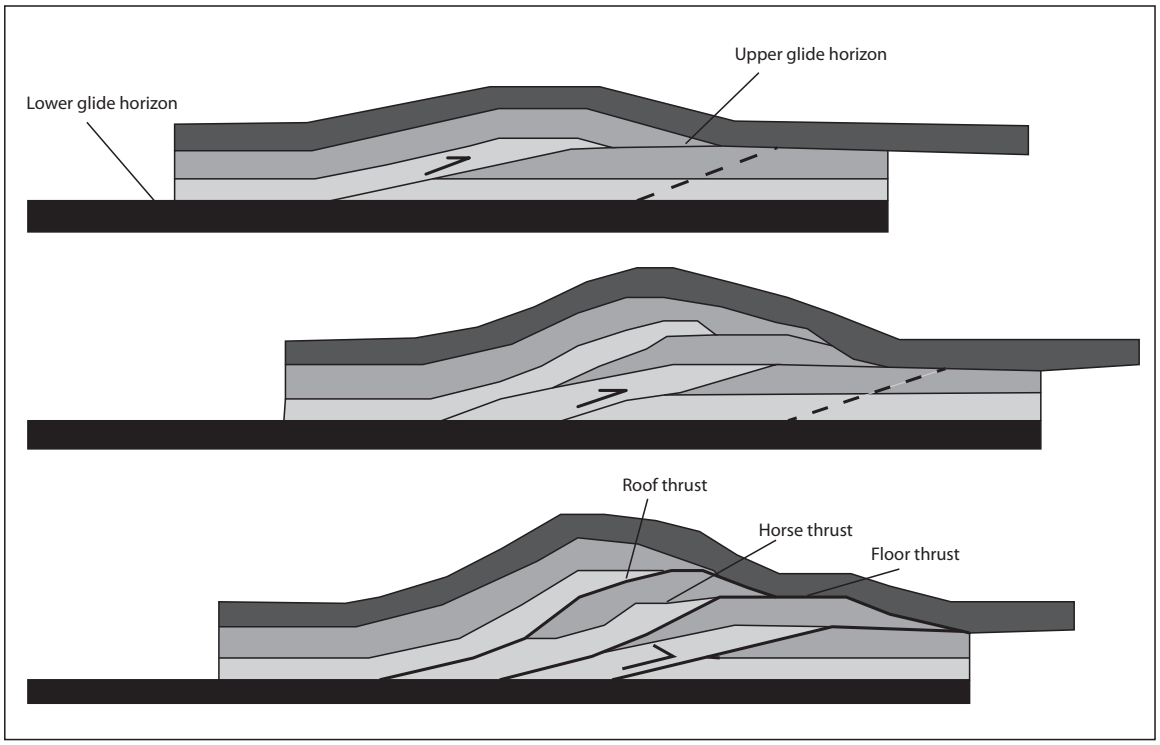

Figure 2.1: Figure of a duplex structure, showing how the horse thrusts are bounded by a floor thrust at the base and a roof thrust at the top (McClay, 1991).

Ductile shear zones result in mylonite development, which are recognized by their fine

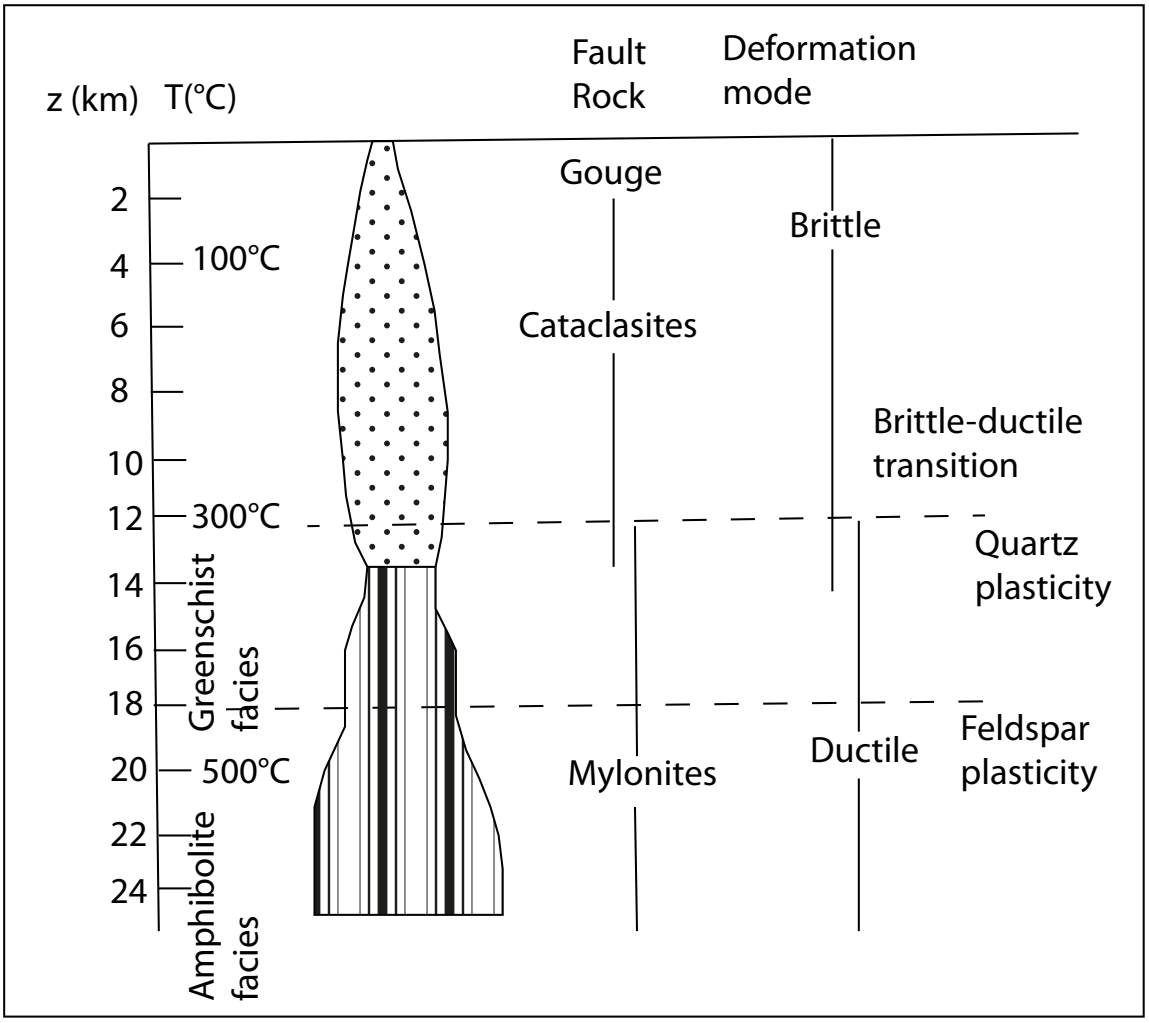

Figure 2.2: The various deformation modes and where in the Earth's crust they operate (Passchier, 2005), assuming a geothermal gradient of 25°C/km and a quartzofeldspathic lithology.

grain size, occurrence in narrow tabular zones and strongly developed foliations and lineations due to strain concentration (Tullis *et al.*, 1982) (Fig. 2.3). Mylonites can vary according to the volume percentage of matrix from proto-mylonites (10-50% matrix) to mylonites (50-90% matrix) and ultramylonites (>90% matrix), the most fine grained. These zones of ductile deformation contain tectonically induced fabrics such as foliations and lineations and usually contain metamorphic minerals (Cosgrove, 2007). Foliation is the preferred orientation of minerals developed in the finite flattening plane (Ramsay, 1980; Passchier, 2005). Lineations form within the foliation plane and are parallel to the greatest finite extension direction (Ramsay, 1980). Stretching lineations form parallel to the shear direction and therefore can show the orientation of transport within the shear zone but not the sense of shear (Carreras, 2001).

With increasing shear strain, lineations can become the dominant fabric, overprinting the foliations (Ramsay, 1980). If pre-existing foliations have a favourable orientation they can get dragged into ductile shear zones and lie nearly parallel to the shear zone boundary. This deflection of pre-existing foliations, shear band cleavages, mantled porphyroclasts, asymmetric lozenges, extensional crenulation and asymmetric folds with hinge lines at a high angle to the stretching lineation can be used as shear sense indicators that show the direction of movement in the shear zone (Carreras, 2001).

Figure 2.3: Photograph showing the fine grained and strongly developed planar foliation of the mylonite within a shear zone.

2.2 Localization mechanisms

Grain size reduction is the result of either dynamic recrystallization or cataclastic processes. It increases the surface area of the grains and therefore increases their susceptibility to reactions that take place on the grain, the reactions result in strain softening. Grain size reduction favours diffusion creep and at high temperatures, grain boundary sliding. For instance, this is the transformation of a large grained K-feldspar to a finer grained myrmekite (Tsurumi *et al.*, 2003). Grain size reduction can also enhance pressure solutions due to the opening of voids and cracks (Rutter, 1976; Gratier *et al.*, 2009). Geometric softening happens due to lattice preferred orientation, which places minerals in a position for easier dislocation glide

(Lister and Williams, 1983; Ji *et al.*, 2004). Fluids may soften rocks by dissolving or removing resistant grains, or they may deposit new, weaker grains (Lister and Williams, 1983). Fluids can also cause hydrolytic weakening (Wintsch *et al.*, 1995), which is the diffusion of water into the crystal lattices of the minerals and causes reaction softening (Kronenberg, 1994; Post and Tullis, 1998). For instance, this may change a strong feldspar to a weaker mica (Mitra, 1978; White *et al.*, 1980). The preferred orientation of weaker minerals will aid deformation because if they are orientated at a low angle to the shear plane then deformation will be accommodated by them easily, compared to if the minerals are orientated at a high angle to the shear plane (Lister and Williams, 1983). If development of a fabric leads to the alignment of easy glide planes, then this will result in fabric softening (Lister and Williams, 1983).

These weakening mechanisms are efficient at localizing strain initially but strain hardening usually follows the initial weakening (Berthe *et al.*, 1979; Holyoke and Tullis, 2006) and in order for a shear zone to exist it needs to remain weak. For example, stress concentrates at the tips of weak biotite grains, this produces semi-brittle deformation in the surrounding quartz and plagioclase grains, and the deformation in the surrounding grains allows for local biotite interconnection by slip along the (001) plane (Holyoke and Tullis, 2006). This causes a transition from a load-bearing framework of quartz to an interconnection of weak biotite, which leads to strain weakening (Holyoke and Tullis, 2006; Johnson *et al.*, 2004; Handy *et al.*, 1999). After yield, the interconnected biotite grains begin to kink, causing a rotation of portions of the grain away from the easy slip orientation and this strengthens them, resulting in strain hardening. For a shear zone to be maintained another weakening mechanism needs to continue the strain softening (Handy *et al.*, 1999; Holyoke and Tullis, 2006). To maintain the weakness highly strained parts of biotite grains could react with quartz and plagioclase to form a fine grained, mixed phase assemblage which then deforms by diffusion-accommodated grain boundary sliding, allowing for further strain weakening and localization (Holyoke and Tullis, 2006). Other mechanisms can also maintain biotite shear zones, such as dynamic recrystallization of new strain-free biotite grains that replace kinked grains and prevents strain hardening (Berthe *et al.*, 1979).

2.3 Shear zone kinematic indicators

Shear zones often contain two planar fabrics, a sigmoidal penetrative foliation (S-foliation) and slip surfaces or shears that displace the foliation (C- or C'-surfaces) (Berthe *et al.*,

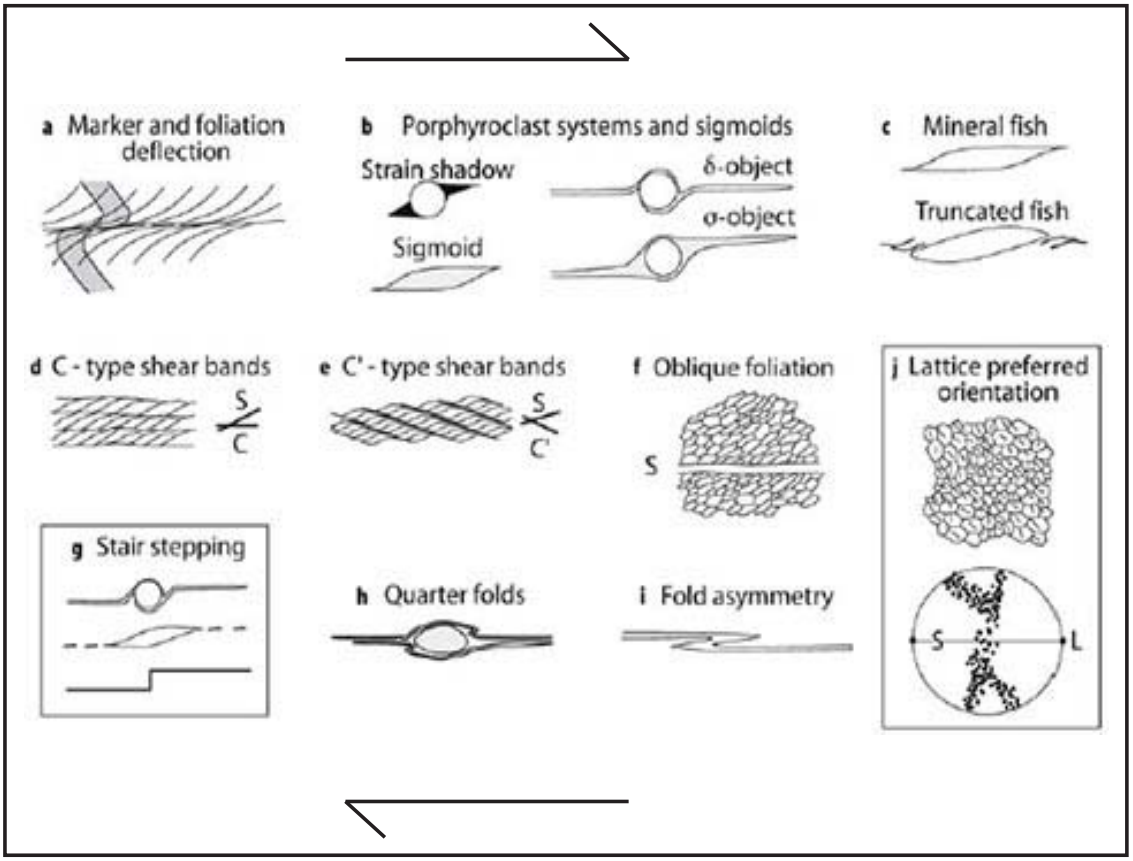

Figure 2.4: Figure showing the various structures used to determine the sense of shear of a shear zone (Passchier, 2005).

1979). S-foliation forms parallel to the XY plane of the local finite strain ellipsoid in between discrete shears that are either parallel (C-surfaces) or oblique (C'-surfaces) to the shear zone boundary. S-surfaces never displace C- and C'-surfaces, therefore showing that no shearing occurs along the S-surfaces (Berthe *et al.*, 1979; Ramsay, 1980; Lister and Snoke, 1984; Blenkinsop and Treloar, 1995). C- and C'-surfaces are planar and show evidence for localized shear displacement from the deformation of S-surfaces (Blenkinsop and Treloar, 1995). C- and C'-surfaces are interpreted to experience higher shear strain than S-surfaces because the grains are finer and have experienced more dynamic recrystallization (Blenkinsop and Treloar, 1995). Platt and Visser (1980) suggested that shear bands form by the development of shears (C- and C'-planes) close to the direction of maximum shear strain rate (slip lines), during deformation of materials with a pre-existing anisotropy which defines the S-foliation. C'-surfaces form as Riedel shears in the orientation of a Coulomb failure surface in a simple shear zone and the development may be controlled by anisotropy. C'-surfaces are inclined in

the opposite direction to the S-surfaces (Blenkinsop and Treloar, 1995). These planar fabrics are separated into two types to be used as shear sense indicators, S-C shear bands and S-C' shear bands (Fig. 5.12 d and e).

Mineral fish are lozenge-shaped porphyroclasts that occur within a finer grained matrix in ductile shear zones and these can be used as shear sense indicators (ten Grotenhuis *et al.*, 2003; Lister and Snoke, 1984). Mineral fish of biotite, tourmaline, K-feldspar, garnet and quartz occur in mylonites but the most common is white mica fish (ten Grotenhuis *et al.*, 2003; Lister and Snoke, 1984). These form by intracrystalline deformation combined with rigid body rotation that results in asymmetric grains (ten Grotenhuis *et al.*, 2003; Lister and Snoke, 1984). Mica fish have a specific shape preferred orientation with their long axis at a small angle with respect to the foliation (ten Grotenhuis *et al.*, 2003) (Fig. 5.12 c).

Mantled porphyroclasts are also commonly used as kinematic indicators. They consist of a strong, resistant core that is undeformed and this commonly has an attached polycrystalline rim that differs in structure and composition to the matrix (Passchier and Sokoutis, 1993; Passchier, 1994). The strong and resistant core often consists of garnet or feldspar minerals. Strain energy is concentrated into the rim of the clast which causes localized dynamic recrystallization, this creates the fine grained mantle. The mantle can consist of the same mineral as its host (core) or be the result of reaction softening and therefore different, for example K-feldspar breaking down to mica (Passchier and Simpson, 1986). There are two types of mantled porphyroclasts, also known as porphyroclast systems, the σ-type porphyroclasts and the δ-type porphyroclasts (Passchier and Simpson, 1986) (Fig. 5.12 b). The σ-type porphyroclasts have wedge shaped recrystallized tails whose median lines are on opposite sides of the reference plane parallel to the tail (Passchier and Simpson, 1986). δ-type porphyroclasts have thin recrystallized tails whose median lines cross the reference plane adjacent to the porphyroclast. This results in embayments of matrix material occurring adjacent to the porphyroclast and bending of the tail, the bends in the tail straighten away from the central clast. Mantle porphyroclasts form because the weak, new, dynamically recrystallized grains in the mantle of the porphyroclast change their shape due to non-coaxial laminar flow in the adjacent matrix (Passchier and Simpson, 1986). During flow the rigid clast causes perturbation and if no secondary shear zones are formed then the clast will rotate (Passchier, 1994; Passchier and Sokoutis, 1993). σ-type porphyroclasts form due to low shear strain and δ-type porphyroclasts form due to high shear strain (Passchier and Simpson, 1986).

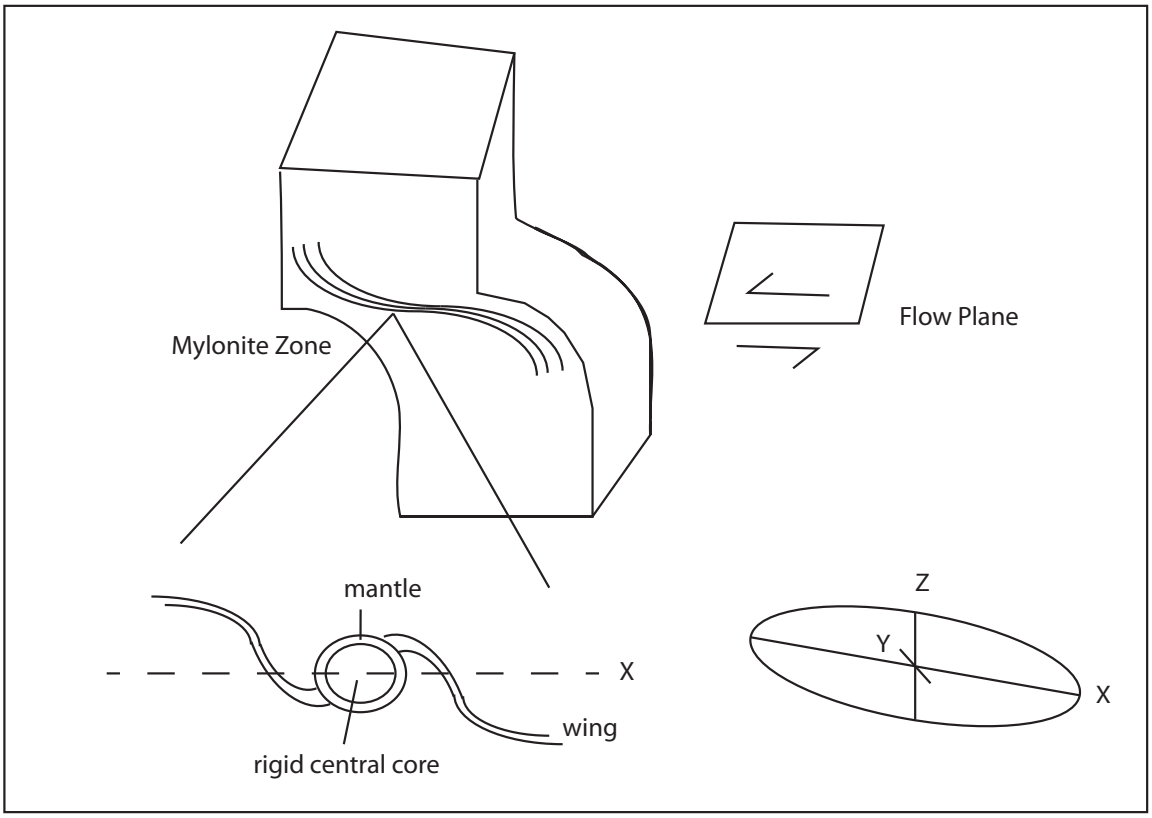

Figure 2.5: Figure illustrating a mylonitic zone with a δ-type porphyroclast displaying the sense of shear direction along with a finite strain ellipsoid for the figure (Passchier and Sokoutis, 1993).

2.4 Ductile deformation mechanisms

Processes of rock deformation vary with depth according to temperature, fluid pressure, confining pressure, mineralogy, differential stress and strain rate (Sibson, 1977). Rocks usually consist of more than one mineral phase and these all might respond to deformation by a different combination of deformation mechanisms. The ductile deformation mechanisms are described below:

•Mechanical twinning, also known as deformation twinning, is achieved by bending rather than breaking of crystal lattices and can be seen under cross polarized light using a petrographic microscope. A mechanical twin is formed when a crystal lattice is bent by shearing parallel to a favourable crystallographic plane (Burkhard, 1993; Passchier, 2005). The crystalline lattice on one side of the twin plane is sheared by a constant angle of rotation compared to the lattice on the other side. The two sides become mirror image reflections of each other

(Burkhard, 1993; Groshong, 1988). Twinning does not require high temperatures or high confining pressures but it does require relatively high differential stresses (plagioglase: <250MPa, jadite: 300MPa, calcite: <90MPa (Stünitz *et al.*, 2003; Küster and Stöckhert, 1999; Craddock *et al.*, 1993)) because it involves energy-intensive bending of lattices (Burkhard, 1993; Groshong, 1988). Mechanical twinning only accommodates a limited amount of strain and often operates along with other deformation mechanisms. The twins are often wedge or tabular in shape and propagate by the movement of the twin tip or twin boundary into untwinned material. Deformation twins often peter out within the grain (Passchier, 2005).

•Diffusion creep is the change in shape due to the movement of vacancies and atoms through crystals and along grain boundaries (Passchier, 2005). Diffusion creep is thermally activated and is more efficient when the rocks are fine grained because the distance that atoms must cover is shorter (Davis *et al.*, 2012). Two types of diffusion creep exist, Coble creep which involves diffusion around grain boundaries and Nabbaro-Herring creep which involves diffusion through grains (Passchier, 2005). Nabbaro-Herring creep is so slow that it only occurs at low differential stresses and extremely high temperatures. It involves the movement of atoms away from high compressive stress to neighbouring sites of lower stress and the movement of vacancies towards high compressive stress (Passchier, 2005). The migration of atoms and vacancies changes the crystal shape and accommodates strain (Passchier, 2005). Coble creep also involves the migration of atoms away from high compressive stress and vacancies towards high compressive stress but it does this by travelling along grain boundaries. The migration path is longer along grain boundaries but the vacancies and atoms can move faster than going directly through crystals, this makes Coble creep more efficient and it can occur at lower temperatures (Passchier, 2005).

When fluid is present, diffusion creep can occur by dissolution-precipitation creep (pressure solution). Dissolution creep is the shape change of a crystal due to dissolution at one place and precipitation of material at another; it requires the presence of fluid along grain boundaries (Durney, 1972; Passchier, 2005). Pressure solution is localised where normal stress on a crystal face is high, increasing the chemical potential, such as on grains in contact with surfaces at high angles to the instantaneous shortening direction. The grain lattices at these contact points are more compressed than elsewhere and this results in dissolution. The dissolved solid is redeposited in free spaces which have experienced lower normal stress and therefore lower chemical potential (Gratier *et al.*, 2009). Dissolution creep commonly occurs

in low grade metamorphic conditions because of the abundance of fluids and typically fine grain size (Passchier, 2005). Dissolution creep can be recognized in rocks by the presence of stylolites and fibres or beards of crystal fibres within pressure shadows (Durney, 1972). Dissolution creep operates over a broad range of temperatures and pressures as long as intergranular fluid is present (Durney, 1972). Grain size is an important factor in dissolution creep because it defines the system size. The system size affects transport distances and the amount of pore space open for fluids to exist in, therefore fine grained rocks are best suited for dissolution creep (Durney, 1972; Gratier *et al.*, 2009, 2013). Dissolution creep works best in immature lithologies, such as shales and carbonate rocks. Dissolution creep causes grain size reduction which leads to faster dissolution, a type of strain softening (Passchier, 2005).

•Dislocation creep is a combination of dislocation climb and dislocation glide (Handy *et al.*, 1999; Passchier, 2005). Dislocation glide and climb are stress and temperature controlled and result in permanent, high strain deformation (Passchier, 2005). Dislocation creep occurs in high temperatures where diffusion rates are high enough to allow for dislocation climb, this enables high strains to occur with relatively low stresses (Tullis *et al.*, 1982) and prevents strain hardening (Passchier, 2005). Dislocation creep produces shape changes by the production, motion and then destruction of dislocations in crystals and grains, these propagate either as edge dislocations or screw dislocations (Passchier, 2005; Handy *et al.*, 1999). Edge dislocations are orientated perpendicular to the direction of slip and screw dislocations are orientated parallel to the direction of slip (Passchier, 2005; Handy *et al.*, 1999). Dislocation creep is the inter-crystalline deformation of crystals by lattice defects and results in lattice-preferred orientations. It can be recognized by undulose extinction, sub-grains (core and mantle structures), sub-grain rotation and grain boundary migration. Different minerals experience dislocation creep at varying conditions, quartz at greenschist facies, K-feldspar at upper greenschist to lower amphibolite facies and plagioclase at middle to upper amphibolite facies conditions (Tullis *et al.*, 1982; Passchier, 2005). As dislocations move through a crystal they may interact with vacancies, interstitial atoms, impurities and other dislocations, this can result in dislocation tangles or the dislocations becoming pinned, this all results in strain hardening of the lattice (Passchier, 2005). As a result of this dislocation glide becomes more difficult and more dislocation are created within a crystal. In order for further deformation to take place these dislocations need to be destroyed or bypassed, for this, recovery and recrystallization act as healers for the crystalline structure, eliminating as many defects as

possible and depleting left-over stored energy in the lattice (Passchier, 2005). For continued dislocation creep to occur, recovery and recrystallization need to keep pace with strain hardening (Passchier, 2005).

•Recrystallization and recovery work in association with dislocation creep in order to reduce the free energy of the system (Passchier, 2005). Recovery involves the moving of dislocations to maximise mutual anihilations in order to form a lower energy configuration (Passchier, 2005). Undulose extinction is an indication of the movement of dislocations (Passchier, 2005). Recrystallization heals by transforming defective grains into strain-free grains or new configurations of grains (Passchier, 2005). Recrystallization involves two types, dynamic recrystallization which occurs during deformation and static recrystallization which occurs post deformation if temperatures are high enough. Dynamic recrystallization involves grain size reduction, by bulging, subgrain rotation, and high temperature grain boundary migration (Tullis *et al.*, 1982; Passchier, 2005; Johnson *et al.*, 2004). Bulging recrystallization occurs at the lowest temperature of all the dynamic recrystallization mechanisms. It forms by grain boundaries bulging into crystals with high dislocation densities. Bulging normally forms along grain boundaries or at triple junctions. It can be recognized by deformation lamella and undulose extinction. Sub-grain rotation recrystallization occurs when dislocations are continuously added to the sub-grain boundaries, this results in the sub-grains commonly being elongated. Sub-grain rotation occurs at higher temperatures than bulging recrystallization. High temperature grain boundary migration recrystallization results in loboid or amoeboid grain boundaries. With relatively high temperatures grain boundary migration increases to a stage when they can sweep through an entire crystal to remove dislocation and sub-grains (Passchier, 2005).

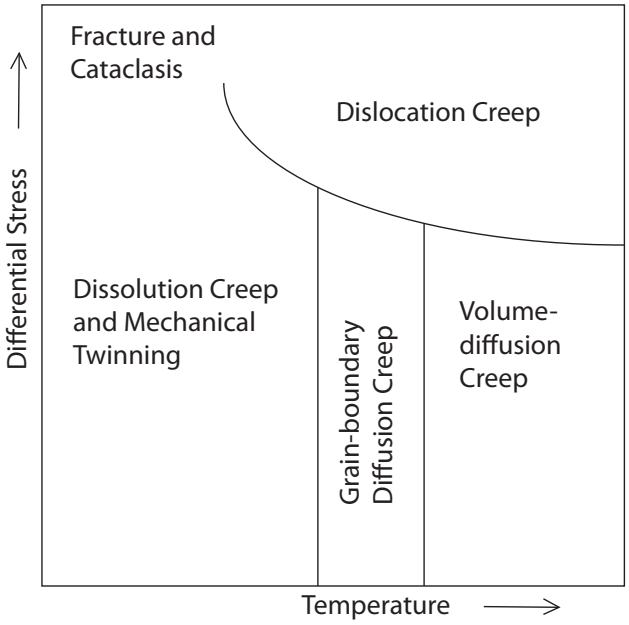

Figure 2.6: Figure illustrating the various deformation mechanisms as a function of temperature and stress (Davis *et al.*, 2012).

2.5 Strain partitioning

As stated above strain is concentrated in narrow zones within the rock. A change in material or deformation conditions in a shear zone compared to its surroundings increases the strain rate at a given stress, narrowing the deforming zone (Montesi, 2013). Rocks are not homogeneous in composition; they are made up of many minerals which have varying strengths. For this reason rocks that are heterogeneous in composition will have large competency contrasts within them (Lister and Williams, 1983). Micas, rheologically the weakest phase in many rocks, form compositional banding (foliation) which is mechanically favourable for deformation because banding facilitates deformation (Goodwin and Tikoff, 2002). These isolated weak phases become interconnected, causing strain localization and therefore facilitate deformation (Holyoke and Tullis, 2006; Johnson *et al.*, 2004). For fabric development a competency contrast is required. Two domains (competent and incompetent) juxtaposed against one another will create this competency contrast. Strain will not be distributed evenly throughout

the rock; the varying domains react differently to various stresses and accommodate strain differently. Strain will be partitioned into the incompetent domain, resulting in higher strain rates and creating fabrics, while the competent domain will only be weakly deformed or remain totally undeformed (Goodwin and Tikoff, 2002; Cosgrove, 2007; Worley and Wilson, 1996). This results in the competent phases forming porphyroclasts while the incompetent phases form flow ribbons around these porphyroclasts. Shear bands are often formed on the margins of large porphyroclasts because of the competency contrast between the competent porphyroclast and the incompetent matrix surrounding it.

An increase in melt content, retrogression and a reduction in grain size are other reasons for strain partitioning into localized zones (Montesi, 2013). Partial melting can cause strain partitioning because the melt is much weaker than the host rocks (Arzi, 1978; Handy *et al.*, 1999), this occurs when critical melt fraction is reached and the partially molten aggregate looses its cohesion and its strength is dominated by the properties of the melt (Arzi, 1978). Strain will be concentrated in this weaker zone, localizing deformation. Migration of large quantities of granite magma through shear zones will result in the introduction of advective heat, which causes thermal softening and an increase in the thermal gradient (Worley and Wilson, 1996). This results in strain partitioning of deformation into these regions of elevated temperatures (Worley and Wilson, 1996). Once the granite crystallizes it becomes more competent than its surrounding host rock, therefore strain is localized into shear zones along the contact of these competent granites and less competent host rocks (Worley and Wilson, 1996). Shear zones commonly have a fine grain size, this grain size reduction could be the cause of strain partitioning or the result of it. Toy et al. (2010) found that reduced grain sizes can come from original heterogeneities in the rock, fine grained layers act as weak zones within a rock, therefore strain will localize in them.

Fault zones can also be relatively weak compared to the surrounding country rock because of weakening processes such as syn-tectonic retrogression and fluid flow (Imber *et al.*, 1997). This occurs by an influx of hydrous fluids that cause grain-scale alteration. The influx of hydrous fluids results in the replacement of a competent framework and chain silicates by fine grained, weaker aggregates of aligned phyllosilicates along with interconnected weak layer structures on all scales within the fault zone (Imber *et al.*, 1997). Prior to the influx of hydrous fluids the bulk rheological behaviour of the rock was controlled by the strength and distribution of the feldspar and hornblende grains making up the load-bearing framework. After the retrogression of these competent grains to interconnected phyllosilicates the bulk

strength of the rock is controlled by the rheology of the fine-grained matrix (Imber *et al.*, 1997). In addition, further syn-tectonic softening by diffusive mass transfer will occur during fluid influx. This softening caused by the retrogression of load-bearing framework to a fine-grained interconnected matrix of weak minerals causes the fault zone to become a zone of long-term weakening (Imber *et al.*, 1997).

The shape of strain ellipsoids, defined by X=the direction of greatest finite elongation, Y=intermediate direction and Z=the direction of greatest finite shortening, is often plotted on a Flinn diagram which visualizes it by plotting the axial ratios $\frac{X}{Y}$ and $\frac{Y}{Z}$ as coordinated axes (Flinn, 1962). The line $\frac{X}{Y} = \frac{Y}{Z}$ represents plane strain (Flinn, 1962). This line separates prolate geometries (cigar or linear shaped) of the upper half of the field from oblate geometries (pancake or tabular shaped) lower half (Flinn, 1962). The shape of the strain ellipsoid is characterized by the k-value, k=$\frac{a-1}{b-1}$, where a=$\frac{X}{Y}$ and b=$\frac{Y}{Z}$ (Flinn, 1962). In this way, when an ellipsoid has been flattened, it's end-member is characterized by k=0 and when an ellipsoid has been stretched, it's end-member is characterized by k=∞. Plane strain is characterized by k=1 (Flinn, 1962).

The magnitude of competency contrast will directly influence the deformation mechanism but the magnitude of competency contrast is influenced by temperature, confining pressure, pore fluid pressure, composition, strain rate and stress orientation (Goodwin and Tikoff, 2002). Grain size and shape, pore space and the ratio of simple to pure shear also play a role in competency contrast and therefore the deformation mechanism (Goodwin and Tikoff, 2002). Pre-existing foliations play an important role in the initiation and evolution of shear zones (Goodwin and Tikoff, 2002; Worley and Wilson, 1996). If the grain orientation of a pre-existing fabric is parallel to the imposed shear plane, the grains will be weak and therefore strain will be partitioned into it. But if the grains are aligned perpendicular to the imposed shear plane they will be stronger and strain will not be partitioned into the grains (Goodwin and Tikoff, 2002; Tullis *et al.*, 1982). If a pre-existing fabric has a favourable orientation and strain is partitioned along the fabric, the strain will reactivate the fabric and result in a composite fabric forming (Worley and Wilson, 1996). A pre-existing shear zone may remain weaker than the adjacent host rock and therefore in future deformation events, strain will tend to re-localize within these weaker zones, even if they are not in the optimal orientation (Holyoke and Tullis, 2006; Worley and Wilson, 1996). For these reasons it is clear that heterogeneous Earth materials are a fundamental control on the localization of strain in shear zones and also the formation of fabrics by shearing (Goodwin and Tikoff, 2002; Lister

and Williams, 1983).

Strain in shear zones can be accommodated by either coaxial or non-coaxial deformation. Compressive stress is defined by $\sigma_1 > \sigma_2 > \sigma_3$, where σ_1 is the maximum and σ_3 the minimum principle compressive stress. Coaxial deformation, pure shear, is defined by no rotation to the principle strain axes during progressive deformation (Hudleston, 1999; Lister and Williams, 1983). Non-coaxial, simple shear, is defined by the σ_1 and σ_3 axes originally orientated at 45° to the plane of greatest shear stress, the principle strain axes rotate with progressive deformation toward the slip plane (Hudleston, 1999; Lister and Williams, 1983). Fossen (1997) stated that because of the large aspect ratio (length and depth >>thickness) of mylonite zones, that pure shear is inefficient in accommodating displacements of the margins compared to simple shear. Therefore it is anticipated that pure shear will be spread over a wide zone and that simple shear will be localized within the mylonite zone/ shear zone (Toy *et al.*, 2013; Lister and Williams, 1983).

A combination of Shimizu's (2008) piezometer with Hirth et al.'s (2001) quartz flow law can be used to determine the strain rate of the rocks if deformed by dislocation creep in quartz (Boutonnet *et al.*, 2013). Firstly Shimizu's (2008) piezometer is used to determine the differential stress σ in MPa by using temperature of deformation T (kelvin) and subgrain size d (μm).

$$\sigma = 3.52 \times 10^2 \times d^{-0.8} exp \frac{6.98 \times 10^2}{T}. \tag{2.1}$$

This describes the processes of SGR (subgrain rotation) and GBM (grain boundary migration) in quartz for intracrystalline nucleation. Once the differential stress is known from the size of the subgrains, the strain rate $\dot{\varepsilon}$ (s^{-1}) can be calculated using Hirth et al.'s (2001) quartz flow law.

$$\dot{\varepsilon} = A\sigma^n f_{H_2O}^m e^{\frac{-Q}{RT}} \tag{2.2}$$

Where Q=135±15 kJ/mol, log A = -11.2±0.6 $MPa^{\frac{-n}{s}}$, m=1, n=4, R=8.3145 J/mol K (ideal gas constant), T = temperature (Kelvin), σ = differential stress and f_{H_2O} = water fugacity (MPa).

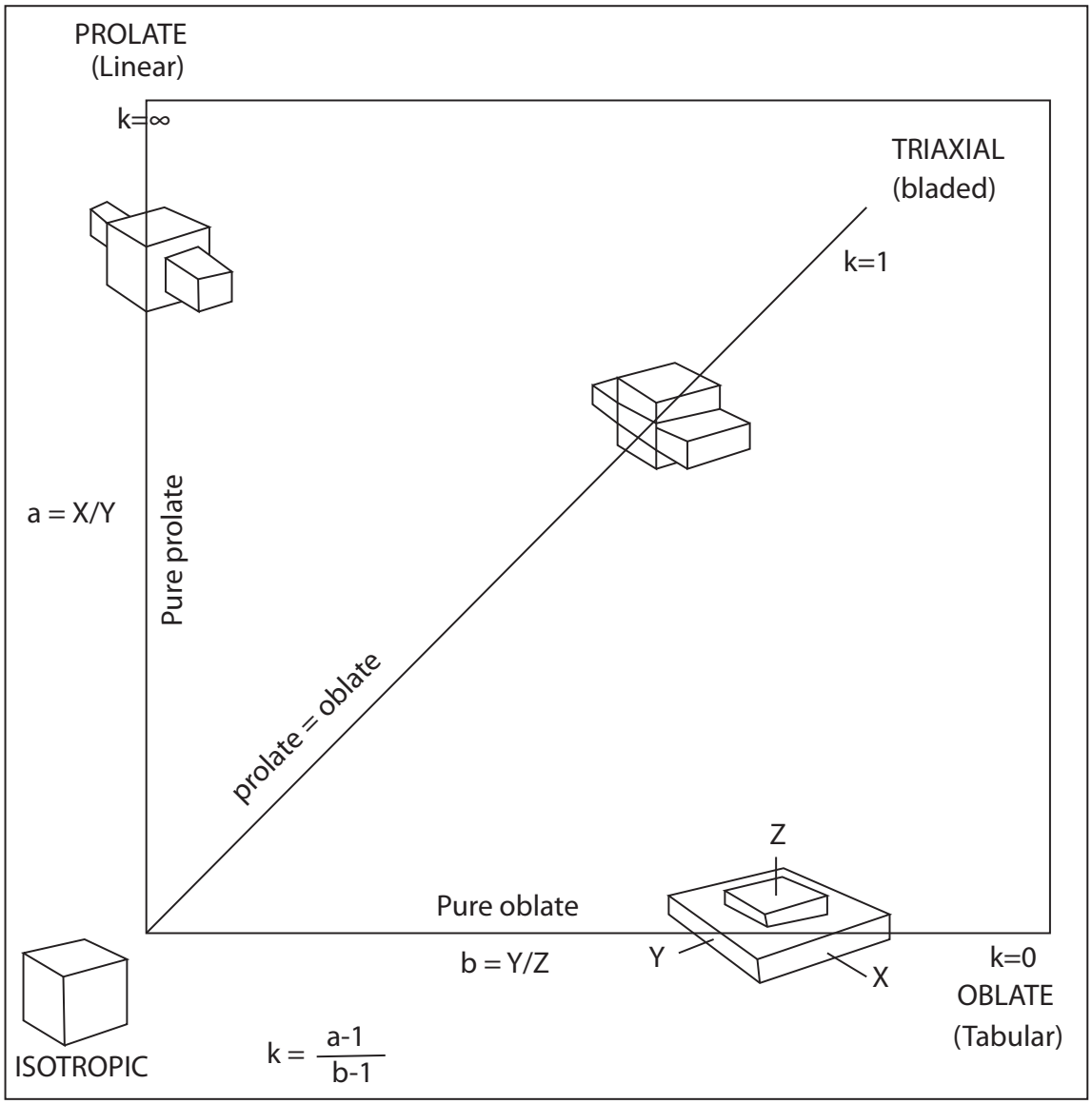

Figure 2.7: Flinn diagram that summarises the range of distortion shapes resulting from ductile deformation of a rock mass (Flinn, 1962).

Chapter 3

Geological Setting

3.1 Antarctica

Antarctica is the southernmost continent on Earth and is almost entirely situated within the Antarctic Circle (66° 33' 44"S). Antarctica covers an area of 14 million km^2 and is totally surrounded by the Southern Ocean. Antarctica is geographically subdivided into two areas by the Transantarctic Mountains, the smaller West Antarctica and the larger East Antarctica.

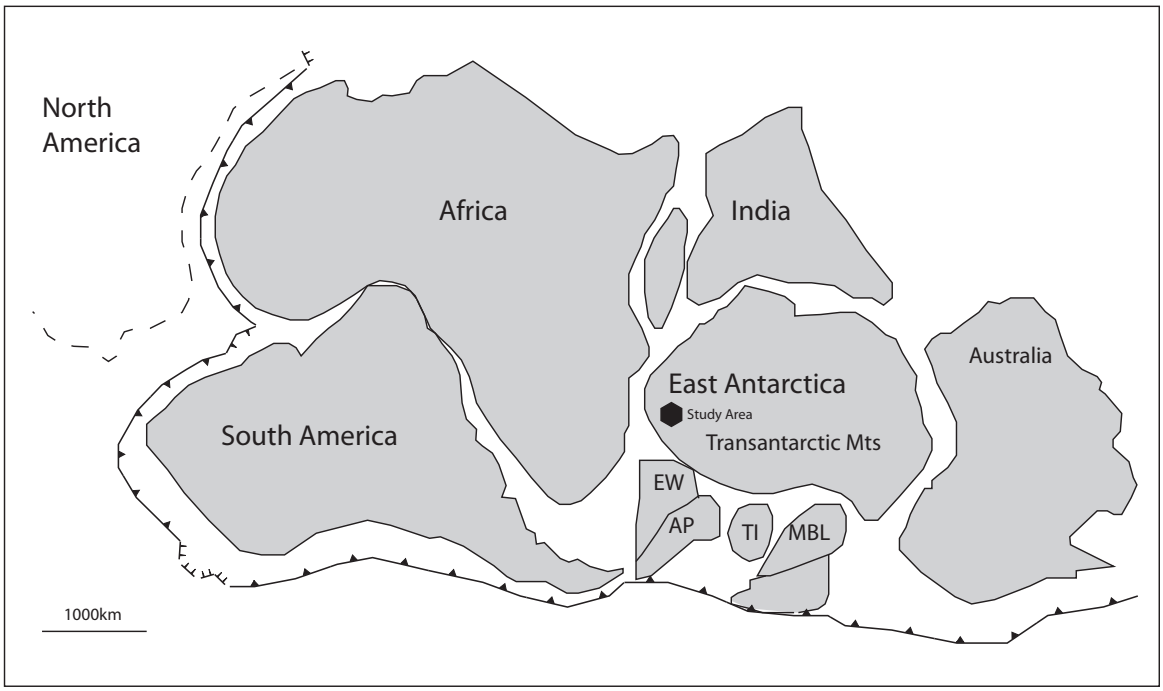

Figure 3.1: Map showing the reconstruction of Gondwana: EW = Ellsworth-Whitmore Block, AP = Antarctic Peninsula, TI = Thurston Island Block, MBL = Marie Byrd Land (Coney *et al.*, 1990).

East Antarctica is considered to have existed by the mid-Proterozoic (Krynauw, 1996). East Antarctica is dominated by the East Antarctic Shield which is made up of Archean nuclei surrounded by polydeformed Proterozoic metamorphic provinces (Krynauw, 1996). Two regionally significant deformation events have affected East Antarctica, the Grenvillian (∼1300 Ma to ∼900 Ma) and the Pan-African (∼600 Ma to ∼450 Ma) orogenies (Fitzsimons, 2000). East Antarctica is made up Dronning Maud Land, Enderby Land, Wilkes Land and the Transantarctic Mountains (Fitzsimons, 2000).

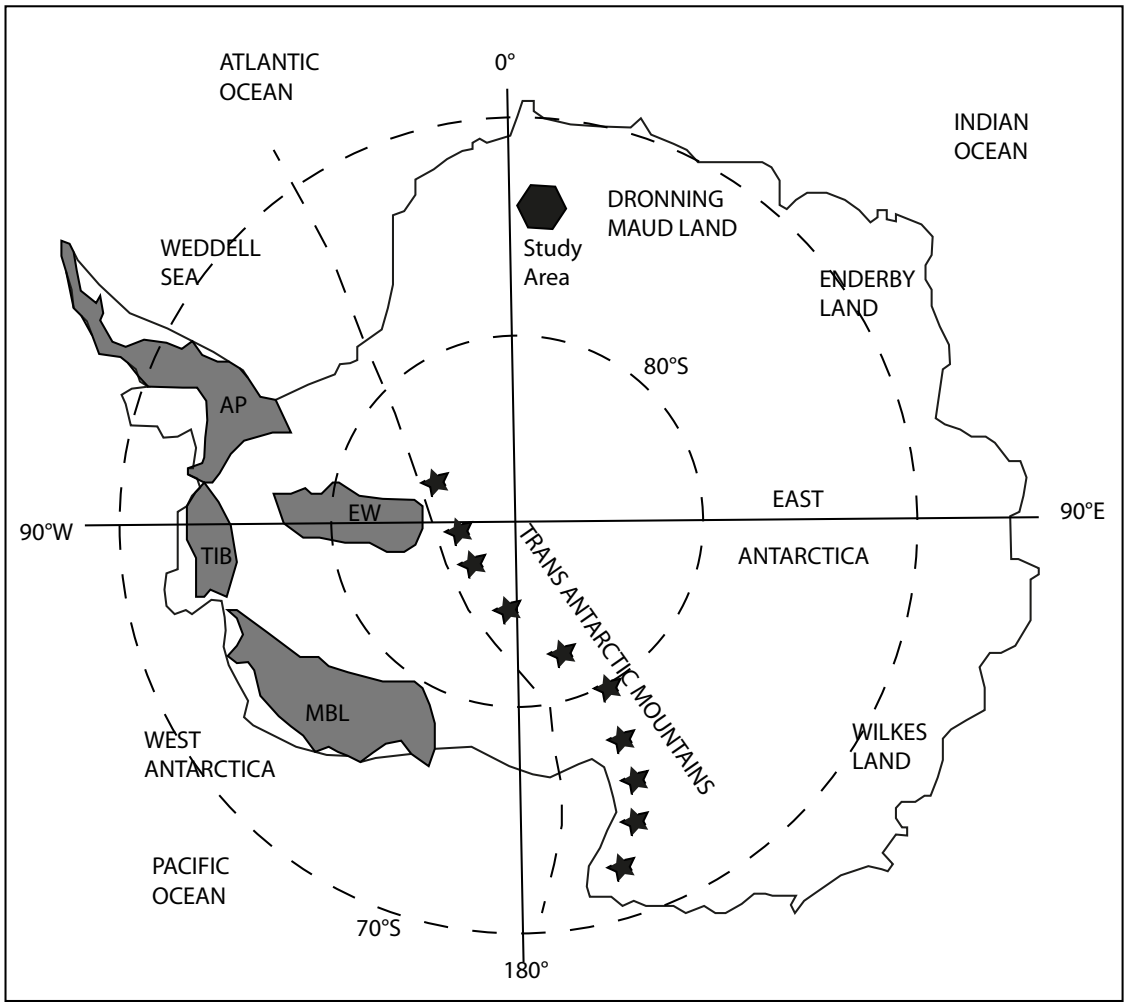

Figure 3.2: Map of Antarctica showing which provinces make up Eastern and Western Antarctica. AP = Antarctic Peninsula, TIB = Thurston Island Block, MBL = Marie Byrd Land and EW = Ellsworth - Whitmore Block (Board, 2001).

3.2 Dronning Maud Land

Western Dronning Maud Land extends from 70°S to 75°S and 15°W to 03°E. Western Dronning Maud Land is made up of two geologically distinct provinces, the Archean to Mesoproterozoic Grunehogna Province (~3100 Ma to ~2950 Ma) and the Mesoproterozoic to early Paleozoic Maud Belt (Halpern, 1970; Barton *et al.*, 1987). The Maud Belt contains the two study areas of this research project, H.U. Sverdrupfjella and Neumayerskarvet (Fig. 3.3). Like the rest of East Antarctica it has experienced at least two regionally significant deformation events, the Grenvillian and the Pan-African orogenies (Fitzsimons, 2000).

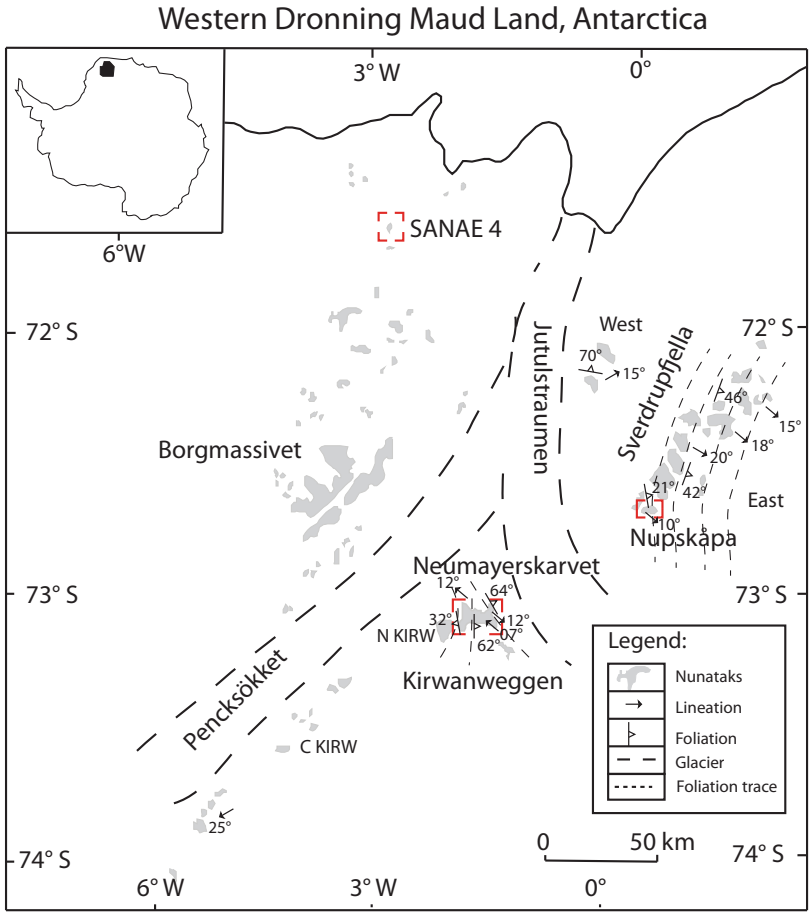

Figure 3.3: Regional map illustrating the field areas - H.U. Sverdrupfjella and Neumayerskarvet within northern Kirwanweggen. Also showing where the South African base (SANAE 4) is situated and the two glaciers (Pencksökket and Jutulstraumen) that seperate the Grunehogna Province from the Maud Belt. (C KIRW=cental Kirwanweggen, N KIRW=northern Kirwanweggen)

3.3 Geology of the Maud Belt

3.3.1 Archean

The Grunehogna Province is made up of a relatively undeformed Archean granite basement and the Mesoproterozoic Ritschersflya Supergroup. The Archean Grunehogna Craton is interpreted as a portion of the Kaapvaal-Zimbabwe Craton (Groenewald, 1995).

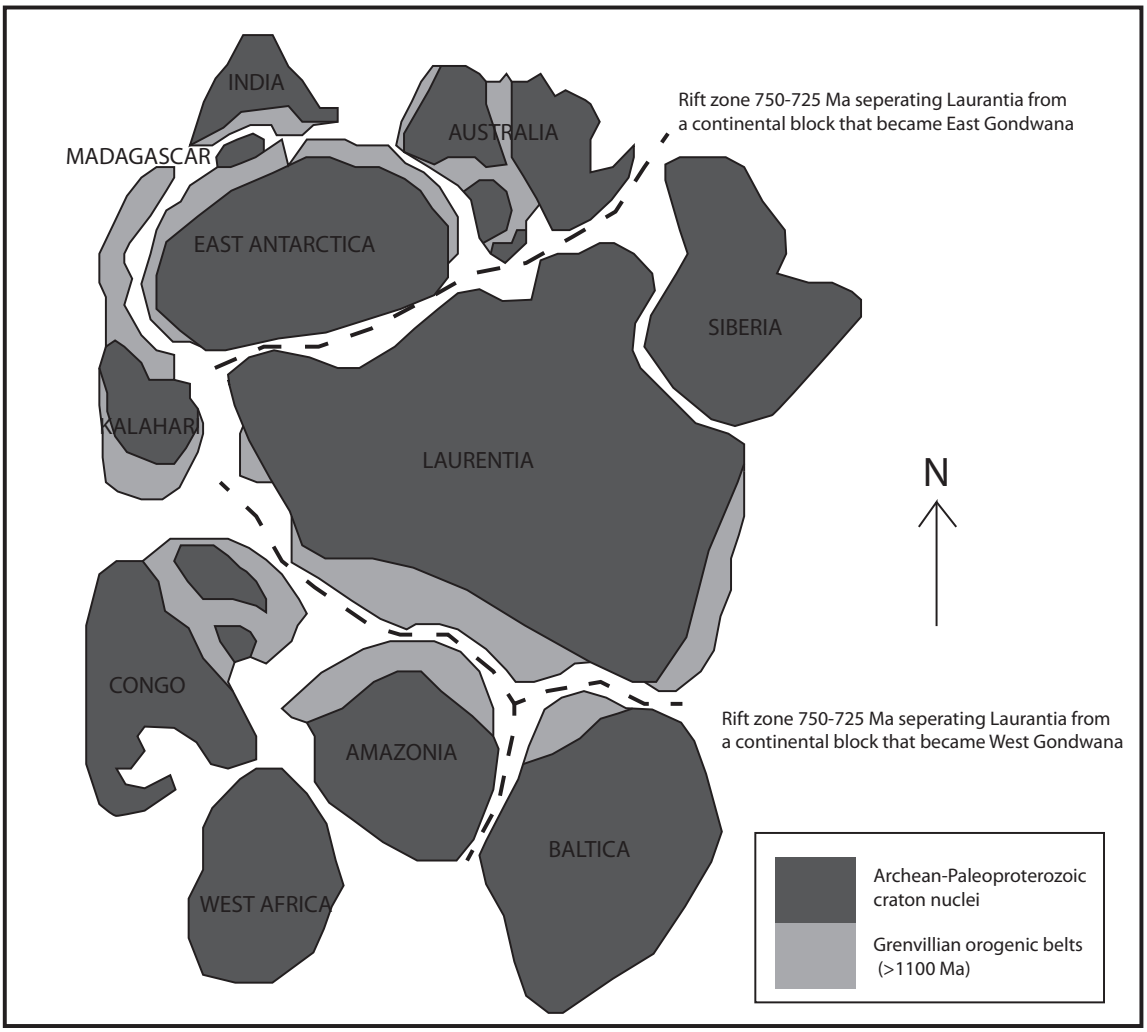

Figure 3.4: Map showing the reconstruction of Rodinia: illustrating the position of the study area and the Grenvillian orogenic belts (Hoffman, 1991; Torsvik *et al.*, 1996; Unrug, 1997).

3.3.2 Grenvillian Orogeny

The Maud Belt developed in the first of the two major orogenic events in western Dronning Maud Land, which involved high grade metamorphism, recumbent folding, and thrusting be-

tween 1200 and 900 Ma (Grantham *et al.*, 1988). The Maud Belt has been tectonically juxtaposed onto the Grunehogna Province along an inferred crustal discontinuity that is masked by the Pencksökket and Jutulstraumen glaciers(Board, 2001). Grantham (1991) proposed that the presence of alkaline complexes along the margins of the Pencksokket and Jutulstraumen glaciers indicates that it was the site of previous thrusting. Gravity and magnetic anomalies show that there is a deep, major graben below the Pencksökket and Jutulstraumen glaciers (Riedel *et al.*, 2012; Jacobs and Lister, 1999). The Maud Belt is made up of Heimefrontfjella, Kirwanveggen, H.U. Sverdrupfjella, Gjelsvikfjella and western Mühlig-Hofmannfjella.
The Grunehogna's Archean granite basement is covered by the Ritschersflya Supergroup (∼1080 Ma) (Moyes *et al.*, 1995) which is predominantly made up of weakly deformed sediments with some volcanogenic contribution from the Jutulstraumen groups. This has been intruded by mafic and ultramafic rocks of the Borgmassivet Intrusive Suite; predominantly tholeiitic sills that were emplaced prior to sediment consolidation (Krynauw *et al.*, 1994) between ∼1000 Ma and ∼1100 Ma (Wolmarans and Kent, 1982; Moyes *et al.*, 1995).

The Grevillian orogeny (1300 Ma to 900 Ma) deformed H.U. Sverdrupfjella and Kirwanweggen in the same way, causing D_1 and D_2 that resulted in isoclinal folds that plunge shallowly to the south/south east and a top-to-the-NW transport direction (Tab.3.1) (Grantham *et al.*, 1995; Groenewald, 1995). The metamorphism associated with the Grenvillian orogeny in both regions in H.U. Sverdrupfjella is high pressure eclogite facies during M_1 and then granulite to upper amphibolite facies in M_2 (Grantham *et al.*, 1995; Groenewald, 1995). This is replicated in Kirwanweggen with M_1 representing an early high pressure eclogite facies and M_2 representing an upper amphibolite facies (Grantham *et al.*, 1995; Groenewald, 1995).

3.3.3 Pan-African Orogeny

The Pan-African orogeny (∼550 Ma to ∼450 Ma) (Board, 2001) added more deformation and metamorphism to the Maud Belt and this resulted in the Maud Belt being characterized by NE-striking shear zones that are attributed to dextral transpression (Grantham, 1992). Previous authors have found it hard to separate the Grenvillian and Pan-African orogenic events on a large scale because they are thought to have transposed each others fabrics and at very similar metamorphic grades.
The deformation caused by the Pan-African orogeny in Western H.U. Sverdrupfjella resulted

in ENE-WSW-trending open folds with axial planar cleavage defined by biotite laths for D_3 and macroscopic warping for D_4 (Grantham, 1992). In Eastern H.U. Sverdrupfjella, D_3 is represented by NE-plunging tight folds with a weak axial planar foliation, defined by biotite, whereas D_4 resulted in continuous folding and late faulting (Tab.3.1) (Grantham *et al.*, 1995). The deformation associated with the Pan-African orogeny in Kirwanweggen is thought to have transposed the Grenvillian fabric (Grantham *et al.*, 1995). Metamorphism related to the Pan-African orogeny throughout these regions is amphibolite facies. The Pan-African orogeny is mainly thought to be M_3 but on occasions in localized areas M_2 also. M_2 and M_3 are very similar in grade (Tab.3.1) (Grantham, 1992; Grantham *et al.*, 1995; Groenewald, 1995).

3.3.4 Gondwana breakup

During the break up of Gondwana (180 Ma) the Grunehogna Province is thought to have been detached from the Kaapwaal-Zimbabwe Craton. Grantham (1991) suggested that during this time rifting was superimposed over the previous thrusting of the Pencksökket and Jutulstraumen glaciers.

D_5 is represented by normal faulting throughout all three regions and it is associated with greenschist facies metamorphism (Tab.3.1).

Table 3.1: Table summarising the deformational features and metamorphic conditions of the tectonic events experienced by the Maud Belt (Board, 2001; Grantham *et al.*, 1995; Groenewald, 1995). The table shows how similar the deformation and metamorphism is throughout the study areas.

Orogeny:	Structure:			Grade:		
	Western H.U. Sverdrupfjella	Eastern H.U. Sverdrupfjella	Kirwanweggen	Western H.U. Sverdrupfjella	Eastern H.U. Sverdrupfjella	Kirwanweggen
Grenvillian (1300 - 900 Ma)	D_1+D_2: -Isolclinal folds plunging shallowly S/SE. -top-to-the-NW transport direction	D_1+D_2: -Isolclinal folds plunging shallowly S/SE. -top-to-the-NW transport direction	D_1+D_2: -SE shallowly dipping. -top-to-the-NW transport direction	M_1 - high pressure eclogite facies M_2 - granulite to upper amphibolite facies	M_1 - high pressure eclogite facies M_2 - granulite to upper amphibolite facies	M_1 - high pressure eclogite facies M_2 - upper amphibolite facies
Pan-African (600 - 450 Ma)	D_3 - ENE-WSW-trending, open folds with axial planar cleavage defined by biotite laths D_4 - macroscopic warping	D_3 - NE-plunging tight folds with axial planr cleavage defined by biotites D_4 - continuous folding and late faulting	Grenvillian and Pan-African deformation fabrics are thought to be transposed	M_3 - amphibolite facies	M_3 - amphibolite facies	M_3 - amphibolite facies
Break-up of Gondwana (180 Ma)	D_5 - normal faulting	D_5 - normal faulting	D_5 - normal faulting	M_4 - greenschist facies	M_4 - greenschist facies	M_4 - greenschist facies

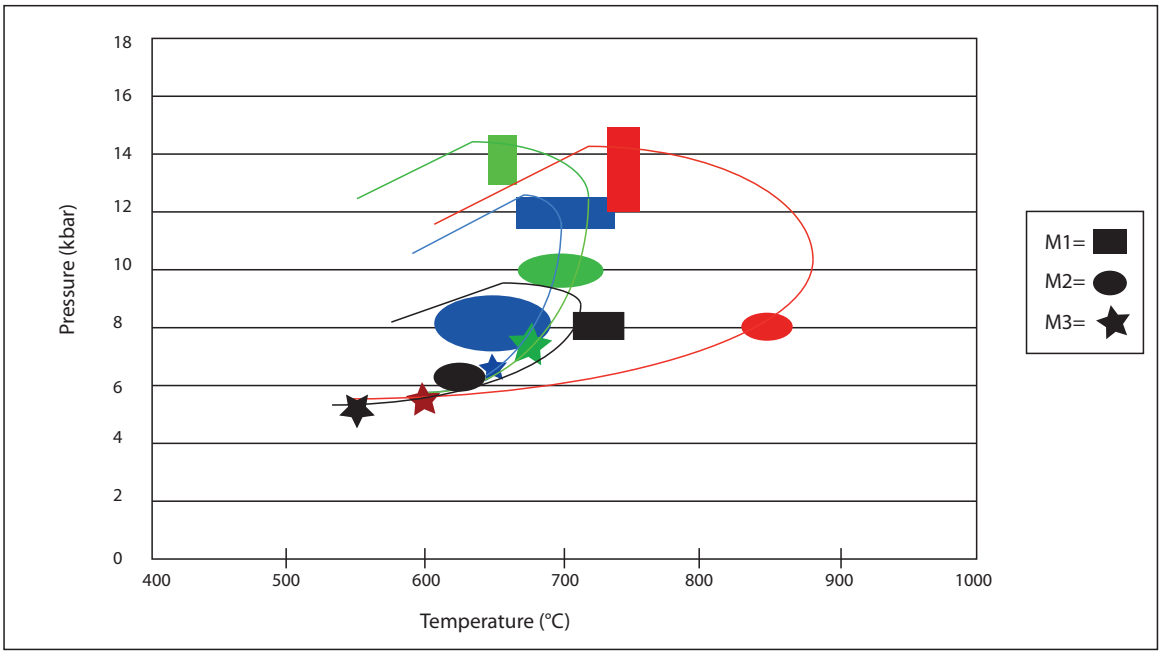

Figure 3.5: Metamorphic estimates and P-T paths that have been proposed for different regions of the Maud Belt: Green=eastern H.U. Sverdrupfjella (Board, 2001), Blue=eastern H.U. Sverdrupfjella (Grantham *et al.*, 1995), Red=eastern H.U. Sverdrupfjella (Groenewald *et al.*, 1995), black=Neumayerskarvet (Harris, 1999).

Previously the Grenvillian orogeny was thought to be the major contributor to deformation in eastern Antarctica (Grantham *et al.*, 1995) but more recently studies have hinted that the Pan-African episode had a larger role to play than previously thought (Board, 2001).

3.4 H.U. Sverdrupfjella and Kirwanweggen

The two study areas which are separated by the Jutulstraumen Glacier have been described as displaying different structural styles but having similar deformation histories (Harris, 1999; Jackson and Jacobs, 1995).

3.4.1 H.U. Sverdrupfjella

Board (2001) divided H.U. Sverdrupfjella into a western and eastern region based on lithological, structural and metamorphic differences (Fig. 3.6). The main difference is that the west is made up of amphibolite facies rocks and the east of granulites to partially retrogressed amphibolite facies (Groenewald, 1995). The east also has a number of E to SE-dipping thrusts sub-parallel to both lithological layering and foliation, whereas the west has been complexly

folded (Groenewald, 1995). A top-to-the-NW transport direction indicates that the higher grade eastern rocks were thrust onto the lower grade western rocks (Groenewald, 1995).

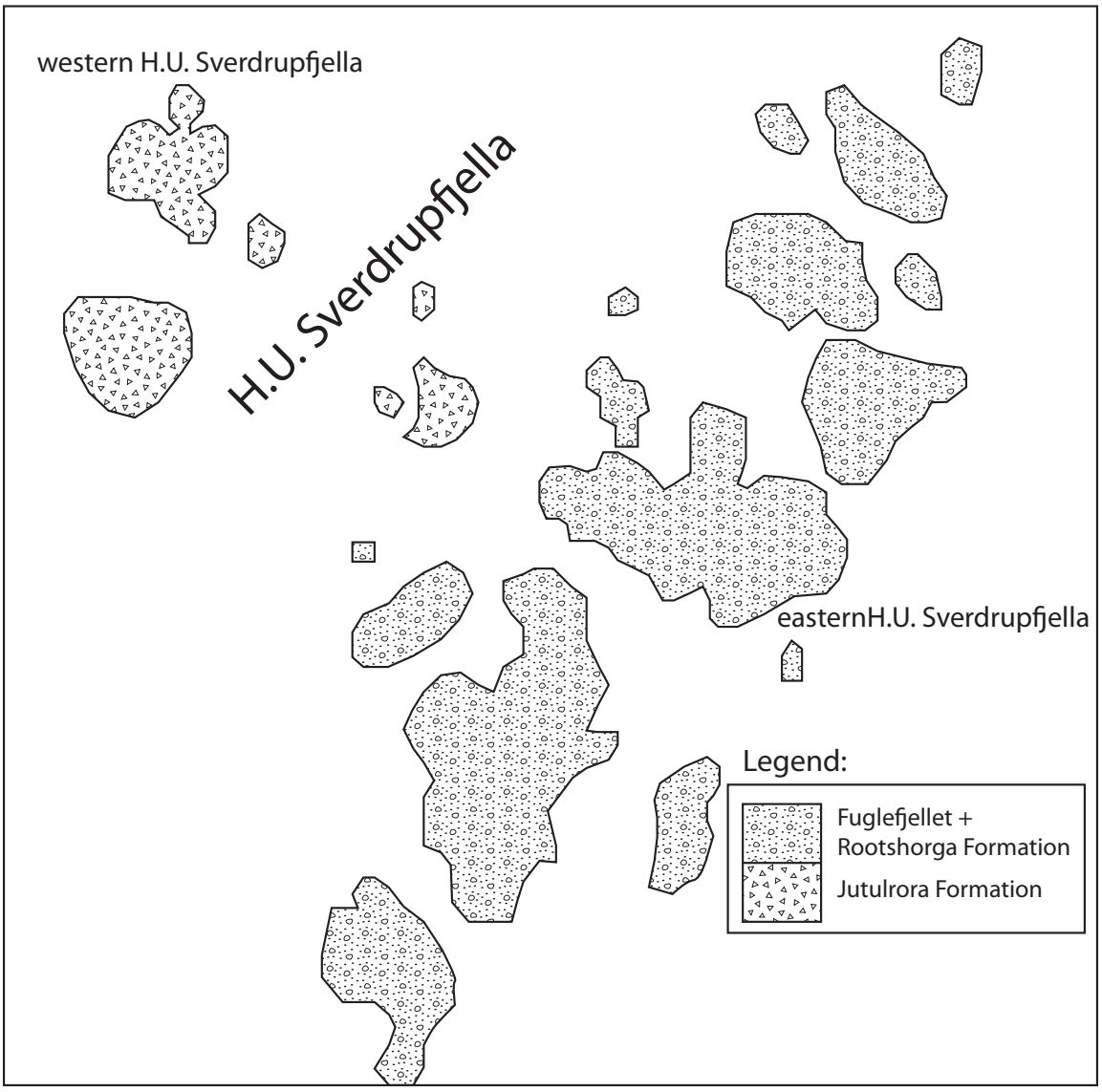

Figure 3.6: Lithological map separating eastern and western H.U. Sverdrupfjella. Western H.U. Sverdrupfjella is dominated by the Jutulrøra Formation, which consists of a hornblende-biotite gneiss and tonalitic orthogneiss (Grantham, 1992; Groenewald, 1995). Eastern H.U. Sverdrupfjella is dominated by the Rootshorga and Fuglefjellet Formations, these consist of high grade gneisses made up of marble, quartzofeldsphatic and pelitic paragneisses and intermediate to felsic orthogneisses (Grantham, 1992; Groenewald, 1995).

Western H.U. Sverdrupfjella

The most abundant rock in this region is a hornblende-biotite gneiss of the Jutulrøra Formation (Grantham, 1992). A Rb-Sr whole rock age of 1145 ± 49 Ma was obtained for the Jutulrøra Formation (Moyes *et al.*, 1995). Inter-layered ortho- and paragneisses are structurally the lowest rocks in this region and are overlain by paragneisses that have been thrust over from eastern H.U. Sverdrupfjella (Board, 2001). The older gneiss has been intruded by tabular granite bodies (1103 ± 17 Ma; Harris et al., 1995), deformed mafic intrusions, post-tectonic monzogranite sheets and dykes (469 ± 5 Ma; Grantham, 1991), Mesozoic alkaline complexes (170 ± 4 Ma; Grantham et al., 1988) and undeformed Jurassic dolerite dykes (Grantham *et al.*, 1991). The Jurassic dolerite dykes are linked to the breakup of Gondwana (Harris and Grantham, 1993).

Grantham (1992) recognized five deformation events. D_1 and D_2 developed in a single continuous deformation event which transposed the S_1 fabric, this is evident in the presence of rootless intrafolial folds. D_2 is characterized by a penetrative shallow east dipping S_2 fabric of tight to isoclinal folds with a top-to-the-WNW sense of shear. Lineations and fold hinge lines plunge to the east and southeast. D_3 is characterized by ENE-WSW-trending open folds with an axial planar cleavage defined by biotite laths. Top-to-the-southeast sense of shear was determined for D_3. D_4 was associated with macroscopic warping of the north- and east-trending fold axes. D_5 the youngest deformation event resulted in sub-vertical normal faults and joints with N-S and NE-SW trends. D_1 and D_2 are linked to the Grenvillian orogeny, D_3 and D_4 to the Pan-African orogeny and D_5 is associated with the breakup of Gondwana (Grantham, 1992).

Four stages of metamorphism are recognized in western H.U. Sverdrupfjella, M_{1-3} all exhibit meduim to high grade metamorphism (P = 3-9 kbar; T = 620-700°C) (Grantham *et al.*, 1995). M_1 experienced early high pressure and represents eclogite facies conditions. M_2 and M_3 are metamorphically similar, both experiencing amphibolite facies conditions, and have been separated by structural relationships of several generations of mafic intrusions (Grantham *et al.*, 1995). M_2 represents high grade granulite to amphibolite facies conditions. M_3 is recognised by biotite laths and includes amphibolitised mafic intrusions that represent amphibolite facies conditions (Grantham *et al.*, 1995). M_4 represents late stage retrogression to greenschist facies and is associated with brittle faults and joints (Grantham, 1992). M_1 and M_2 have been associated with the Grenvillian orogeny (D_1 and D_2), M_3 with the Pan-African

orogeny (D_3 and D_4), and finally M_4 is interpreted as related to the breakup of Gondwana (∼180 Ma, D_5) (Grantham, 1992).

Eastern H.U. Sverdrupfjella

The eastern domain is made up of the Fuglefjellet and Rootshorga formations; these consist of high-grade gneisses made up of marble, quartzofeldsphathic and pelitic paragneisses and intermediate to felsic orthogneisses (Grantham, 1992; Groenewald, 1995). Groenewald (1995) concluded that granitic and mafic bodies that intruded these rocks formed during a prolonged period of collisional tectonism because of changes in the melt composition.

Eastern H.U. Sverdrupfjella records a similar deformation history to that of western H.U. Sverdrupfjella with five deformation episodes (Grantham *et al.*, 1995). D_1 and D_2 resulted in moderate SE-dipping composite fabrics associated with SE-plunging tight to isoclinal folds, moderate SE-plunging lineations and a top-to-the-NW sense of shearing. D_3 is characterized by shallow NE-plunging tight to isoclinal folds with localized foliation over-printing and the development of a weak axial planar foliation defined by biotite. Late brittle faulting is also associated with D_3. D_4 is characterized by mesoscale, open, upright folding on NE-trending axes, this reflects the waning stages of deformation in eastern H.U. Sverdrupfjella (Board, 2001). D_5, just like in the western domain has resulted in normal faults and joints. Like the western domain, D_1 and D_2 are thought to be linked to the Grenvillian orogeny, D_3 and D_4 to Pan-African orogeny and D_5 to the breakup of Gondwana (Grantham *et al.*, 1995; Groenewald, 1995).

Similar to western H.U. Sverdrupfjella, eastern H.U. Sverdrupfjella experienced four metamorphic events. M_1 is an early high-pressure stage (P= 9-20kbar; T = 720-850°C), this then underwent decompression to amphibolite and granulite facies for M_2 (P= 5-8 kbar; T = 600-790°C), M_3 has similar conditions to M_2 but experienced retrograde re-hydration. Finally late-stage greenschist facies conditions occurred during M_4 (Groenewald, 1995). Groenewald, (1995) argued that M_2 and M_3 are linked to D_2 and D_3 because of the similarities in structural styles and metamorphic conditions and that M_4 is related to D_5. In this way thermal resetting of mineral isotopes at ∼500 Ma is the only signature of D_4, the Pan-African episode.

3.4.2 Kirwanweggen

Kirwanweggen is situated south-west of the Jutulstraumen glacier. It is made up of high grade paragneisses and orthogneisses which deformed tectonically during the Grenvillian (1130 Ma to 1150 Ma), and were intruded by younger orthogneisses and leucogranites (1080 Ma to 1130 Ma). Kirwanweggen also experienced the younger Pan-African (550 Ma to 450 Ma) deformational event but 1000 Ma and 500 Ma fabrics are probably parallel and collinear, making them indistinguishable in the absence of structurally well constrained time markers such as intrusive dykes (Grantham *et al.*, 1995). Central Kirwanweggen (Fig. 3.3) is described as shallow SE-dipping composite fabrics, with associated SE-plunging mineral stretching lineations and fold hinge lines. The high strain zones show a top-to-the-NW movement. Northern Kirwanweggen (Fig. 3.3) varies from the central Kirwanweggen by having a shallow NNW-plunging lineation and a steep, sub-vertical, foliation; this has been interpreted as a lateral ramp (Harris, 1999). Kirwanweggen is inferred to have experienced four metamorphic episodes. M_1 is described as an early high pressure eclogite facies, M_2 experienced upper amphibolite facies conditions, M_3 is similar to M_2 with upper amphibolite facies associated with biotitisation and the final M_4 stage of metamorphism was greenschist facies. M_1 is thought to have occurred between ∼1096 Ma and ∼1150 Ma, M_1 and M_2 are thought to be linked to the Grenvillian orogeny and M_3 has been associated with the Pan-African episode and finally M_4 is associated to the breakup of Gondwana (Ferrar, 1995). Harris (1999), however, classified the two amphibolite facies, M_2 and M_3, as Grenvillian and M_4 as Pan-African.

Chapter 4

Field relations and Petrography

A very broad description of the field areas is that they are dominated by paragneisses and orthogneisses. H.U. Sverdrupfjella is made up of paragneisses varying from psammitic to pelitic and orthogneisses which in places contain pre-tectonic mafic lenses. All of these units are cut by leucogranites and a ∼50 meter wide dolerite dyke in the eastern section of the field area. Neumayerskarvet has a greater variety of rock types, with paragneisses varying from banded paragneiss to migmatitic paragneiss and migmatitic paragneisses containing mafic lenses. There are many generations of orthogneiss, ranging from a weakly foliated orthogneiss to a strongly foliated orthogneiss and then there is also a generation of unfoliated granite which is found within two shear zones in eastern Neumayerskarvet.

4.1 H.U. Sverdrupfjella

On a large scale the petrography of H.U. Sverdrupfjella consists of alternating units of granitic orthogneisses and quartzfeldspathic paragneisses that have been thrust above one another forming a duplex structure. The sub-horizontal lithological units are approximately 100 to 200 meters thick. The top exposed lithology of the duplex structure in this area is a metapelite. The duplex structure has been intruded by multiple leucogranites phases and a dolerite dyke. The dolerite dyke is approximately 50 meters wide.

4.1.1 Orthogneiss

The orthogneisses are very uniform throughout H.U. Sverdrupfjella, consisting predominantly of K-felspar (microcline), plagioclase (albite), quartz and biotite with garnet, apatite and

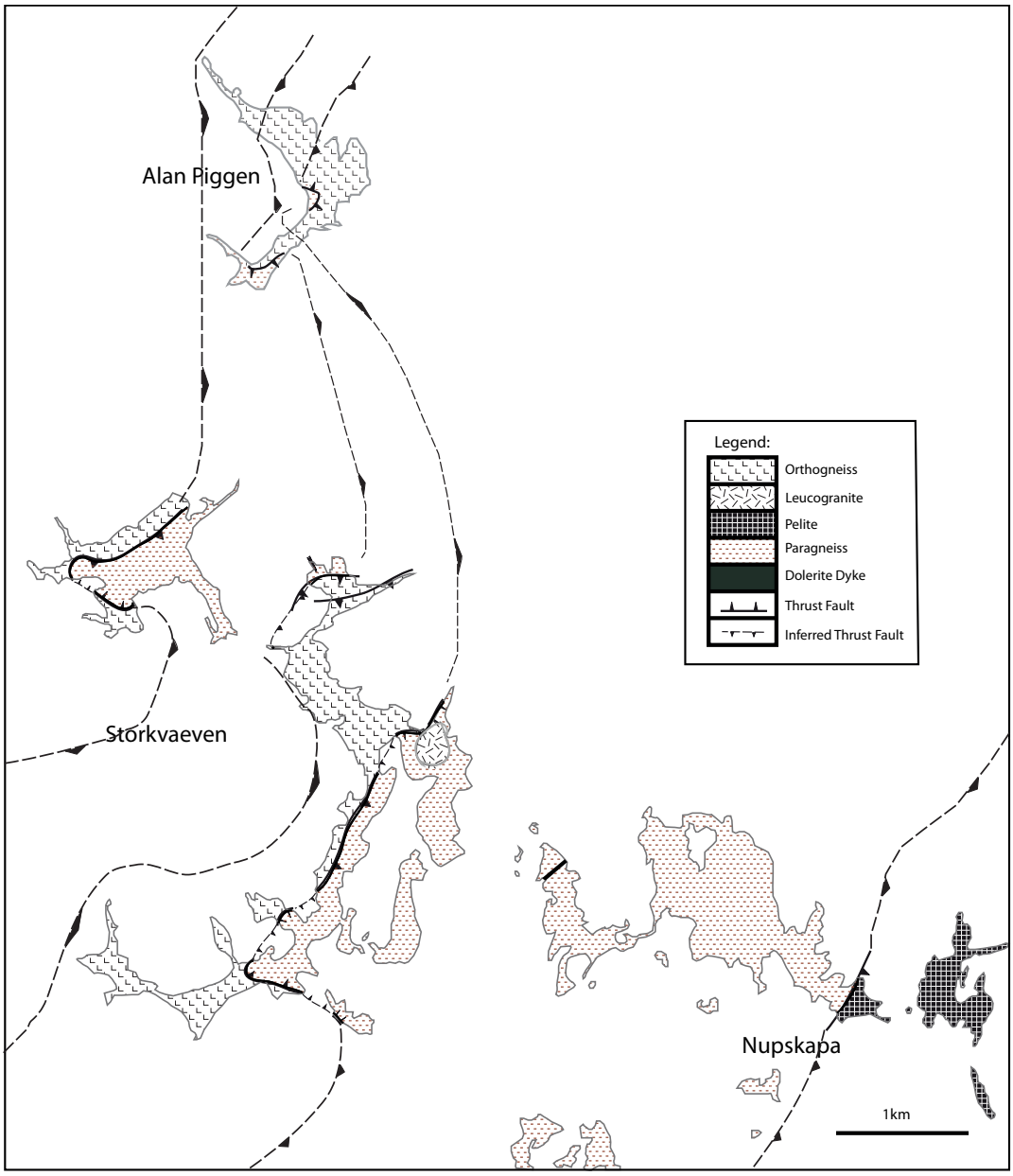

Figure 4.1: The major lithologies occurring in H.U. Sverdrupfjella are paragneisses, orthogneisses, a leucogranite, a pelite unit and a dolerite dyke.

sphene occurring locally. The orthogneisses commonly occur as augen gneisses because of the large (2-5cm) feldspar porphyroclasts present within them (Fig. 4.2). There is however a variation in grain size when in a close proximity to shear zones, the feldspar and quartz grains become finer (0.5-2cm). Some of the orthogneisses contain mafic lenses (50cm-200cm); these mafic lenses have a high proportion of hornblende (∼40%).

Figure 4.2: A photograph of an augen gneiss (orthogneiss) in H.U. Sverdrupfjella, with large porphyroclasts of feldspar and cross-cut by a leucogranite.

The biotite grains wrap around the larger porphyroclasts of microcline and quartz, defining a planar fabric. There is, however, a smaller average proportion of biotite in the orthogneisses (<15%) compared to the paragneisses (>20%). The dominant feldspar in the orthogneisses is microcline with smaller portions of albite (<10%) also appearing (Fig. 4.3 a). Microcline is commonly surrounded by fine grained albite which has quartz intergrowths within it (Fig. 4.3 e and f). This is known as a myrmekite texture. Grains of albite commonly look dirty in PPL as they are replaced by fine grained muscovite. The garnet grains are all very fractured, with a pseudomorph replacement texture of quartz and biotite (Fig. 4.3 c and d).

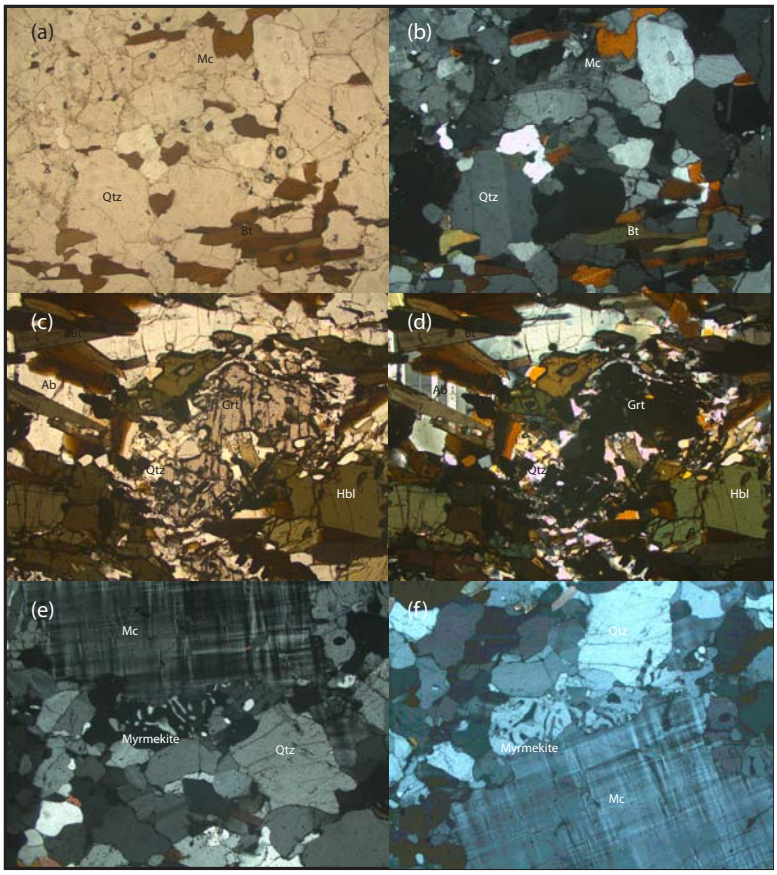

Figure 4.3: The general characteristics found in orthogneiss samples: (a) The general make up of a orthogneiss sample - quartz, biotite, microcline and albite (PPL). (b) XPL version of (a). (c) A garnet grain that has broken down into quartz and albite (PPL). (d) The XPL version of (c). (e) Myrmekite - small grains of albite that have inter-growths of quartz, myrmekite grains surround the microcline porphyroclast (XPL). (f) A microcline porphyroclast with sub-grains of albite and inter-growths of quartz (myrmekite). (Ab-albite, Bt-biotite, Grt-garnet, Hbl-hornblende, Mc-microcline, Qtz-quartz)

4.1.2 Paragneiss

The paragneiss is also uniform on a large scale but on a smaller scale it is rather heterogeneous between individual layers. The paragneiss alternates from quartz-rich layers to mica-rich layers and to hornblende-rich layers on a cm scale (Fig. 4.4). This heterogeneity is likely inherited from the parental sedimentary rocks and in places by retrogression. The top lithological unit of the duplex structure is a pelitic paragneiss, it is similar to the rest of the paragneisses but has a higher proportion of phyllosilicates.

Figure 4.4: A photograph of a strongly foliated paragneiss in H.U. Sverdrupfjella.

Although the paragneisses are fairly heterogeneous because of their layering, they mainly consist of quartz, microcline, albite, biotite, sphene and apatite in variable proportions (Fig. 4.5 a and b). In places there are grains of hornblende, garnet, epidote and rutile present. In the samples where layers alternate between hornblende-rich and quartz-rich layers, the biotite grains do not abide to this layering and occur throughout the rocks. Epidote is commonly altered to allanite along grain boundaries. The dominant feldspar in the paragneisses is albite with only minor amounts of microcline (<5%) appearing. These albite grains are very fractured, and fine grained quartz has grown in these fractures. On the other hand, like in the orthogneiss, albite has experienced retrogression and is replaced by fine grained muscovite (Fig. 4.5 c and d). The more retrogressed samples contain less hornblende which seems to have been replaced by epidote and biotite.

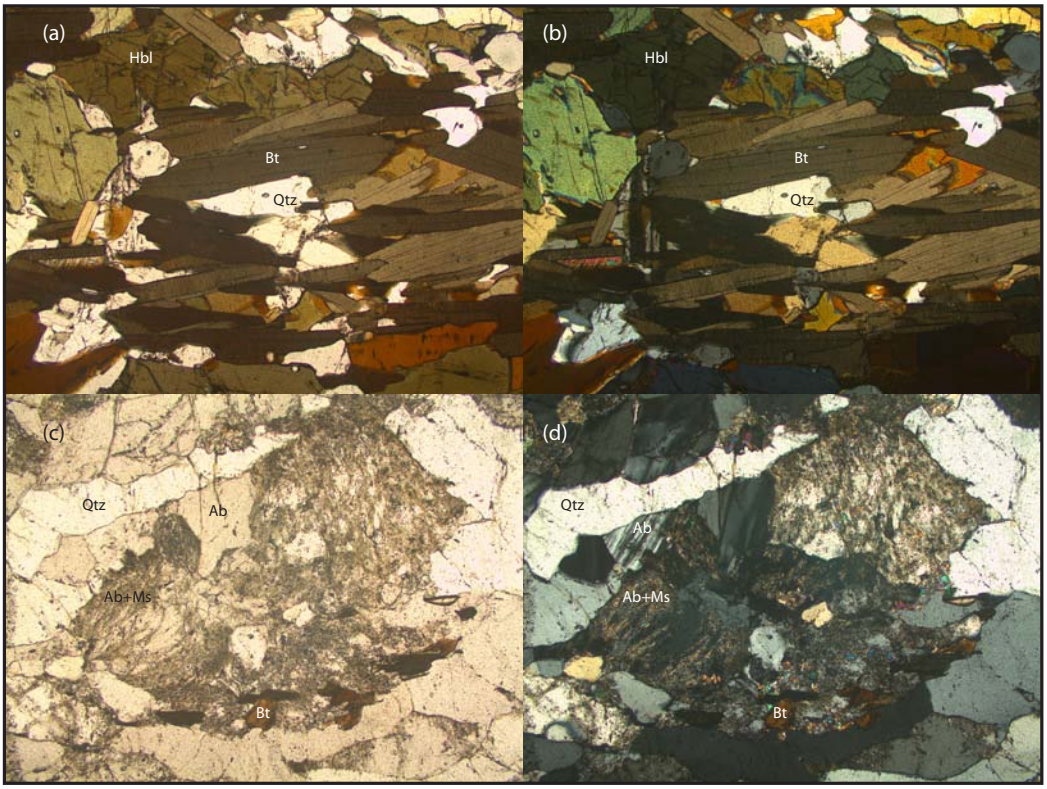

Figure 4.5: The general characteristics found in paragneiss samples: (a) The general make up of a paragneiss sample - quartz, biotite, microcline, albite and hornblende. (b) PPL version of (a). (c) Albite replaced with fine grained muscovite. (d) The PPL version of (c). (Ab-albite, Bt-biotite, Hbl-hornblende, Ms-muscovite inclusions, Qtz-quartz)

4.1.3 Leucogranites

Two generations of leucogranites are found at H.U. Sverdrupfjella. There is an early generation that is mostly foliation-parallel and deformed and another dyked generation that cross-cuts the fabrics. The leucogranites predominantly consist of coarse grained (0.5-4cm) quartz and feldspar.

Figure 4.6: A photograph of inter-layers of paragneiss (top) and orthogneiss (bottom), with a leucogranite cross-cutting them, H.U. Sverdrupfjella.

4.2 Neumayerskarvet

The lithology of Neumayerskarvet is more diverse than H.U. Sverdrupfjella with a number of different paragneisses and orthogneisses occurring in the region. Each individual paragneiss is also heterogeneous on a cm scale much the same as in H.U. Sverdrupfjella, resulting in quartz-rich, mica-rich and hornblende-rich layers (Fig. 4.10). Various phases of leucogranite are also found, cross-cutting the fabrics.

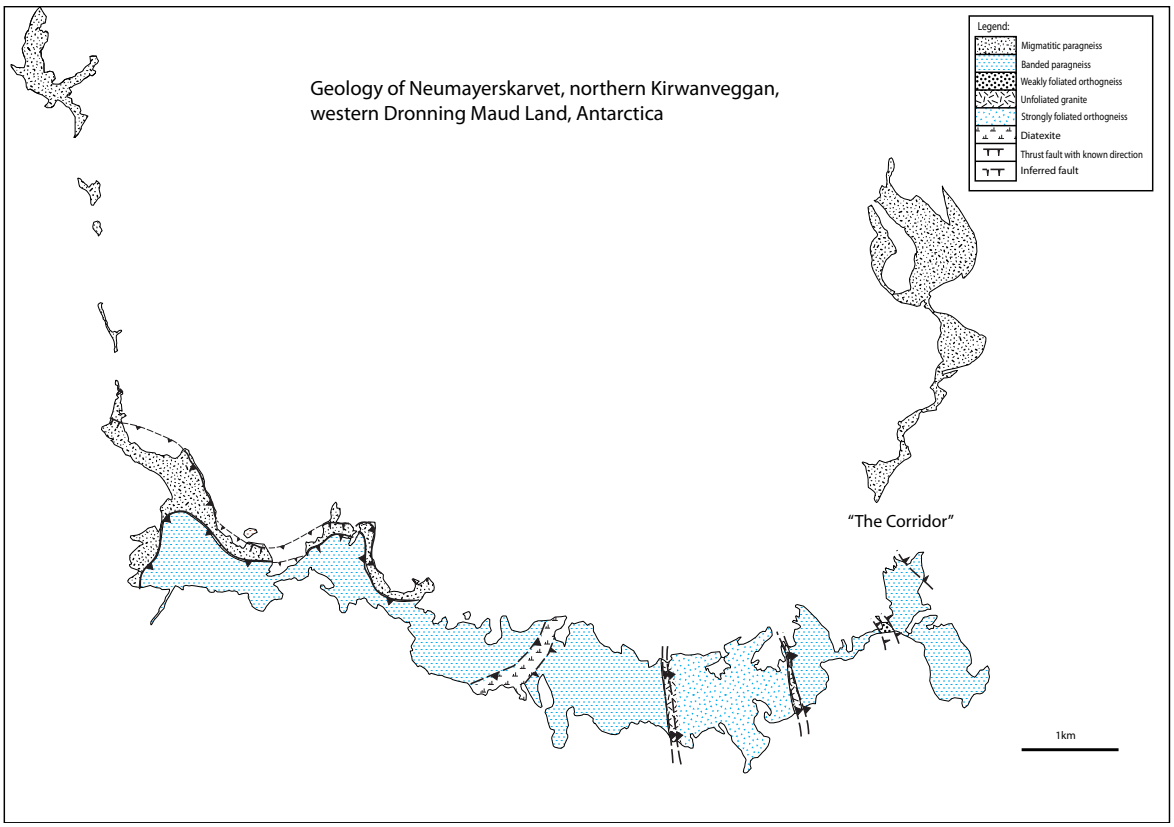

Figure 4.7: The major lithologies occurring in Neumayerkarvet are banded paragneiss, migmatitic paragneiss, strongly foliated orthogneiss, weakly foliated orthogneiss and a unfoliated granite.

4.2.1 Foliated Orthogneisses

Two foliated orthogneisses are found at Neumayerskarvet, a strongly foliated orthogneiss and a weakly foliated orthogneiss (Fig. 4.8). The two orthogneisses are made up of the same major minerals, quartz, K-feldspar (microcline), plagioclase (albite), apatite, hornblende and in places garnet (Fig. 4.9). Commonly the orthogneisses are augen gneisses because of the large porphyroclasts of feldspar.

The biotite and frequently hornblende form a planar fabric that wraps around the large feldspar porphyroclasts (Fig. 4.9 a and b). The biotite that defines the planar fabric is, however, not interconnected as in the paragneisses but instead scattered in that fabric's orientation. The orthogneisses commonly contain albite that looks dirty because it has been replaced by fine grained muscovite. In most samples that contain large microcline porphyroclasts, mymerkite textures are found along its edges (Fig. 4.12 b).

Figure 4.8: Photograph of a weakly foliated orthogneiss intrusion into a banded paragneiss at Neumayerskarvet.

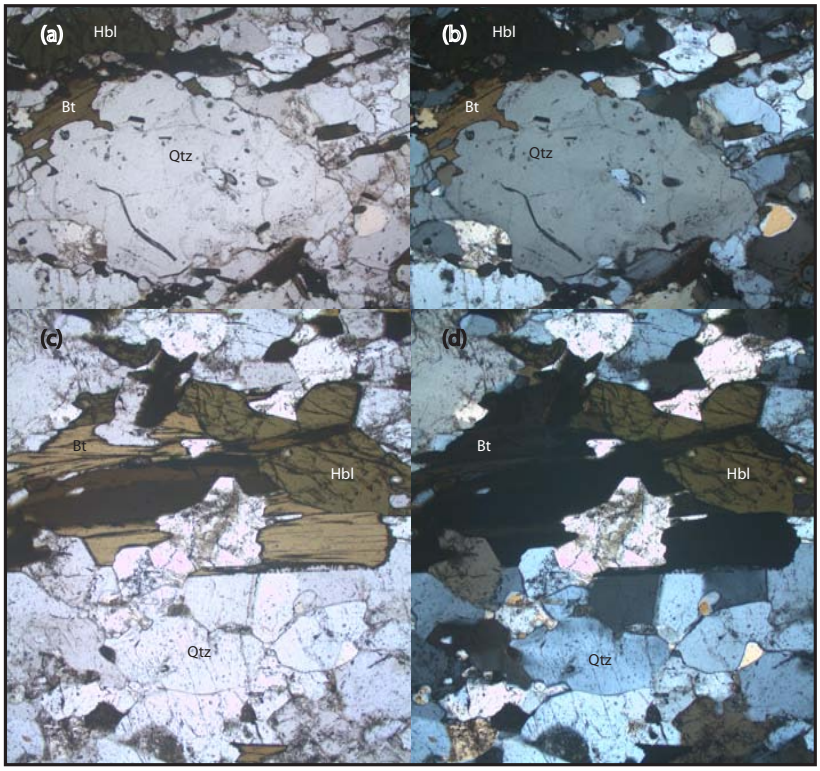

Figure 4.9: Thin sections taken from the foliated orthogneiss on either side, east and west, just alongside the unfoliated granite intrusion: (a) Sample taken from the western section of the foliated orthogneiss, this specific augen gneiss has biotite and hornblende forming a fabric that wraps around large quartz and feldspar porphyroclasts, this is viewed through PPL. (b) The XPL version of (a). (c) Sample taken from the eastern section of the strongly foliated orthogneiss, this does not contain porphyroclasts but hornblende and biotite still make up the planar fabric. It can also be seen that quartz is elongated parallel to the hornblende and biotite, forming a lineation. (d) Is the XPL version of (c). (Bt-biotite, Hbl-hornblende, Qtz-quartz)

4.2.2 Migmatitic Paragneiss and Banded Paragneiss

The first type of paragneiss is a migmatitic paragneiss containing $\sim 20\%$ leucosome (Fig. 4.11 a and b). The second type is a banded paragneiss, it is very similar to the migmatitic paragneiss but only contains $\sim 5\%$ migmatite (Fig. 4.11 c and d). A third type of paragneiss is located north of "The Corridor", Figure 5.13, it is a migmatitic paragneiss that contains mafic boudins but on a map scale it is included with the migmatitic paragneiss.

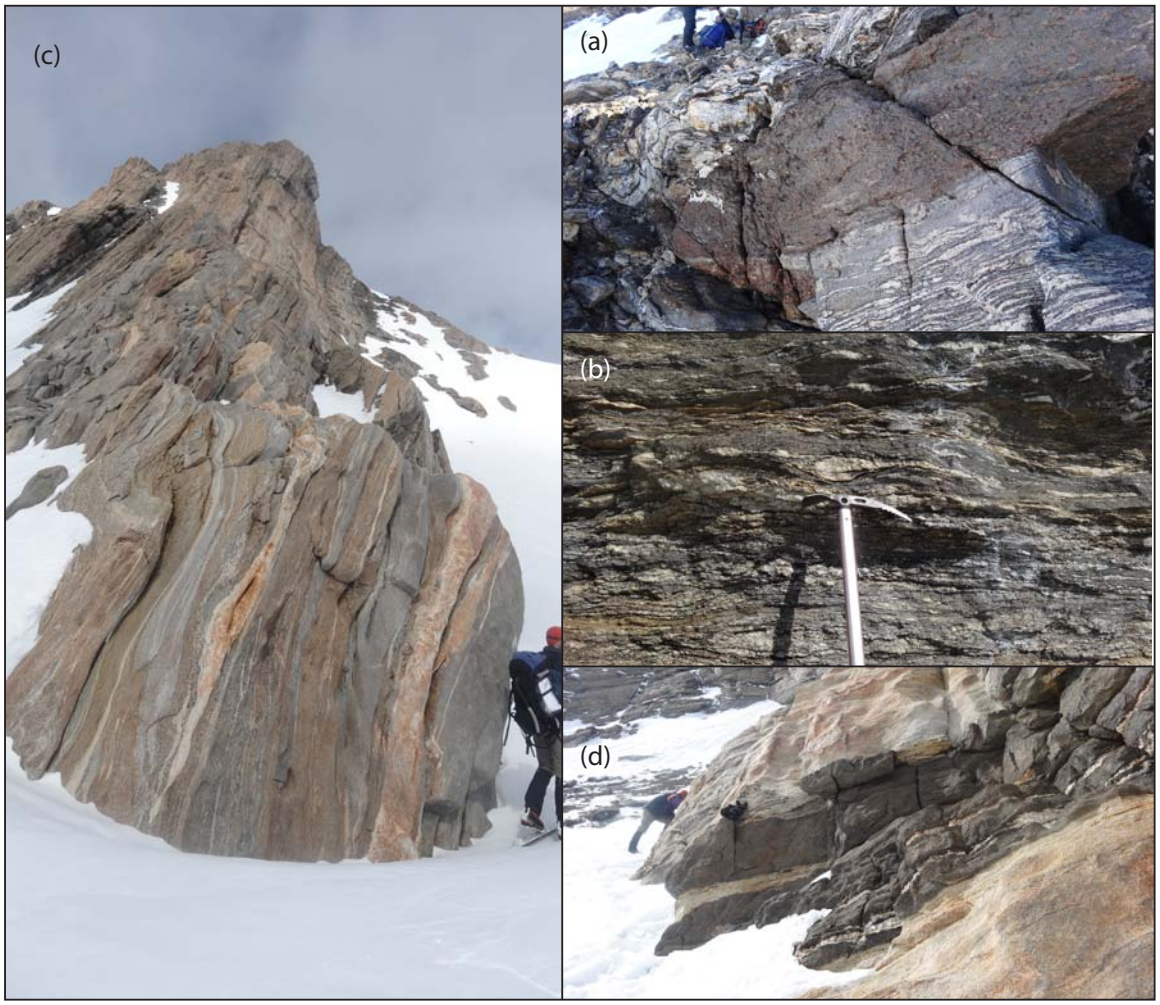

Figure 4.10: Photographs of the paragneisses that occur at Neumayerskarvet: (a) A garnet rich layer within the migmatite rich paragneiss. (b) Migmatite rich paragneiss showing large quartz porphyroclast. (c) Sub-vertical banded paragneiss situated south of "The Corridor". (d) Mafic layer within a leucosome occurring north of "The Corridor" in a migmatitic paragneiss layer containing mafic boudins.

The various types of paragneiss that occur at Neumayerskarvet are relatively similar in composition. The mineral composition of the three paragneisses is quartz, K-feldspar (microcline), plagioclase (albite), biotite, hornblende with the additions of apatite, epidote, garnet, gedrite, sillimanite and sphene. The various paragneisses only differ in the proportions of the minerals that they are composed of. The banded paragneiss has more biotite (>30%) and these layers of biotite are closer together than in the migmatitic paragneiss which contains less biotite ($\sim$ 20%) and more quartz and feldspar. The migmatitic paragneiss that contains mafic boudins is very similar to the migmatitic paragneiss, apart from the addition of mafic

boudins which consist of biotite, hornblende, epidote, quartz and albite (Fig. 4.12 e and f). A number of the paragneiss samples also contain mymerkite textures alongside the larger microcline porphyroclasts (Fig. 4.12 a and b).

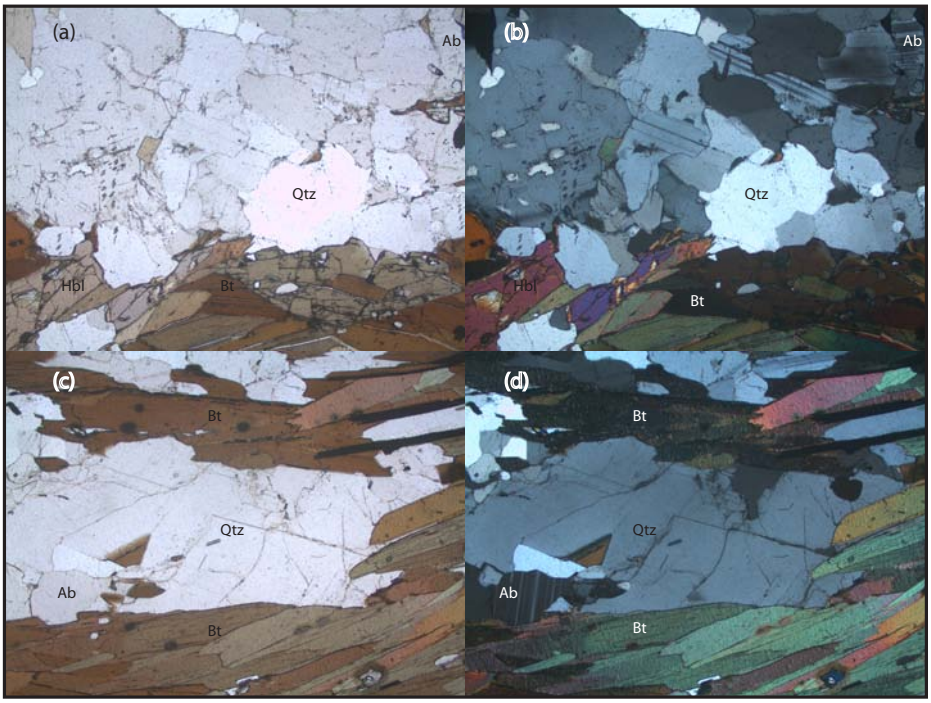

Figure 4.11: Photomicrographs of the two dominant paragneisses at Neumayerskarvet: (a) Migmatitic paragneiss viewed through plane polarized light. Biotite defining the foliation, with quartz and hornblende elongated parallel to the foliation. (b) The XPL version of (a). (c) Banded paragneiss viewed through plane polarized light. Biotite defining a foliation, quartz and albite forming thin layers between the biotite layers. (d) The XPL version of (c). (Ab-albite, Bt-biotite, Hbl-hornblende, Qtz-quartz)

4.2.3 Unfoliated Granite

A sub-vertical unfoliated granite is found in the contact between the strongly foliated orthogneiss and banded paragneiss, it has a pinkish colour and contains large K-feldspar porphyroclasts (2 to 5 cm in diameter). The granite is made up of the major minerals, quartz, K-feldspar (microcline), plagioclase (albite), apatite, hornblende and in places garnet and biotite. The unfoliated granite is approximately 20-50 meters thick and does not contain a magmatic or solid foliation.

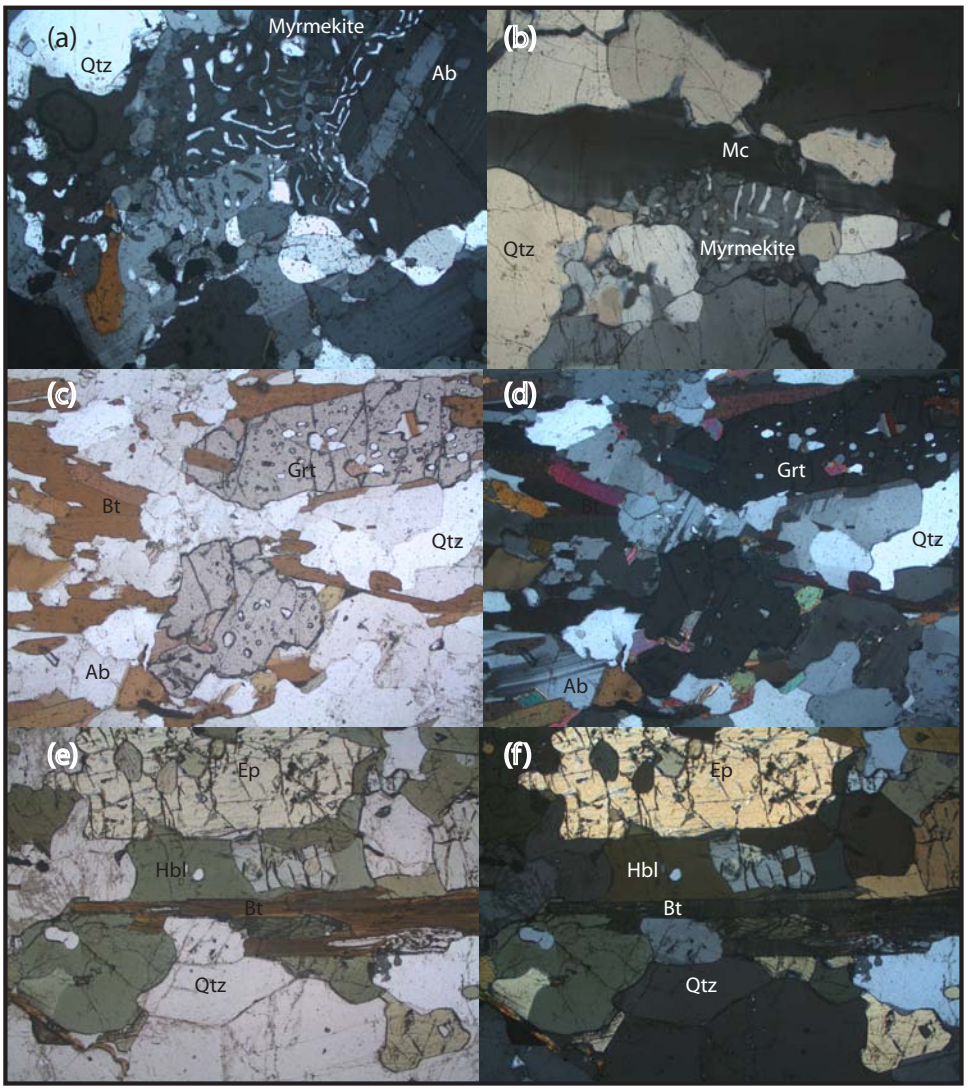

Figure 4.12: Thin sections showing the heterogeneity of layers found in paragneisses at Neumayerskarvet: (a) Myrmekite forming in albite grains, seen through cross polar lights. (b) Myrmekite situated next to a large microcline grain, seen through cross polarized light. (c) A garnet rich layer, garnets are elongated parallel to the biotite fabric, this layer corresponds to (Fig. 4.10 a). (d) The XPL version of (c). (e) A mafic boudin containing large amounts of epidote and hornblende, these minerals are elongated parallel to the biotite fabric. (f) XPL version of (e). (Ab-albite, Bt-biotite, Ep-epidote, Hbl-hornblende, Mc-microcline, Qtz-quartz)

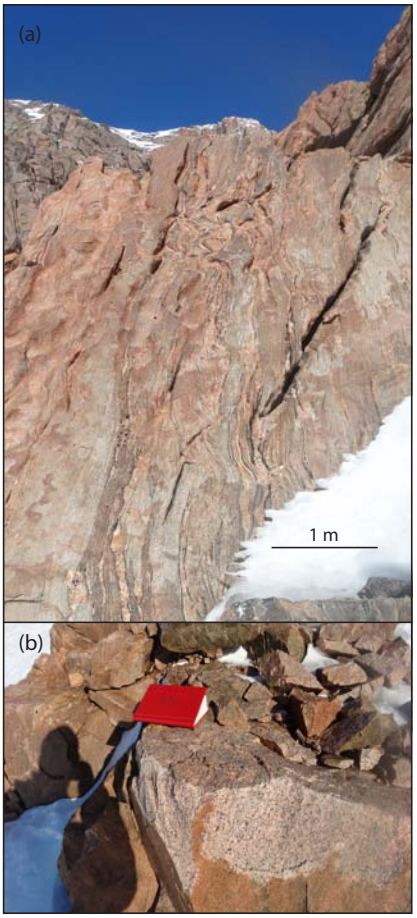

Figure 4.13: Photographs of the unfoliated granite that occurs at Neumayerskarvet: (a) Unfoliated granite intrusion in the contact between banded paragneiss on the left and foliated orthogneiss on the right. (b) Unfoliated pink granite.

4.3 Differences and Similarities

The lithology of the two study areas, H.U. Sverdrupfjella and Neumayerskarvet is broadly similar. On a large scale both areas consist predominantly of paragneisses and orthogneisses. The variation between them is that Neumayerskarvet has a greater variety of compositions of paragneisses and orthogneisses and contains more migmatite than H.U. Sverdrupfjella. H.U. Sverdrupfjella has more post-deformation leucogranites intruding it compared to Neumayerskarvet.

Mineralogically the two study areas are very similar, the paragneisses of both areas mainly consist of quartz, albite and biotite with minor hornblende, garnet, apatite, silliminite, sphene and gedrite. The paragneisses have a greater mineralogical variation than the orthogneisses but this is likely caused by the heterogeneity of the parental sedimentary rocks that they

originate from. The orthogneisses are very uniform, mainly consisting of quartz, microcline and some albite and biotite with minor apatite, sphene, garnet and hornblende. The additions of apatite, sphene, garnet and hornblende can also be the result of mafic lenses within the orthogneisses.

Chapter 5

Fabrics, Structures and Kinematics

This section presents all of the geometrical observations on maps, cross-sections and lower hemisphere, equal area stereographic plots. In both areas the foliation is commonly defined by biotite. The lineation is commonly defined by elongated quartz grains and in places feldspar, epidote, sillimanite and hornblende.

5.1 H.U. Sverdrupfjella

5.1.1 Shear Zones

The detailed geological map of H.U. Sverdrupfjella, Figure 5.1, shows that a number of shear zones occur in the region. Major shear zones, ∼10m wide, separate packages of orthogneiss and paragneiss but there are also minor shear zones, ∼5-10 m wide, within these packages. The major shear zones form within the contacts between the paragneiss and orthogneiss but tend to concentrate mainly in the paragneiss. Using three-point-problems the strike and dip of the shear zones can be calculated. The shear zones all dip shallowly to the SE. The lowermost major shear zone has an orientation of 037°/11° SE, the second major shear zone above that has an orientation of 019°/8° SE, the third major shear zone above that has an orientation of 024°/15° SE (Fig. 5.2). All of the major shear zones are roughly parallel and therefore the fourth and uppermost major shear zone is assumed to have a similar orientation. The cross section, Figure 5.3, shows how the shear zones are sub-horizontal and are stacked in a duplex structure, in which the rock types alternate with shear zones separating them. The most northern outcrop studied is called Alan Piggen, it contains two shear zones that separate orthogneiss from paragneiss above and below (Fig. 5.1).

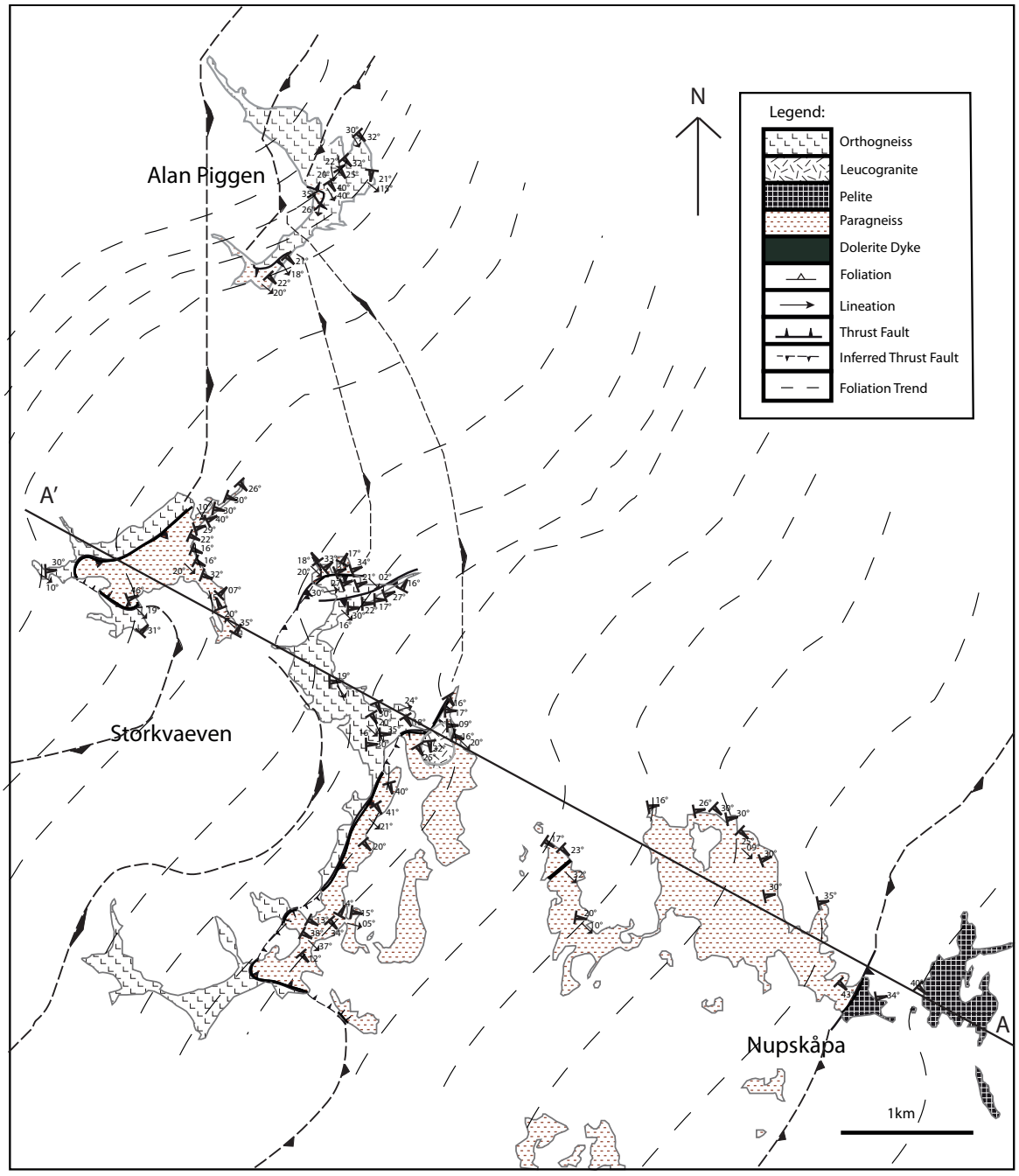

Figure 5.1: Detailed structural map of Nupskapa, H.U. Sverdrupfjella.

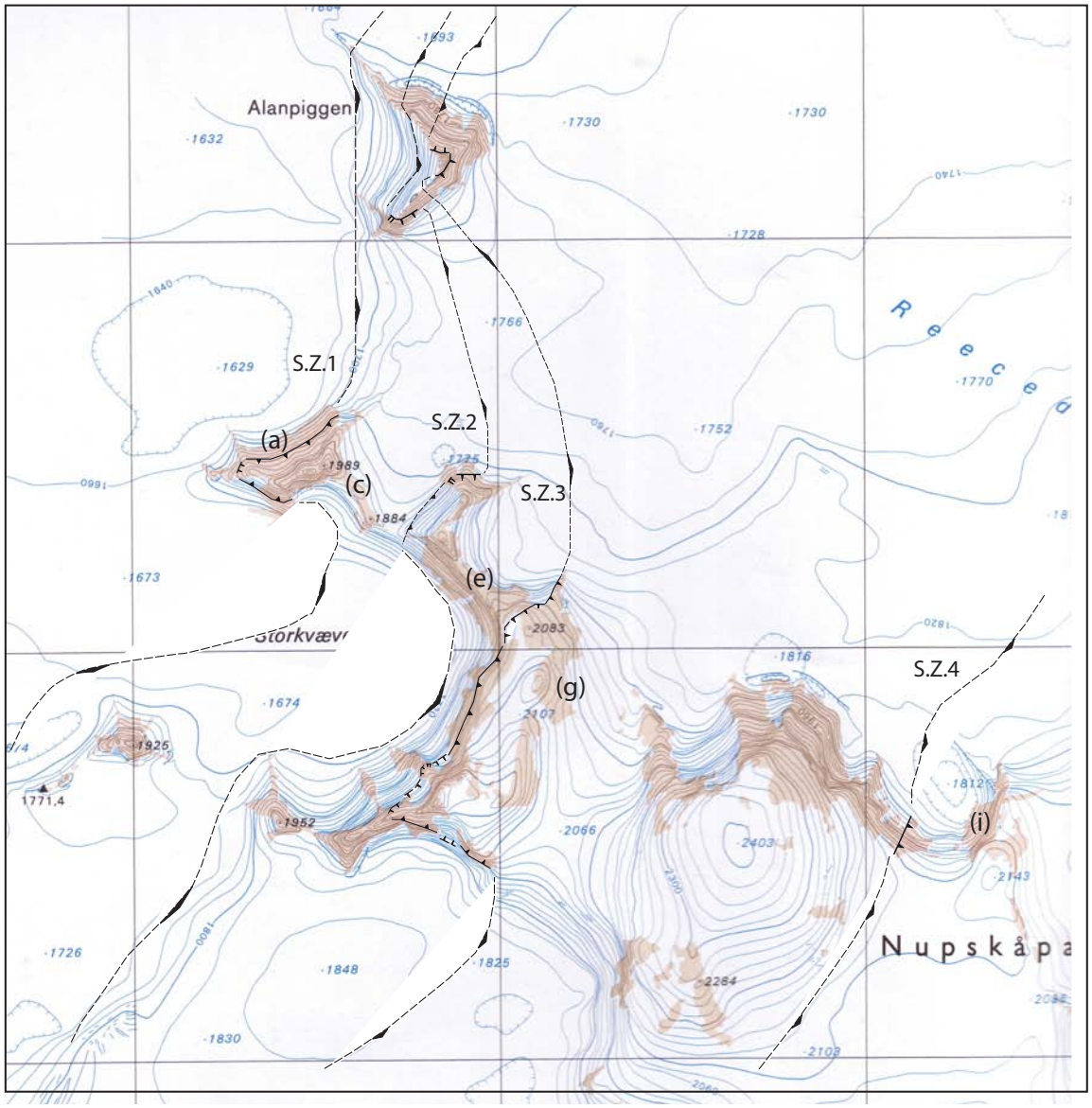

Figure 5.2: Topographic map of Nupskapa, H.U. Sverdrupfjella displaying the major shear zones. The variation in the topography causes the shear zones to have a meandering shape on the map. (S.Z.1= lowermost major shear zone, S.Z.2= the second major shear zone, S.Z.3= the third major shear zone and S.Z.4= the uppermost major shear zone, (a-i) relates to the rock types used later in the chapter.)

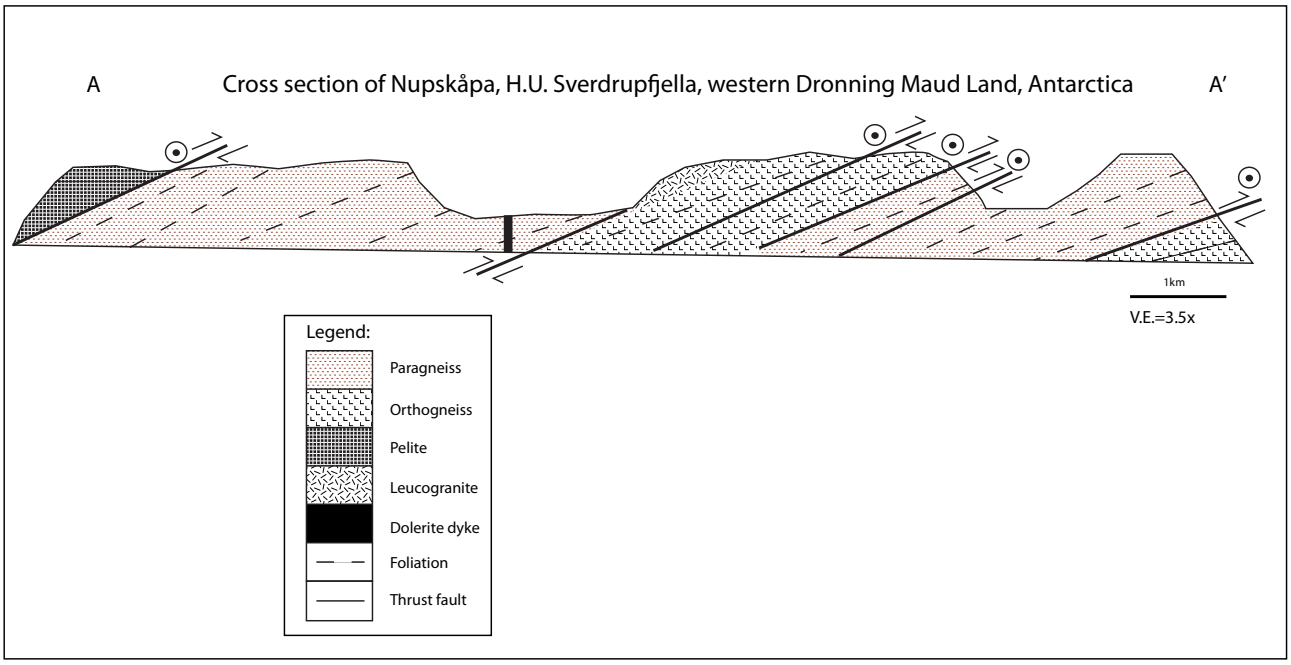

Figure 5.3: Cross section of Nupskapa, H.U. Sverdrupfjella, illustrating the sub-horizontal shear zones dipping SE, the dolerite dyke and the large leucogranite intrusion.

5.1.2 Foliations

The foliations all dip shallowly and in most places have an approximate strike of 020°, dippin SE but changes locally to a strike of 170°, dipping east.

Shear zones

Shear zone foliations are more uniform in orientation than the host rock foliations (Fig. 5.4) (Fig. 5.6). The shear zone foliations themselves change from a strike of 170°, dipping east in the structurally lowest shear zone (Fig. 5.4 b) to a strike of 050°, dipping SE in the uppermost shear zone (Fig. 5.4 h).

Host rock

The host rock foliations from (a) to (i) in Figure 5.2 are similar but they are very scattered and cover a wide range of dip directions. The dip angle is shallow throughout H.U. Sverdrupfjella, ranging from 31° in (a) through 20° in (e) and 40° in (i) (Fig. 5.4).

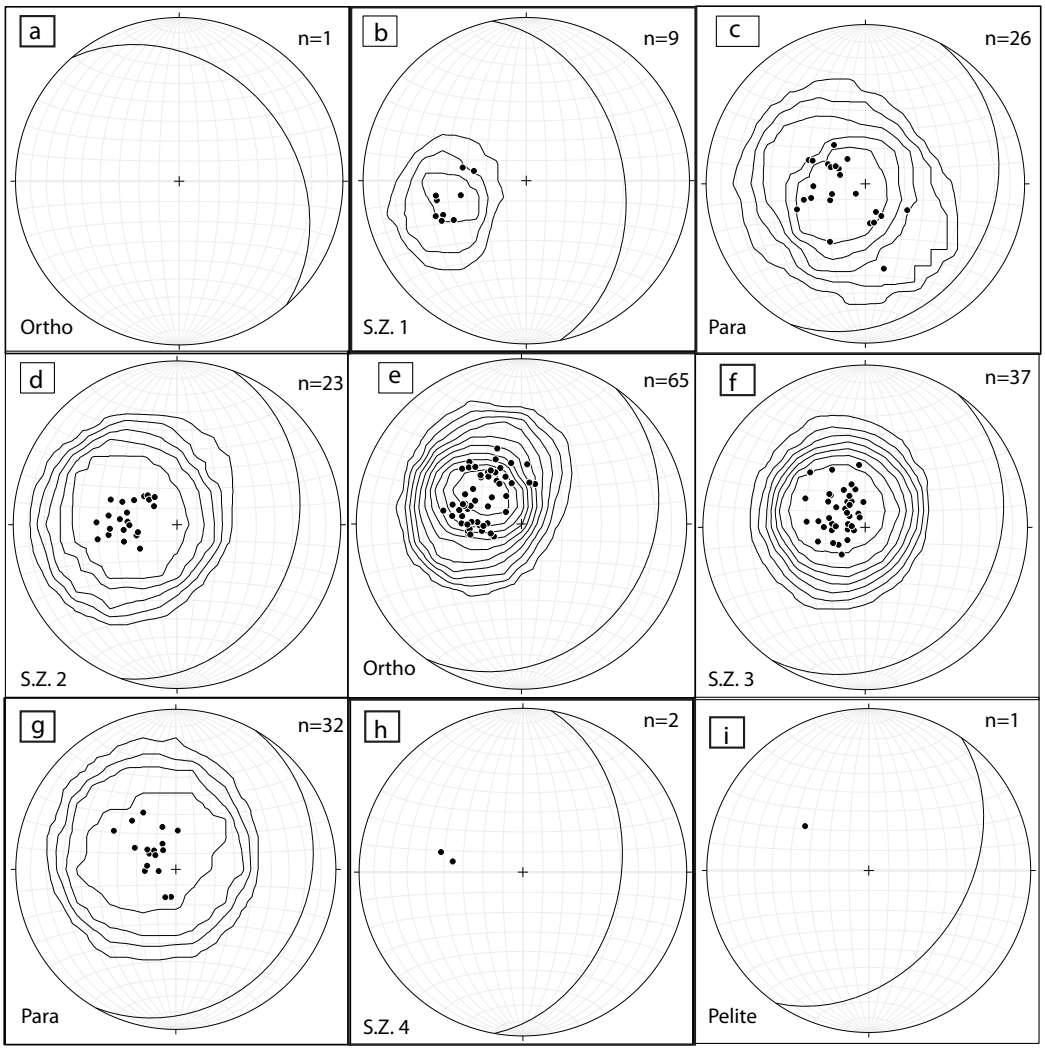

Figure 5.4: The foliations from H.U. Sverdrupfjella plotted in stereoplots as poles with an average plane for each. The stereoplots have also been contoured to show the density of populations. (S.Z. = shear zone, 1 is the bottom and 4 is the top) The stereoplots have been split up into different shear zones and host rock values from the lower most area to the upper most. (a) The foliations of the lowermost orthogneiss host rock. (b) The foliations of the lower shear zone between orthogneiss and paragneiss. (c) The foliations of the host rock paragneiss above the lower shear zone. (d) The foliations from the second shear zone between paragneiss and orthogneiss. (e) The host rock foliations of the orthogneiss above the second shear zone. (f) The foliations of the third shear zone between orthogneiss and paragneiss. (g) The foliations of the paragneiss above the third shear zone. (h) The foliations of the fourth and upper shear zone between paragneiss and pelites. (i) The foliations of the upper pelite zone.

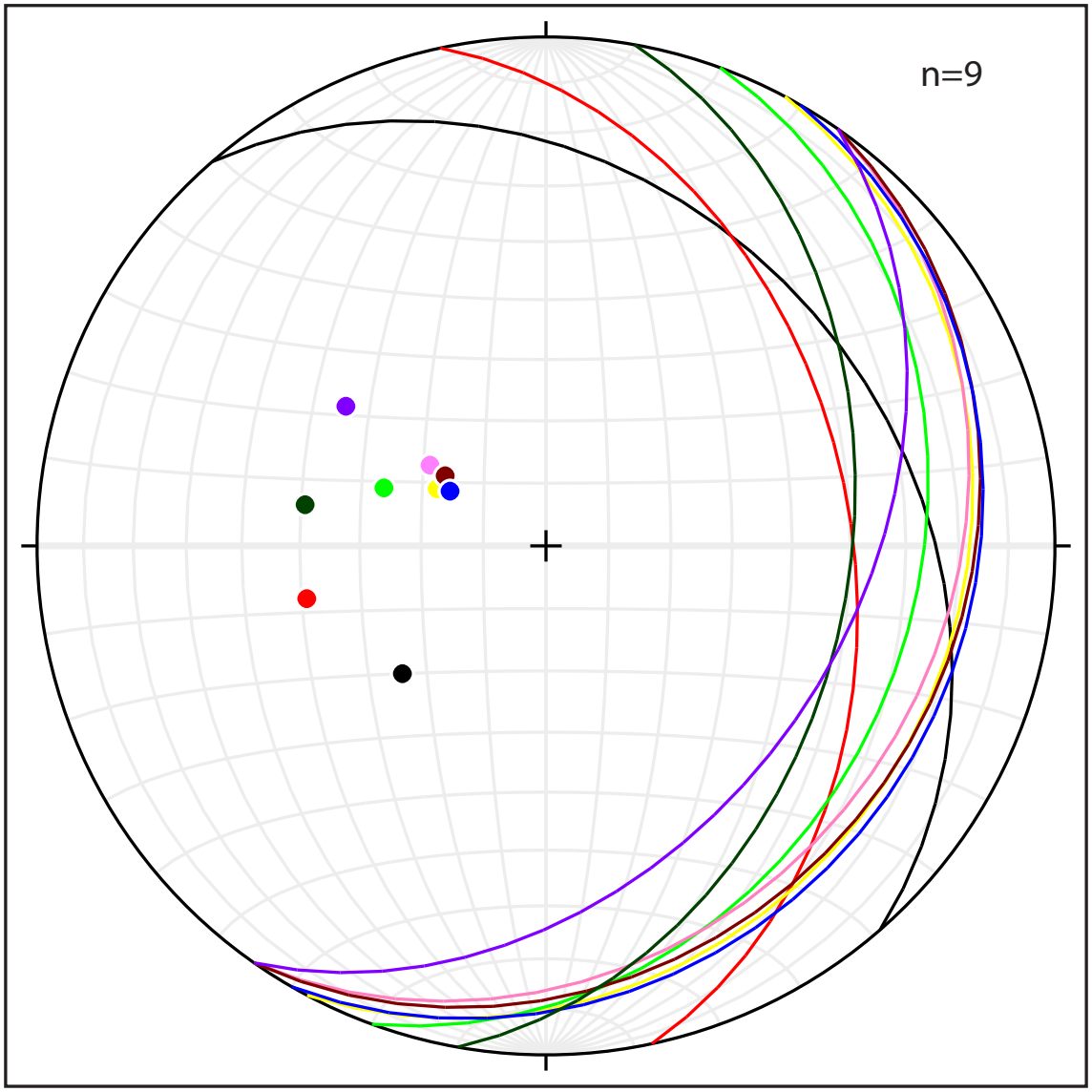

Figure 5.5: The average foliations from H.U. Sverdrupfjella plotted in stereoplots as poles with an average plane for each. The letters refer to Figures 5.4 and 5.2. Black = bottom orthogneiss (a), Red = lowermost shear zone between orthogneiss and paragneiss (shear zone 1) (b), Yellow = paragneiss above shear zone 1 (c), Green = shear zone 2 between paragneiss and orthogneiss (d), Pink = orthogneiss above shear zone 2 (e), Maroon = shear zone 3 between orthogneiss and paragneiss (f), Blue = paragneiss above shear zone 3 (g), Dark green = uppermost shear zone (shear zone 4) between paragneiss and pelite (h), Purple = pelite above shear zone 4, the uppermost unit in the area (i).

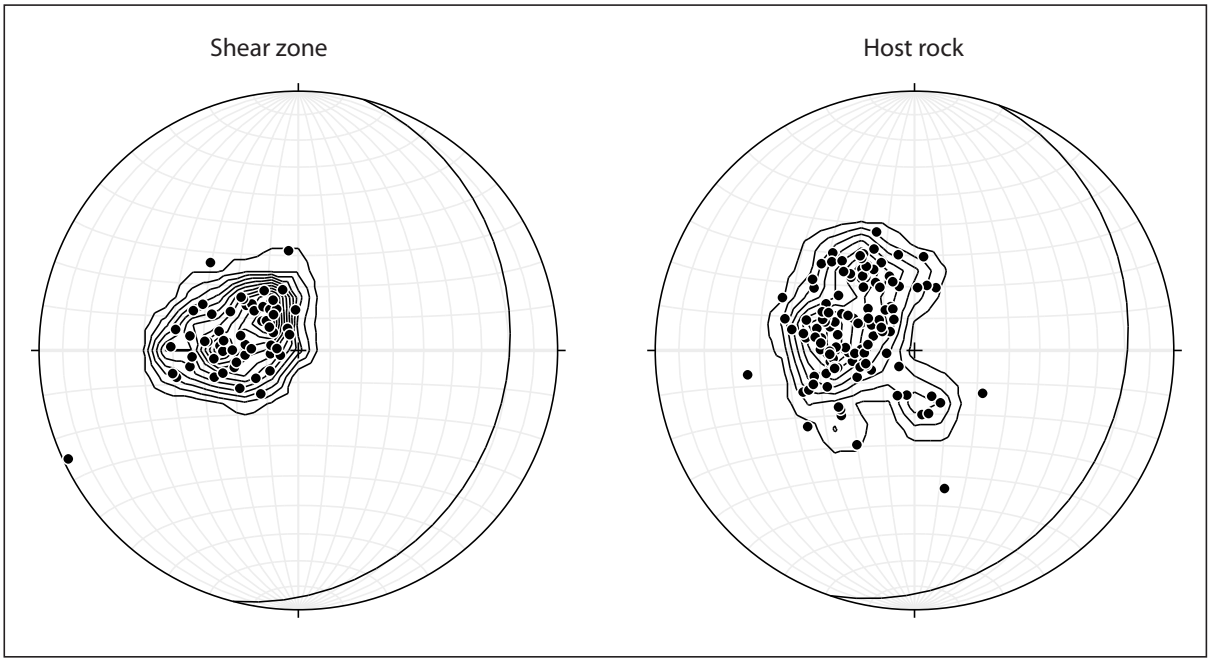

Figure 5.6: The average foliations within shear zones and outside shear zones (host rock) from H.U. Sverdrupfjella plotted in stereoplots as poles with an average plane for each. The stereoplots have also been contoured to show the density of populations.

Alan Piggen

A section up Alan Piggen, the northern-most outcrop in the study area, was studied in order to determine if there was any variation in the foliation from one shear zone to the next. Figure 5.7 illustrates the variation of the foliation from the lower shear zone through a package of orthogneiss to the upper shear zone of Alan Piggen. Surrounding the lower shear zone the foliations have an orientation of $\sim 170°/32°$ E and ascending towards the top shear zone the foliations orientation becomes closer to $050°/34°$ SE. There is a significant variation in dip direction but the shallow dip angle is constant throughout the section up Alan Piggen. The angle between the strike of the foliation planes of the lowest to the summit of Alan Piggen is 24°, the dip direction changes systematically from east at the base to SE at the summit of Alan Piggen (Fig. 5.7).

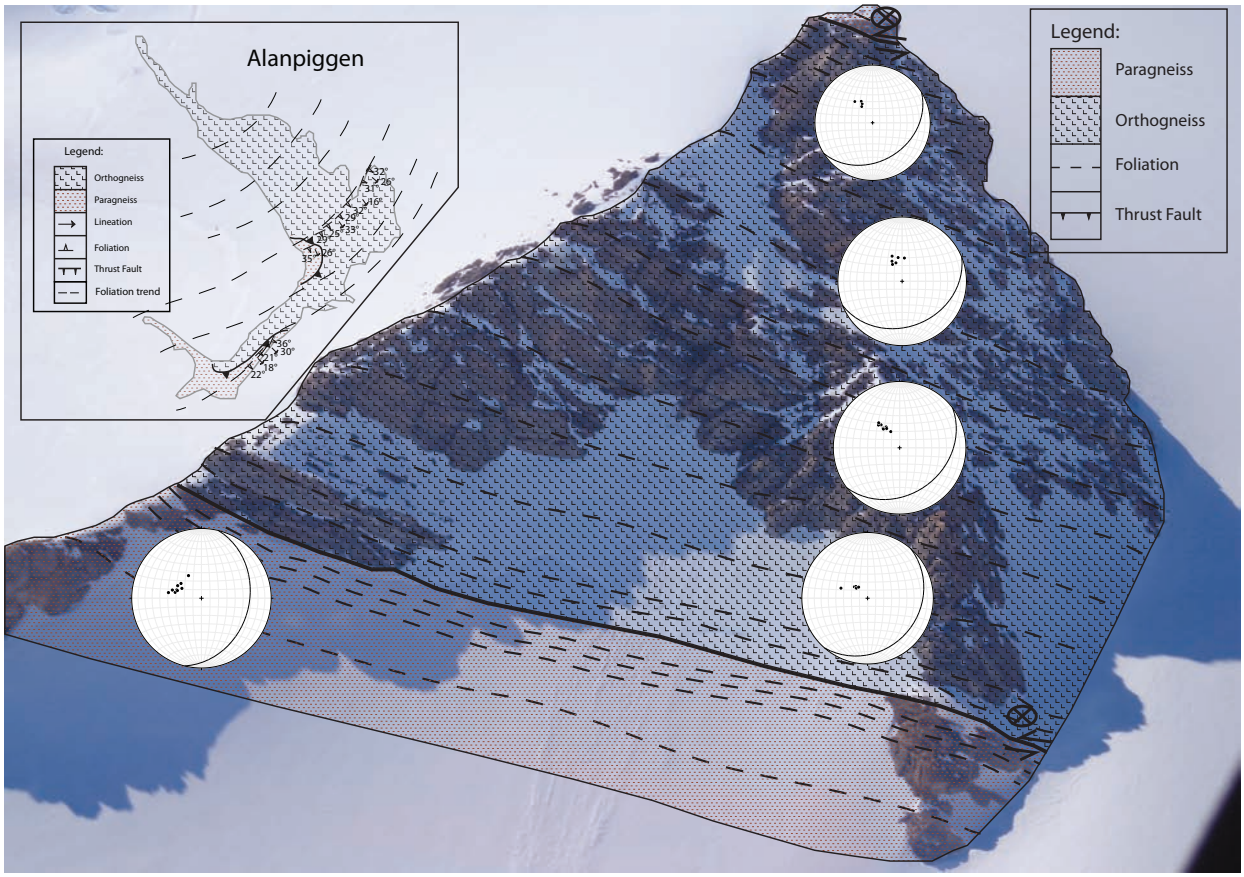

Figure 5.7: Detailed photograph of Alan Piggen showing rock types, shear zones and variations in foliations on stereoplots ascending towards the top shear zone. The photograph was taken looking NW. The foliation changes from shallowly dipping to the east at the bottom to shallowly dipping to the SE at the top of Alan Piggen. In the top left corner is a detailed structural map of Alan Piggen.

5.1.3 Lineations

There are three distinct groupings of lineations, the first has a trend of ∼080°, the second ∼140° and the third ∼320° but they all plunge shallowly. A 140° trending lineation is the strongest and most common but a 080° trending lineation was found locally but with the dominant 140° also present in the same rock (Fig. 5.9). The lineation is mostly formed by elongate quartz grains and in places sillimanite, epidote, feldspar and hornblende. Shear zone lineations are more uniform in orientation than the host rock lineations (Fig. 5.8). The 140° and 320° trending lineations can be combined because it just takes a variation of <40° in the dip angle and then it's trend is in the opposite direction. A 140° and 320° trending lineation have a similar orientation of elongation. Therefore there are two groups of lineations at H.U. Sverdrupfjella, a 140°/320° trending lineation and a 080° trending lineation.

Shear zones

Within the shear zones throughout H.U. Sverdrupfjella only the 140°/320° trending lineation is present.

Host rock

The 140°/320° trending lineation is found alongside the weaker 080° trending lineation throughout the host rocks of H.U. Sverdrupfjella.

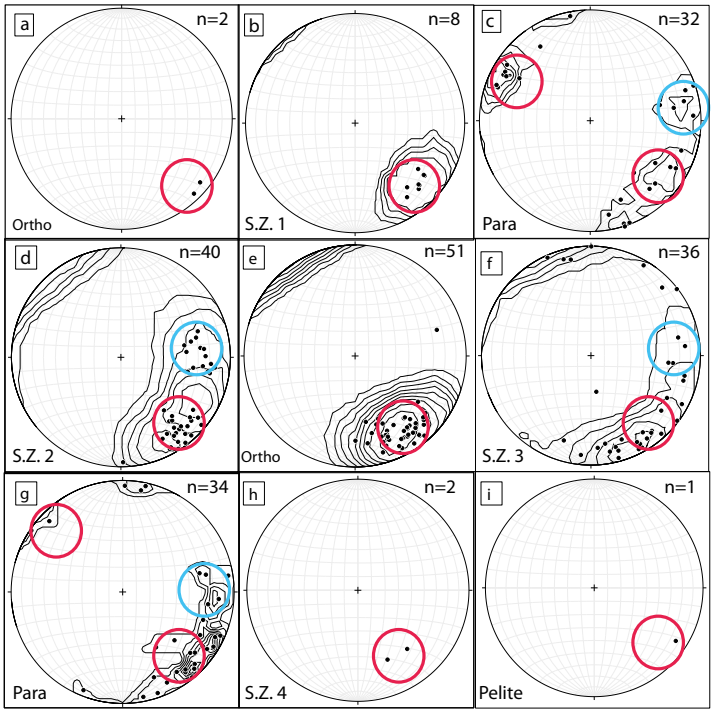

Figure 5.8: The lineation from H.U. Sverdrupfjella plotted in lower hemisphere, equal area plots. The stereoplots have been contoured. The stereoplots have been split up into different shear zones and host rock values from the lower most area to the upper most. (S.Z. = shear zones, S.Z.1 is the lowermost to S.Z.4 which is the uppermost shear zone) (a) The lineations of the lowermost orthogneiss host rock. (b) The lineations of the lower shear zone between orthogneiss and paragneiss. (c) The lineations of the host rock paragneiss above the lower shear zone. (d) The lineations from the second shear zone between paragneiss and orthogneiss. (e) The host rock lineations of the orthogneiss above the second shear zone. (f) The lineations of the third shear zone between orthogneiss and paragneiss. (g) The lineations of the paragneiss above the third shear zone. (h) The lineations of the fourth and upper shear zone between paragneiss and pelites. (i) The lineations of the upper pelite zone. The red circles highlight an area of lineations with a trend in the region of 140° or 320° and the blue circles highlight an area of lineations with a trend in the region of 080°.

Figure 5.9: Photograph showing the two lineations that are found at H.U. Sverdrupfjella.

5.1.4 Folds

Folds of varying scales appear throughout H.U. Sverdrupfjella, Figure 5.10 displays areas that have experienced intense folding. The folds range from tight to open and are inclined to the NW from sub-vertical to recumbent. The wavelength of the folds varies from a cm scale to tens of meters scale. The plunges of the fold hinges are all very shallow, but the trend varies significantly from NW through S and to NE, covering most azimuths (Fig. 5.11).

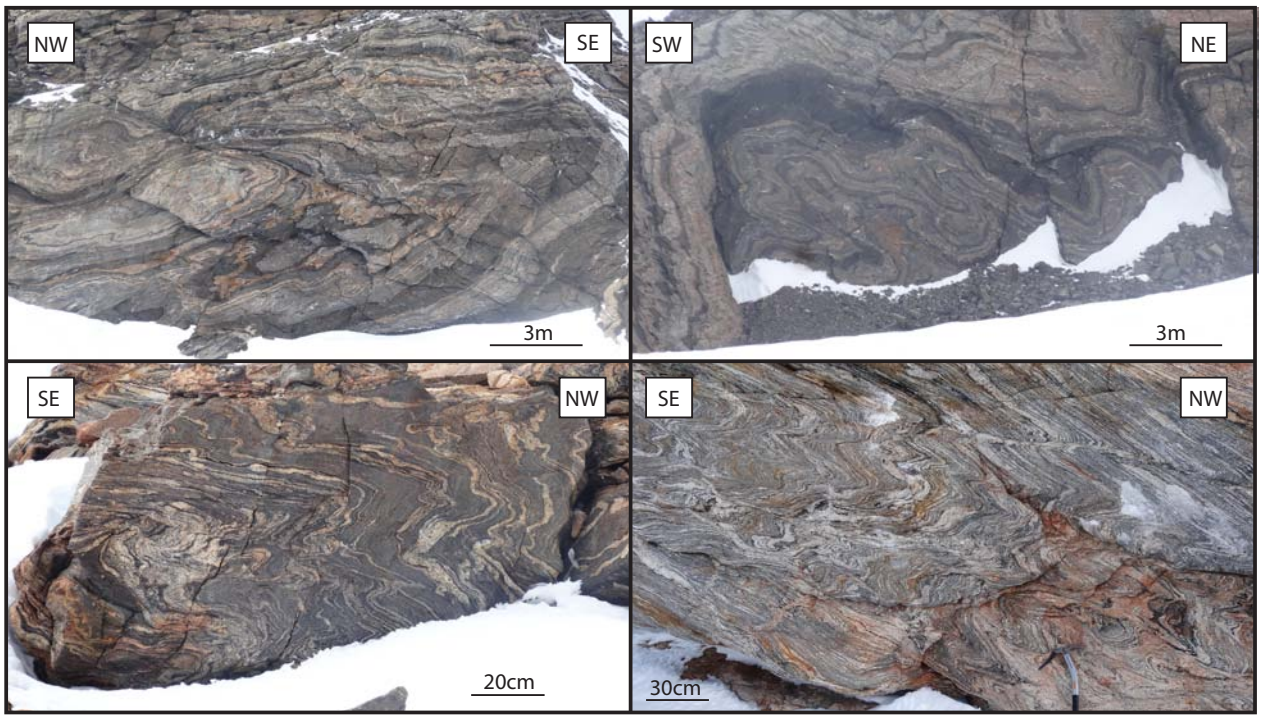

Figure 5.10: Photographs of folds observed in the two study areas, H.U. Sverdrupfjella and Neumayerskarvet.

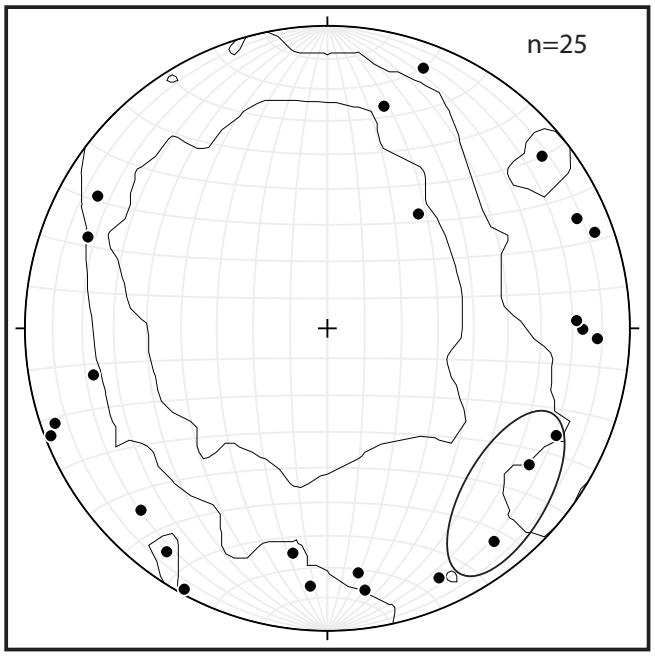

Figure 5.11: Lower hemisphere, equal area plots illustrating the trend and plunge of all the fold hinges measured at H.U. Sverdrupfjella. The circled area is parallel to the 140° trending lineation, shear direction, in the study area.

5.1.5 Kinematic Indicators

Folds throughout the shear zones of H.U. Sverdrupfjella are inclined to the NW, indicating a transport direction of top-to-the-NW. Asymmetric lozenges and mantled porphyroclasts also consistently indicate a top-to-the-NW transport direction (Fig. 5.12).

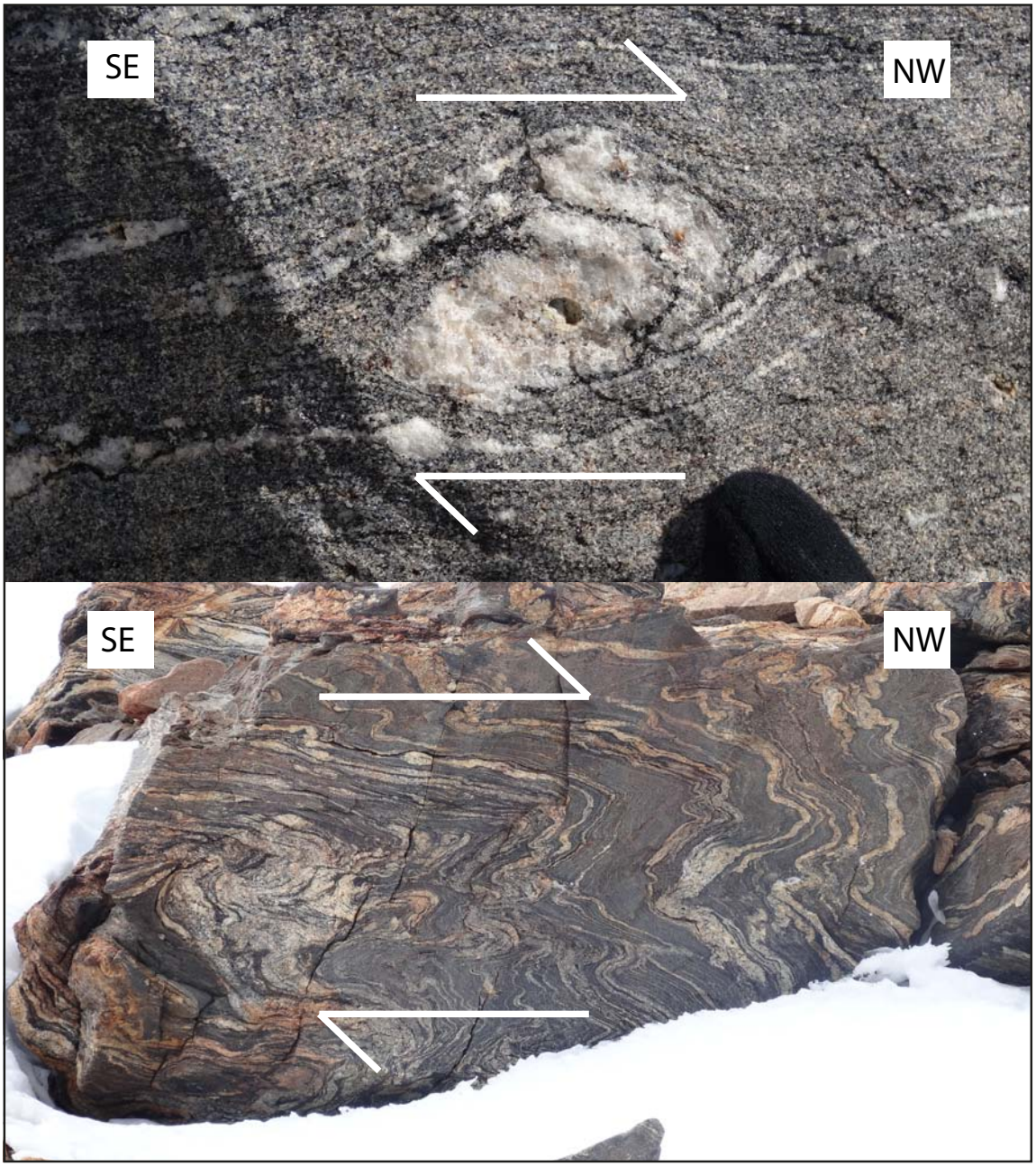

Figure 5.12: Examples of δ-clast porphyroclasts and asymmetric folds used to determine the sense of shear in H.U. Sverdrupfjella as top-to-the-NW.

5.2 Neumayerskarvet

5.2.1 Shear Zones

Neumayerskarvet contains two map-scale sub-horizontal shear zones and five sub-vertical strike-slip shear zones (Fig. 5.13). The one sub-horizontal shear zone is major as it separates the migmatitic paragneiss from the banded paragneiss, the other sub-horizontal shear zone is minor, situated within the migmatitic paragneiss. The shear zones are all approximately 10-20 meters wide. Apart from the most easterly sub-vertical strike-slip shear zone which is situated within the banded paragneiss, the rest separate orthogneisses from paragneisses. Figure 5.13 and Figure 5.14 show that Neumayerskarvet can be separated into a western region characterized by sub-horizontal fabrics and an eastern region of sub-vertical fabrics. The western region is dominated by paragneisses and the eastern region is made up of a combination of paragneisses and orthogneisses. The lineations are similar throughout both the eastern and western regions.

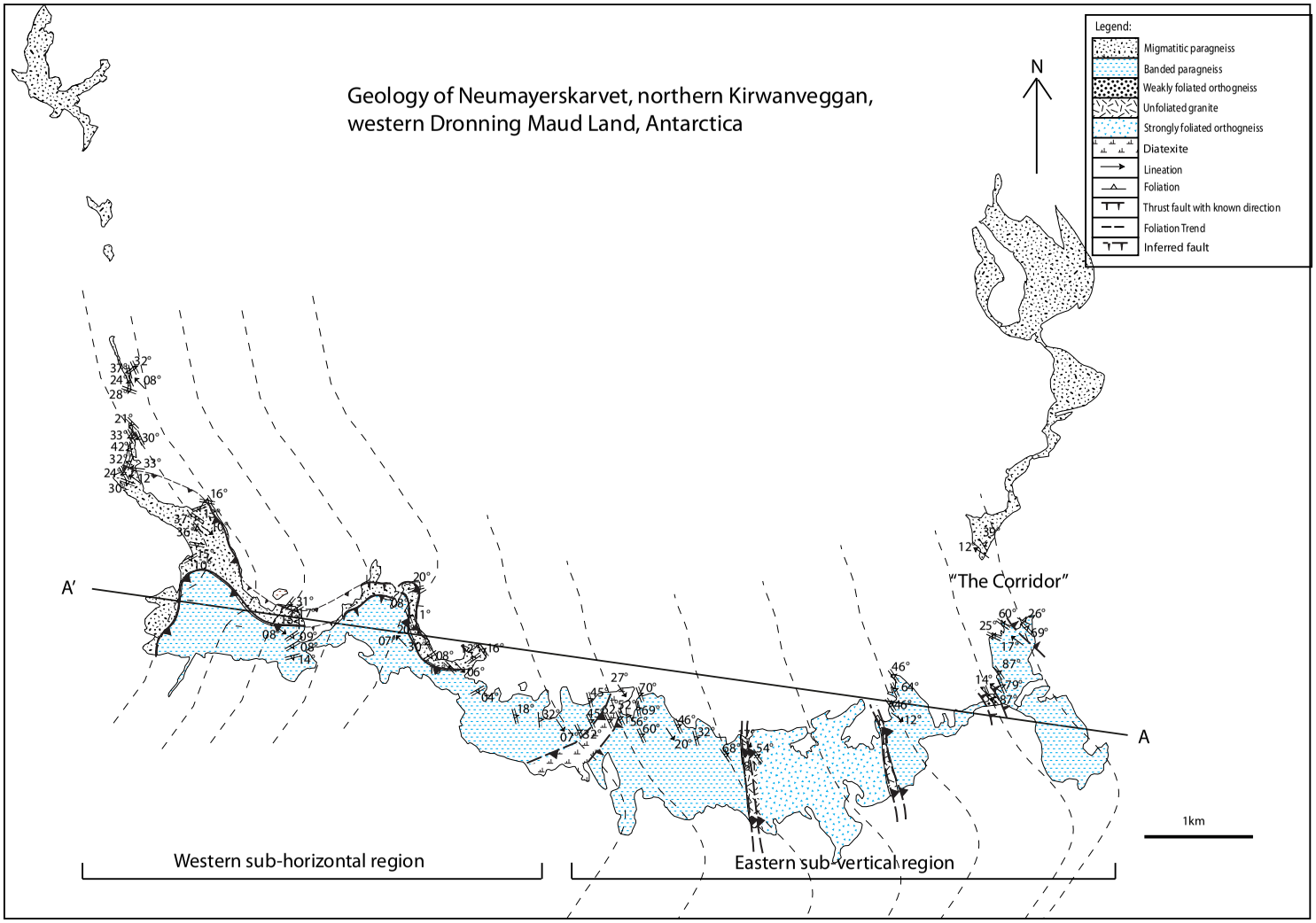

Figure 5.13: Detailed structural map of Neumayerskarvet.

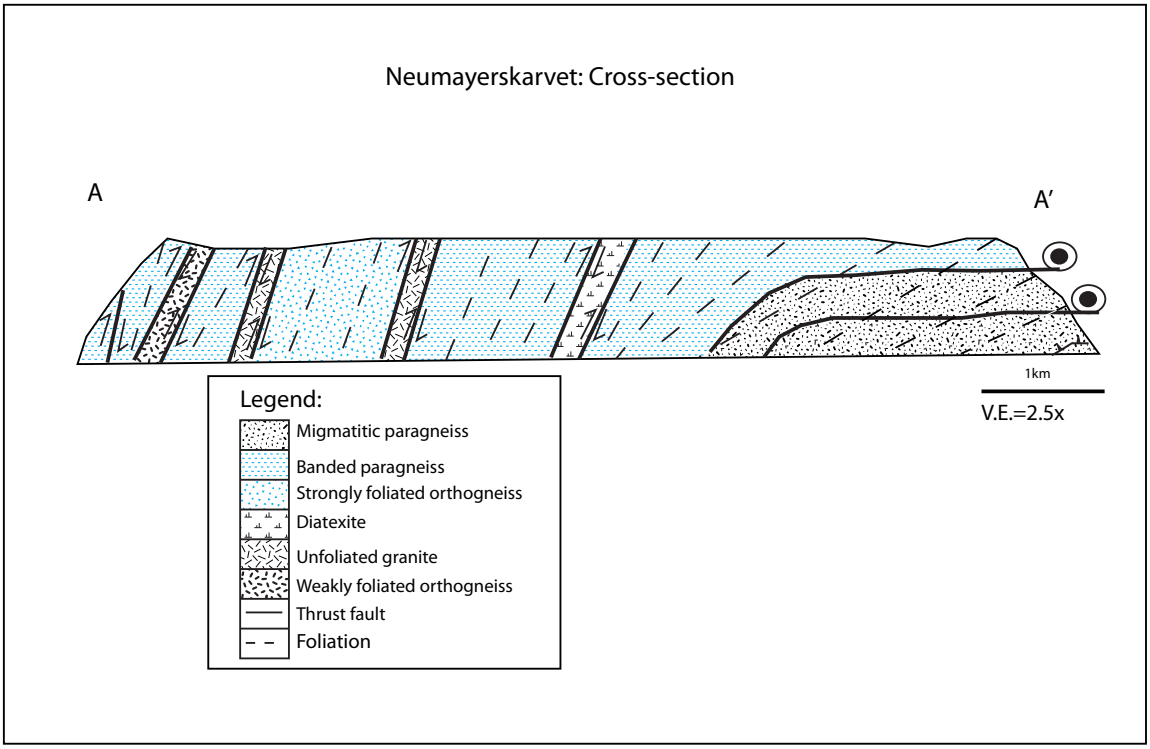

Figure 5.14: Cross section of Neumayerskarvet, illustrating the two sub-horizontal shear zones and the five sub-vertical shear zones. They all show a transport direction of top-to-the-NW. The unfoliated granite intrusion can be seen occurring within the two shear zones in the middle of the cross-section.

5.2.2 Foliations

The foliations of the western region of Neumayerskarvet are plotted in Figure 5.15 and the foliations of the eastern region of Neumayerskarvet in Figure 5.16.

Shear zones

In the western region the foliations of both the sub-horizontal shear zones are very similar, the lower shear zone dips shallowly NW and the upper shear zone dips shallowly SE. The dip angle of the foliation in the western region of Neumayerskarvet is always very shallow, $<30°$. In the eastern region of Neumayerskarvet the shear zones have a very steep foliation compared to the host rock, the contact of the unfoliated granite intrusions dips steeply NE but not as steeply as the shear zones. The foliations of the five sub-vertical shear zones are all very similar, dipping NE to E with a dip angle between 50° and 87°. The shear zones readings are again more tightly clustered than the host rock for both domains.

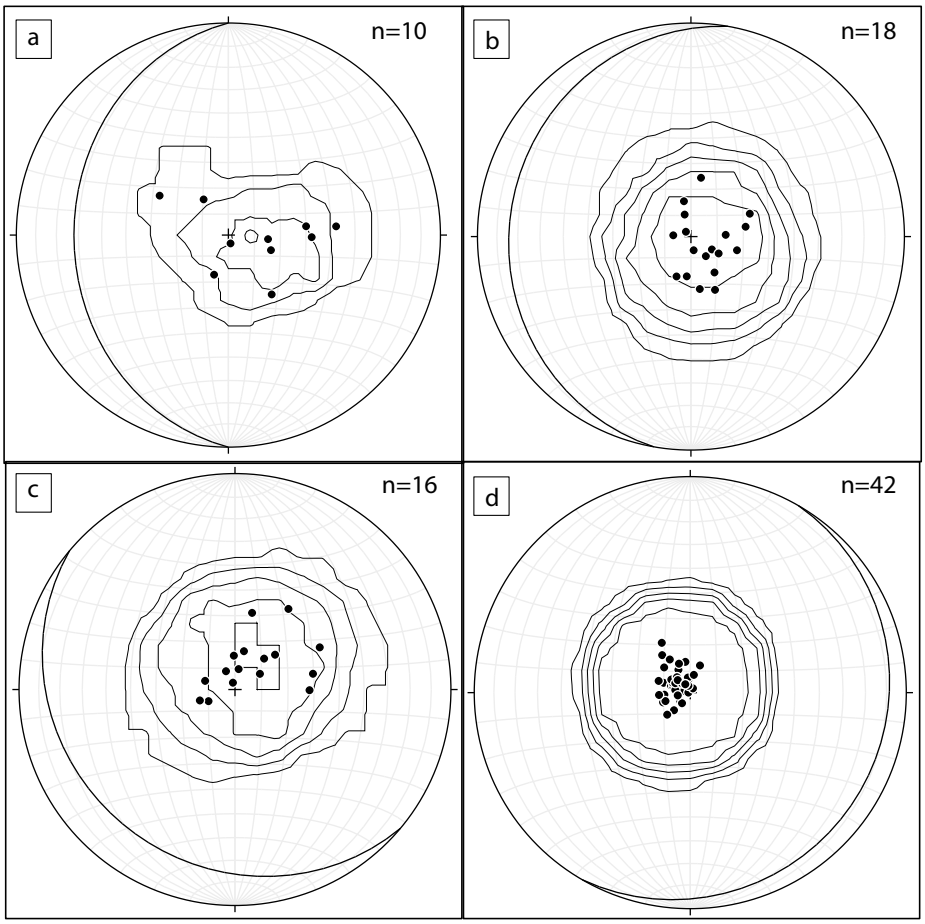

Figure 5.15: The foliations from the sub-horizontal shear zones of Neumayerskarvet plotted in lower hemisphere, equal area plots as poles with an average plane for each. The stereoplots have also been contoured to show the density of populations. (a) Host rock foliation values below the lower shear zone. (b) Lower shear zone foliations. (c) Host rock foliation values between the lower and upper shear zone. (d) Upper shear zone foliations.

Host rock

The host rock values of the western region are more scattered, dipping shallowly between SW and W. The dip angle of the foliation in the western region of Neumayerskarvet is always very shallow, <30°. In the eastern region the foliation within the host rock dips steeply to the NE but not as steeply as the shear zones.

Figure 5.17 compares shear zone foliations to host rock foliations for the western and eastern domains.

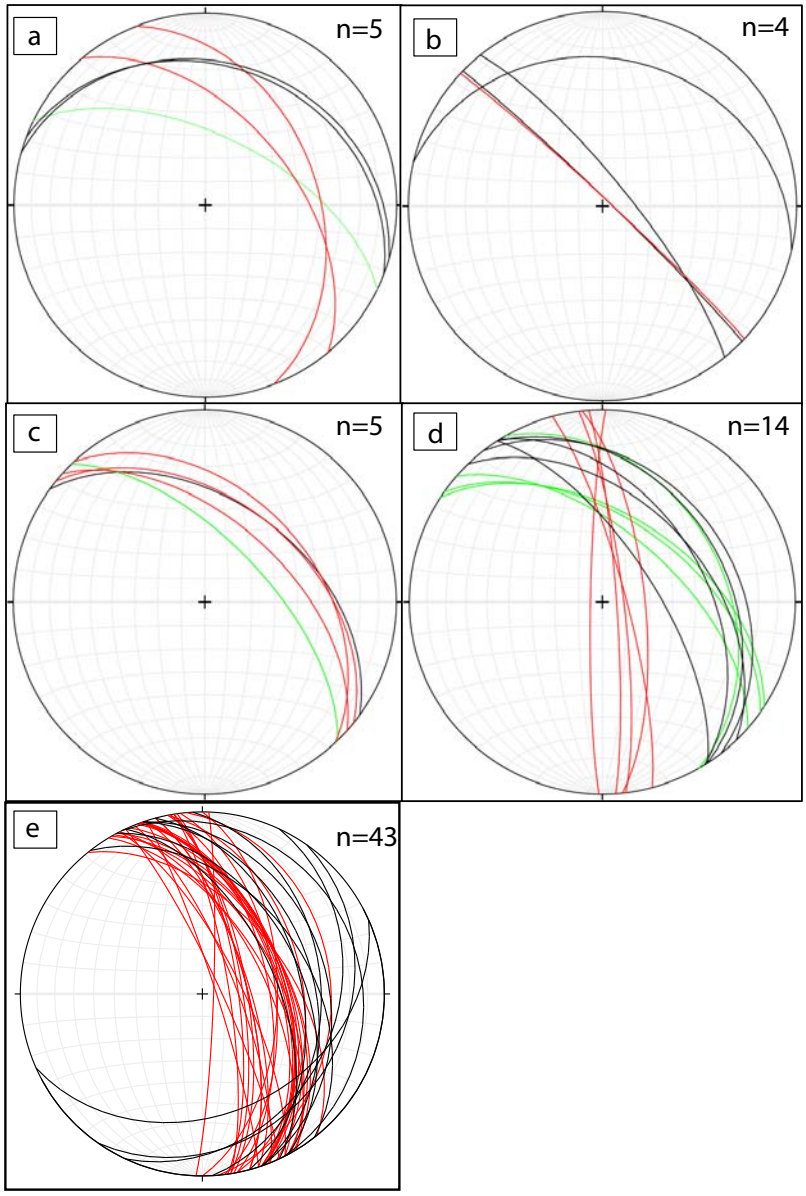

Figure 5.16: The foliations from the sub-vertical shear zones of Neumayerskarvet plotted in lower hemisphere, equal area plots as planes. Data is shown from east to west in alphabetical order. Red symbolizes the shear zone foliations, black symbolizes the host rock foliations and green the contact of the unfoliated granite intrusion.

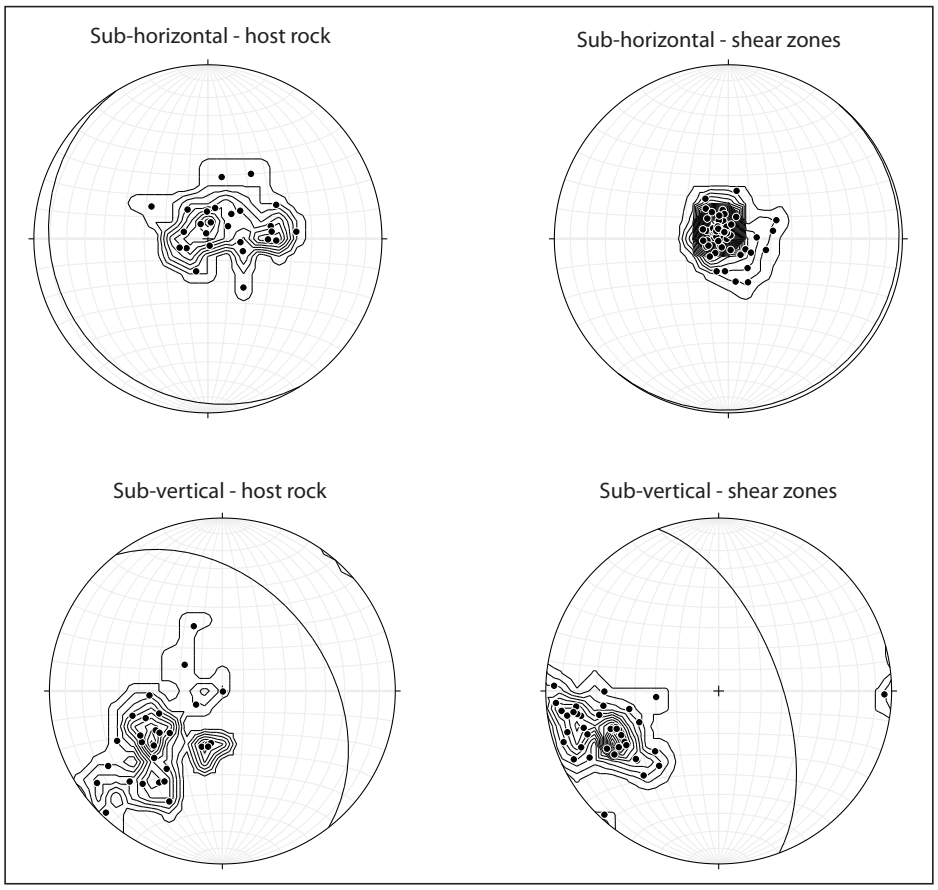

Figure 5.17: The foliations from within shear zones and their host rocks of the sub-horizontal shear zones and sub-vertical shear zones of Neumayerskarvet. The stereoplots have also been contoured to show the density of populations.

A digitized photograph of the western region of Neumayerskarvet illustrates the two sub-horizontal shear zones within the paragneiss units (Fig. 5.18). The lower minor sub-horizontal shear zone exists within the migmatitic paragneiss. The upper major sub-horizontal shear zone separates the migmatitic paragneiss from the banded paragneiss. The lower hemisphere, equal area stereographic plots on the photograph illustrate how the foliation varies from the base of the mountain, across the two shear zones to the top. At the base of the mountain the host rock foliations dip shallowly west and the lower shear zone foliations dip shallowly NW. The plots further up the mountain show that host rock foliations dip shallowly SW and that the upper shear zone foliations dip shallowly SE. The plots and the foliations drawn in on the photograph illustrate how shallow the dip of the foliation is.

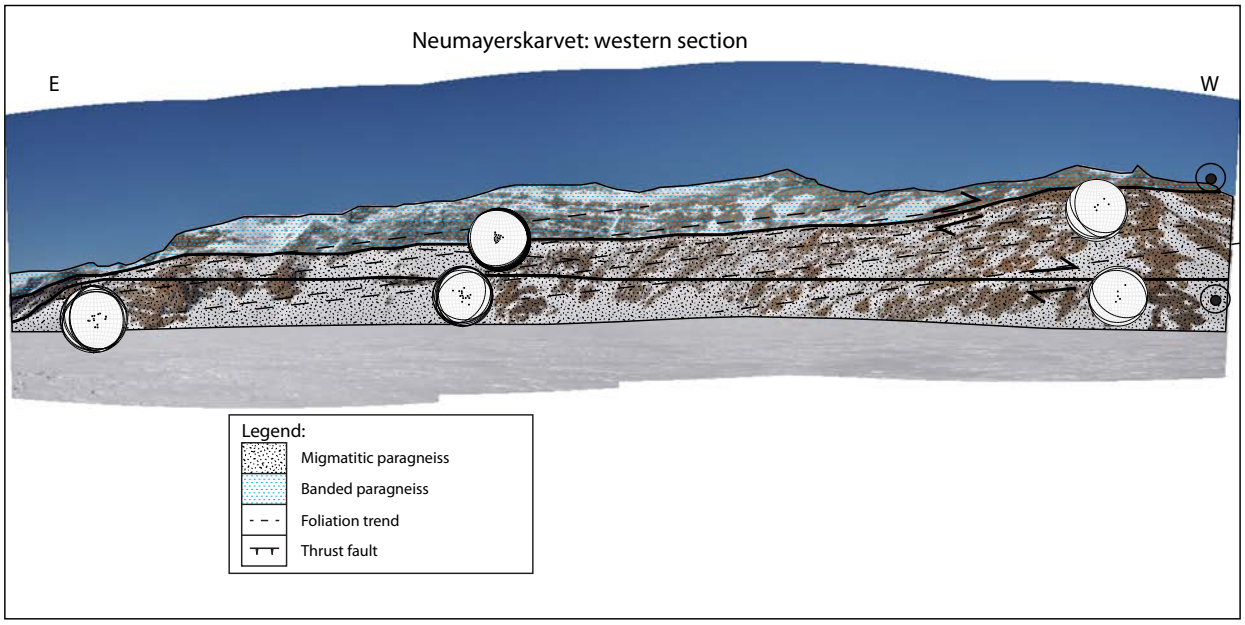

Figure 5.18: Photograph of Neumayerskarvet: the western section showing two sub-horizontal shear zones.

Figure 5.19 is a photograph of the central region of Neumayerskarvet. This region moves out of the sub-horizontal shear zones, this can be seen in the bottom right hand corner of the photograph, the upper sub-horizontal shear zone goes below the surface and can no longer be traced. To the left of the photograph there is a large portion of diatexite, which almost entirely consists of leucogranite. This diatexite does not contain a foliation but does have a strong lineation parallel to the host rocks lineation. The plot on the right hand side of the photograph illustrates how shallow the foliation is dipping still, but further east the foliations become steeper. This can be seen on the plots, as they change from a sub-horizontal dipping foliation (058°/06° SE), to (005°/45° E) in the middle of the photograph and then alongside the diatextite the foliation becomes sub-vertical (170°/75° ENE). As the foliations steepen, the dip direction changes from SE to NE.

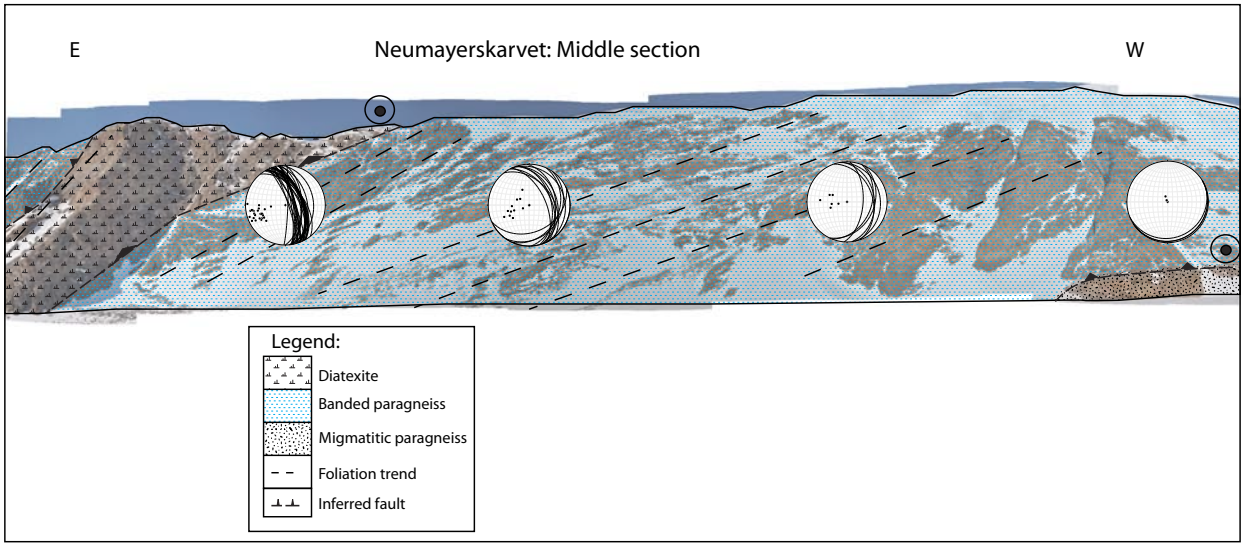

Figure 5.19: Photograph of Neumayerskarvet: the central section showing foliations becoming steeper and a diatexite.

Figure 5.20 is a photograph of the eastern region of Neumayerskarvet. It differs to the western region because of the appearance of various orthogneisses, unfoliated granite intrusions and sub-vertical shear zones. The foliations dip steeply to the NE, this is typical of all the sub-vertical shear zone regions. The unfoliated granite frequently occurs between the orthogneiss and paragneiss. By referring to Figure 5.16 d it can be seen that the unfoliated granite contact has a similar orientation to the host rock foliation but not as steep as the shear zones themselves. The foliations within the banded paragneiss on the right hand side of the photograph have orientations of 130°/52° NE, further to the east the shear zones foliations steepen to 172°/80° E. The contact of the unfoliated granite is not as steep as the foliations within the shear zone, its orientation is 131°/60° NE and the furthest plot to the east on the photograph is outside the shear zone in the strongly foliated orthogneiss, its orientation is 125°/54° NE. The foliations steepen as they approach a shear zone, and a unfoliated granite is found within the shear zone forming the contact between the banded paragneiss and the strongly foliated orthogneiss.

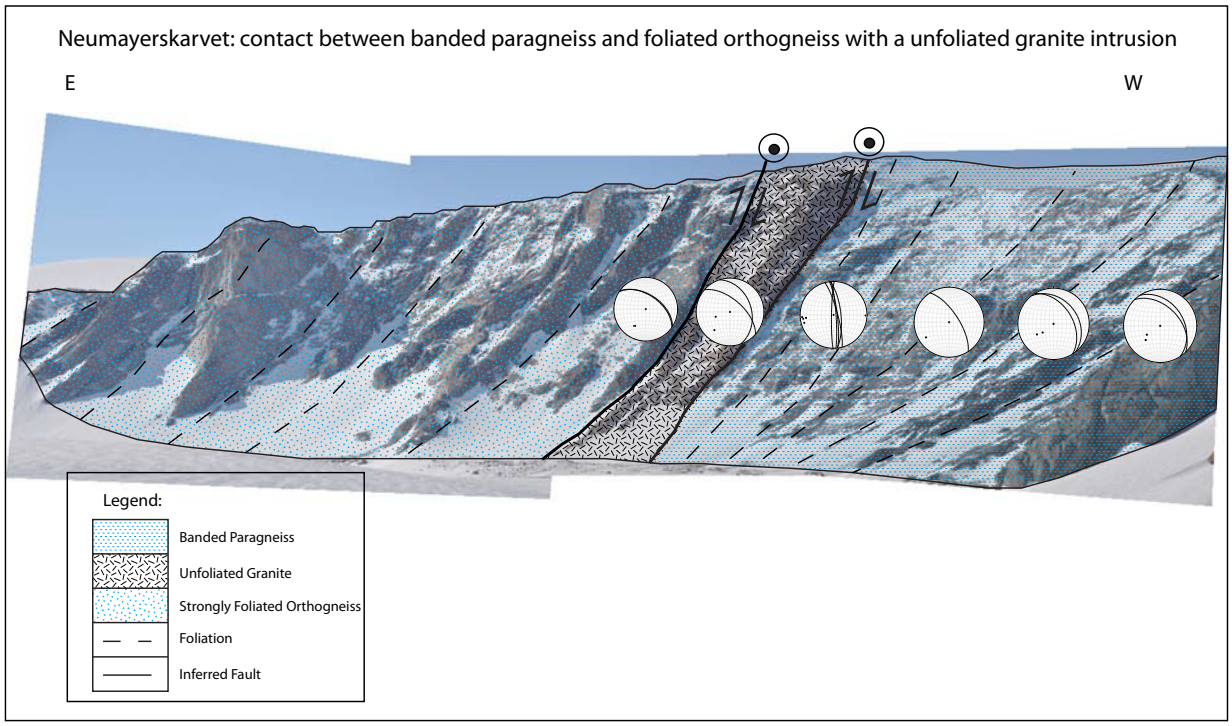

Figure 5.20: Photograph of Neumayerskarvet: the eastern section displaying sub-vertical shear zones and granite intrusions.

5.2.3 Lineations

The lineations of the western region of Neumayerskarvet are plotted in Figure 5.21 and the lineations of the eastern region of Neumayerskarvet in Figure 5.22. The plunge of the lineations throughout Neumayerskarvet, in the western and eastern region is very shallow, 5° to 20°.

Shear zones

The lineations from the sub-horizontal shear zones are scattered but with a main clustering of ∼140° or ∼320° trend (Fig. 5.21 b and d). The sub-vertical shear zone lineations are very uniform in orientation, ∼140° or ∼320° trend and shallowly plunging (Fig. 5.22).

Host rock

The lineations of the host rock in the western region are scattered around an 080° trending lineation, which is only found within the host rock and a 140° or 320° trending lineation that is always found alongside it (Fig. 5.21 a and c). The lineations of the host rock in the eastern region are uniform around a 140° or 320° trending lineation (Fig. 5.22).
By comparing the sub-horizontal and the sub-vertical areas together there is definitely a dominant 140° or 320° orientation in the trend of the lineations. The 080° trending lineation is found in the host rocks of the western region of Neumayerskarvet but it is not found in the sub-vertical eastern region.

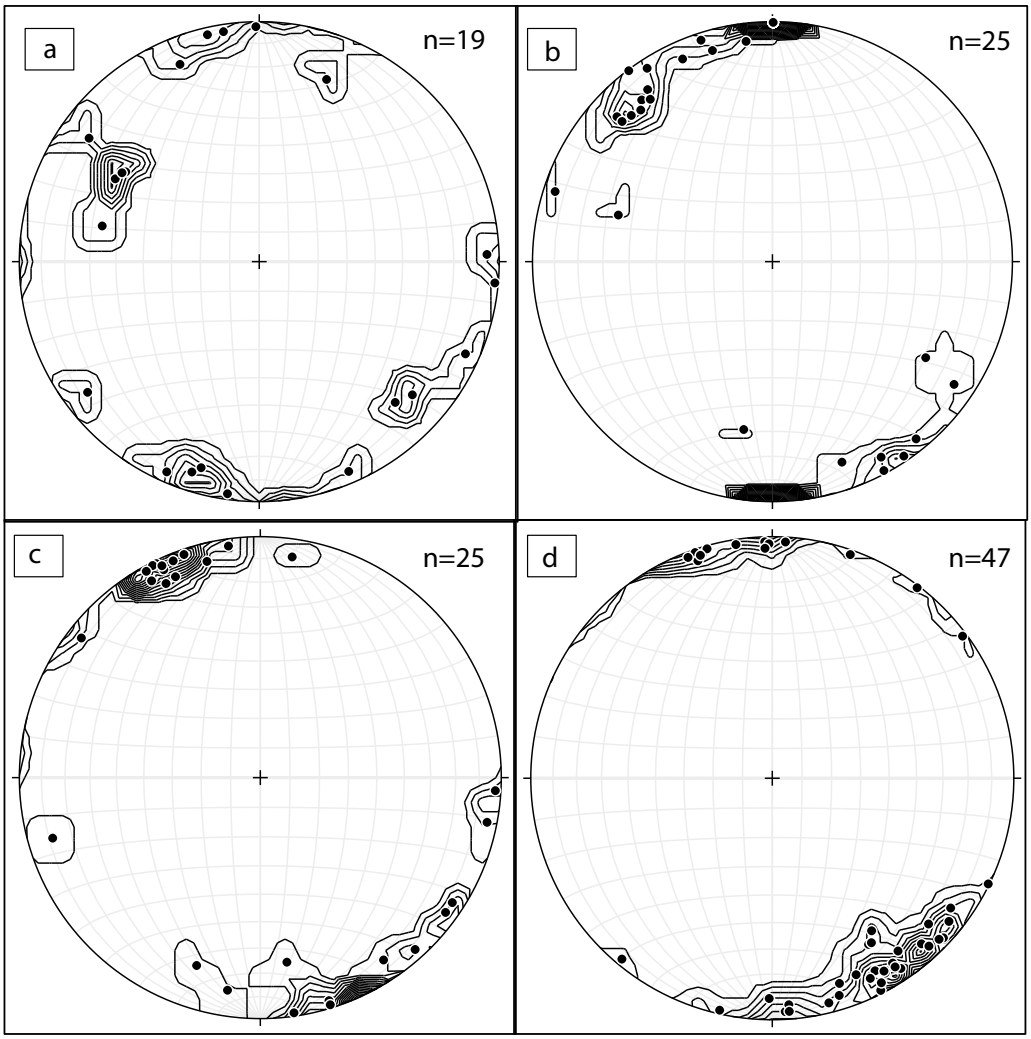

Figure 5.21: The lineations from the sub-horizontal shear zones of Neumayerskarvet plotted in lower hemisphere, equal area plots. The stereoplots have also been contoured to show the density of populations. (a) Lineations below the lower shear zone. (b) Lineations in the lower shear zone. (c) Lineations between the two shear zones. (d) Lineations in the upper shear zone.

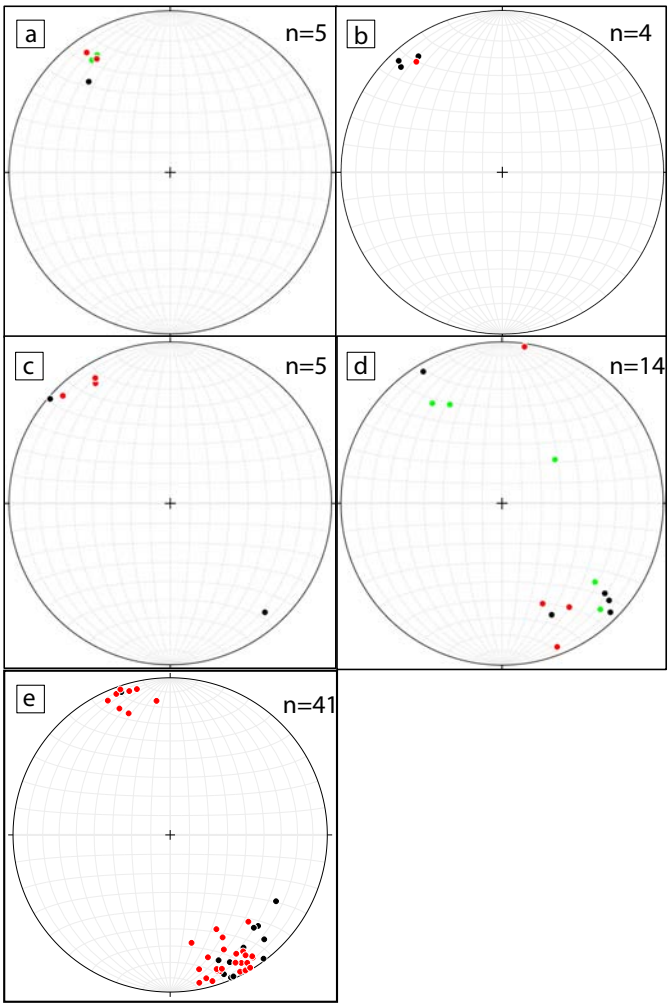

Figure 5.22: The lineations from the sub-vertical shear zones of Neumayerskarvet plotted in lower hemisphere, equal area plots. (a)-(e) are the lineations of the different sub-vertical strike-slip shear zones from east to west. Red symbolizes the shear zone lineations, black symbolizes the host rock lineations and green the contact of the unfoliated granite intrusion.

5.2.4 Folds

Folds of varying sizes are found throughout the shear zones of Neumayerskarvet (Fig. 5.10). The folds range from tight to open and are inclined to the NW from sub-vertical to recumbent. The wavelength of the folds varies from a cm scale to tens of meters scale.The plunges of the fold hinges are all very shallow, but the trend varies significantly from S through N and to E, covering most azimuths.

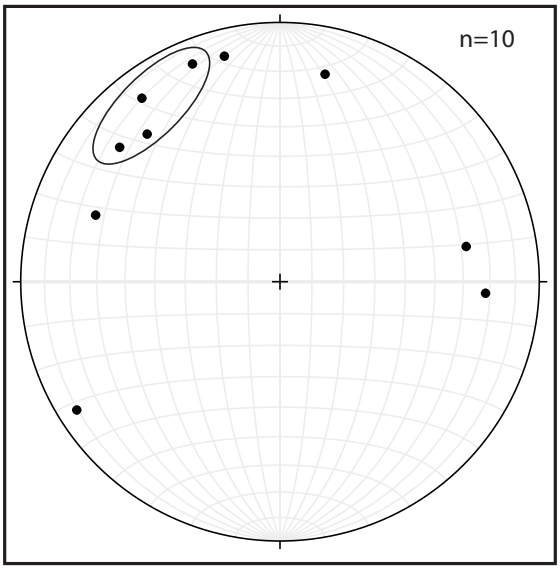

Figure 5.23: Lower hemisphere, equal area plot illustrating the trend and plunge of all the fold hinges measured at Neumayerskarvet.The circled area is parallel to the lineation, shear direction, in the study area.

5.2.5 Kinematic Indicators

All shear zones show a transport direction of top-to-the-NW, based on asymmetric lozenges, mantled porphyroclasts and asymmetric folds (Fig. 5.12).

5.3 Differences and Similarities

H.U. Sverdrupfjella and Neumayerskarvet both contain sub-horizontal shear zones, in Neumayerskarvet the two sub-horizontal shear zones occur in paragneiss layers, one is major and separates the migmatitic paragneiss from the banded paragneiss. In H.U. Sverdrupfjella the sub-horizontal shear zones alternate between orthogneiss and paragneiss layers, forming a duplex structure. Neumayerskarvet also contains a steep domain with sub-vertical strike-slip shear zones, these sub-vertical shear zones occur alongside vertical orthogneiss and unfoliated granite intrusions. The orthogneiss layers at H.U. Sverdrupfjella are allochthonous because they have been transported to their current duplex situation by the major sub-horizontal shear zones found in the region.

The plots of the foliations from the two study areas show that they have a uniform distribution apart from the sub-vertical foliations in the eastern region of Neumayerskarvet. Firstly in both H.U. Sverdrupfjella and Neumayerskarvet the shear zones foliations are clustered

around a SE or NW orientation but the host rocks foliation orinetations are spread throughout a range, from NE to W. At H.U. Sverdrupfjella the foliation dip direction is 140° and at Neumayerskarvet the foliation dip direction is 320°. The dip directions of the foliations for the two study areas differs by 180°, the cause of this is that they dip so shallowly, that a rotation of the foliations dip by <36° would cause a difference in dip direction of 180°. The only variation in terms of the foliations between the two study areas is the vertically foliated region at Neumayerskarvet, this does not occur at H.U. Sverdrupfjella. This difference occurs alongside the vertical orthogneisses which are not observed at H.U. Sverdrupfjella. The leucogranite dykes at H.U. Sverdrupfjella are post-deformation and cross-cut the fabrics.

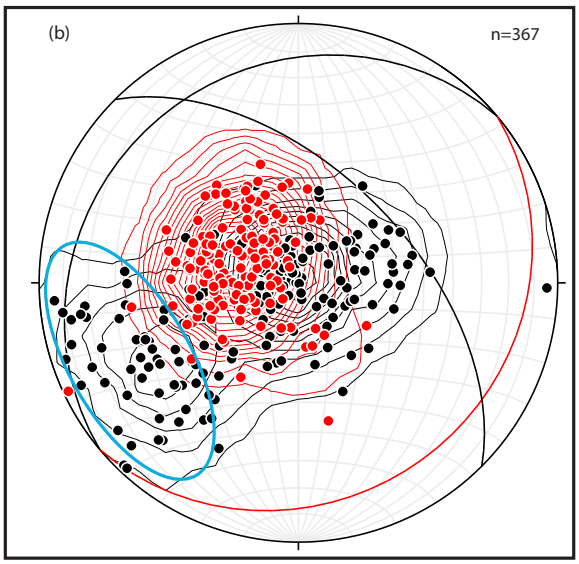

Figure 5.24: Lower hemisphere, equal area plot illustrating the dip direction of foliations in H.U. Sverdrupfjella and Neumayerskarvet: Black represents Neumayerskarvet, it is separated into east and west, the blue circle surrounds the steep eastern foliations, the red represents H.U. Sverdrupfjella. An average plane is plotted for the sub-horizontal and sub-vertical Neumayerskarvet domains and for H.U. Sverdrupfjella. (b) Is a contoured version of (a) to show the density of populations. The angle between the sub-horizontal plane of Neumayerskarvet and H.U. Sverdrupfjella is 36°, showing that only a slight rotation will cause a 180° change in the dip direction of the foliation. 55° is the angle between the sub-vertical eastern domain and the sub-horizontal western domain of Neumayerskarvet.

Field observations only found one foliation that is more uniform within the shear zones than in the host rock. The foliation is interpreted as been transposed because at least two deformation phases have affected the region and only one foliation is found. The transposed foliation in H.U. Sverdrupfjella and Neumayerskarvet is therefore grouped as a S_{1+2} foliation.

The S_{1+2} foliation is found within the shear zones and host rocks.

The lineations from both study areas are very similar in orientation. H.U. Sverdrupfjella mainly contains a shallowly SE-plunging lineation with a lesser easterly plunging lineation. Neumayerskarvet mainly contains a shallowly SE/NW-plunging lineation and rarely a lesser easterly plunging lineation is found. The dominant lineation has a trend of 140°/320° with a less dominant 080° trending lineation occurring in places. The dominant 140°/320° trending lineations is still consistent through the sub-vertical orthogneiss intrusions at Neumayerskarvet. Shear zones only contain the 140°/320° trending lineation but outside this, in the host rock, both the weaker 080° and stronger 140°/320° trending lineations are found within the same rock. All of the lineations have a shallow plunge, ranging from 5° to 20°. The presence of only the 140°/320° trending lineation in the shear zones implies that the 140°/320° trending lineation is associated with a more recent deformation phase, D_2, and that the weak 080° trending lineation is associated with an older deformation phase, D_1.

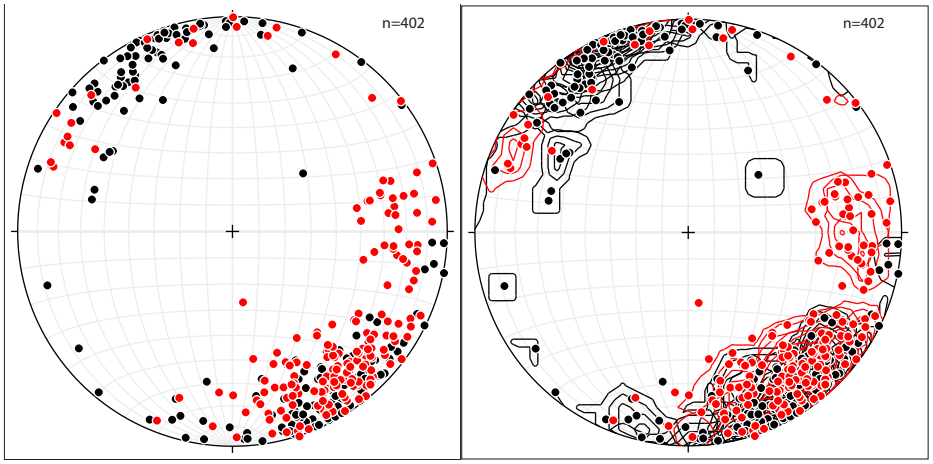

Figure 5.25: Lower hemisphere, equal area plot illustrating the orientation of lineations at H.U. Sverdrupfjella and Neumayerskarvet: Black represents Neumayerskarvet, the red represents H.U. Sverdrupfjella. There is a tight cluster of lineations plunging shallowly SE and NW, with Neumayerskarvet having more lines trending NW than H.U. Sverdrupfjella, which is dominantly trending SE. There are lineations plunging shallowly east but to a lesser extent than the ones trending SE and NW and these are dominated by the points from H.U. Sverdrupfjella. (b) Is a contoured version of (a) to show the density of populations.

The measurements taken from the fold hinges at both study areas are not clustered as was found for the foliations and lineations. The fold hinges are all plunging shallowly but in different directions throughout the plot, however frequently the fold hinges plot parallel

to the lineations found at the study areas. Fold hinges initially form at 90° to the shear direction but as the strain increases they can be rotated, to lie parallel to the shear direction (Bell, 1978). The circled areas in Figure 5.11 and Figure 5.23 show that frequently the fold hinges have been rotated parallel to the 140°/320° trending lineation, shear direction, but they are not all clustered there and instead spread around these areas.

The kinematic indicators, inclined folds, asymmetric lozenges and mantled porphyroclasts, all show a consistent top-to-the-NW transport direction for both Neumayerskarvet and H.U. Sverdrupfjella.

Chapter 6

Microstructure

6.1 H.U.Sverdrupfjella

6.1.1 Foliation

In both the paragneisses and the orthogneisses, biotite and quartz define the foliation. Commonly in the paragneiss, hornblende, sillimanite and epidote have formed parallel to this fabric, and in orthogneisses, K-feldspar aligned parallel to this fabric. In the paragneiss the biotite defines the main fabric, quartz is elongated but not as much as biotite. In the orthogneiss there is ∼20 % less biotite than in the paragneiss and the quartz grains are more elongated than in the paragneiss. Figure 6.5 c and d illustrates how elongated the quartz grains are, this is most noticeable in the thin sections cut along the 140° trending lineation.

A minor shear zone within an orthogneiss unit at H.U. Sverdrupfjella is studied in detail to determine how the fabric changes from outside the shear zone to the centre. Figure 6.1 illustrates where the samples were taken and the variation in grain size surrounding the shear zone. The grain size changes from fine grained in the centre of the shear zone to medium to coarse towards the edges (Fig. 6.2).

Furthest above the shear zone, the orthogneiss is medium grained but contains many porphyroclasts (2 mm diameter) of quartz and microcline. The fine grained matrix of biotite, muscovite, albite and quartz makes up ∼30 % of the rock, it therefore resembles a protomylonite. Myrmekites are also found surrounding microcline porphyroclasts. The biotite (15 %) in the sample is scattered but still in a preferred orientation that resembles a foliation, elongated quartz grains form a lineation (Fig. 6.3 a and b). The sample taken below this is

also medium grained but it contains less porphyroclasts and has a more developed foliation of biotite (20 %) and quartz (50 %) compared to above. The quartz grains are very elongated and the rock contains ∼50 % matrix, consisting of biotite, quartz, albite and muscovite, which classifies it as a mylonite (Fig. 6.3 c and d). The fine grained zone in the centre of the shear zone, is finer grained and contains more subgrains than the other parts of the shear zone. The rock is made up of ∼60 % matrix, this consists of subgrains of quartz, albite and muscovite with a small portion of biotite (10 %). The quartz grains are more elongated than any other part of the shear zone and it contains the most developed foliation in the shear zone. The centre of the shear zone is fine grained with a well-defined foliation and large proportion of matrix and is therefore classified as a mylonite (Fig. 6.3 e and f). The host rock below the shear zone contains many very large porphyroclasts (4mm) of quartz, albite and microcline. The biotite grains (20 %) are also more coarse than in the other samples and they form ribbons around the larger porphyroclasts. The quartz grains are elongated parallel to the biotite grains forming a foliation and lineation. This coarse grained area of the shear zone is classified as protomylonite because of the abundance of large porphyroclasts and the small proportion of matrix (∼10 %) (Fig. 6.3 g and h).

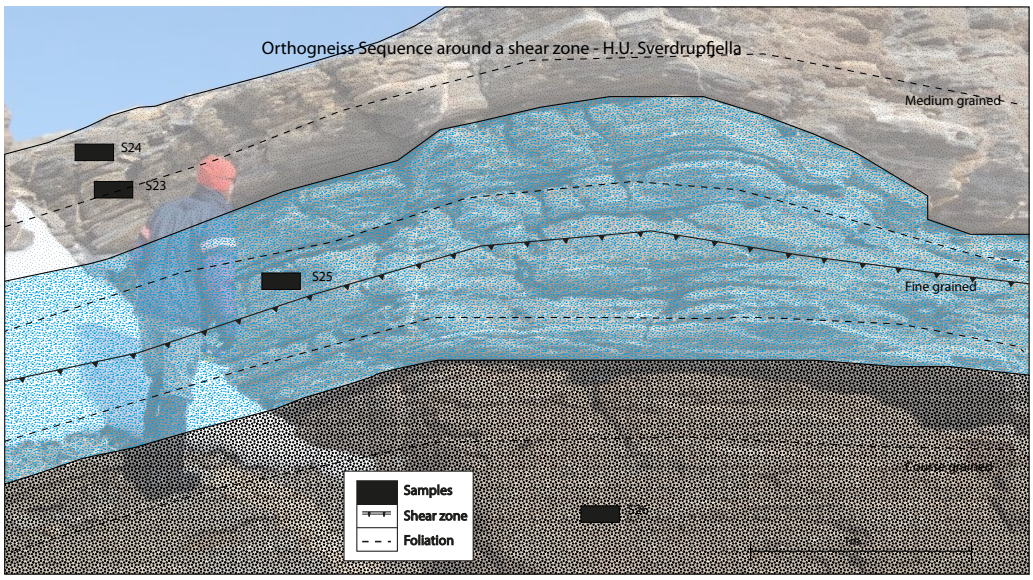

Figure 6.1: A detailed photograph illustrating where samples were taken from a shear zone within a orthogneiss unit.

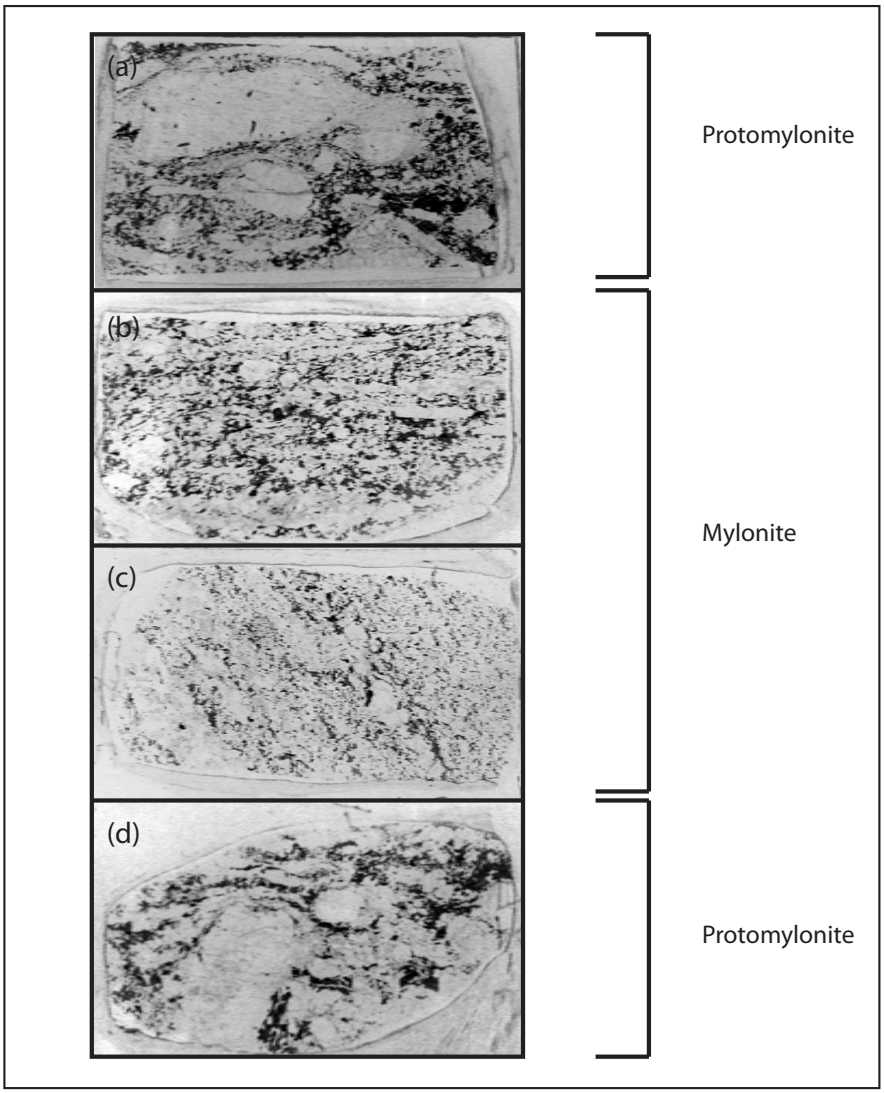

Figure 6.2: Photographs of thin sections taken from a shear zone within a orthogneiss unit (Fig. 6.1). (a) Photograph of sample (S24), it is a medium grained orthogneiss at the top of this sequence. (b) Photograph of sample (S23), it is a medium to fine grained orthogneiss just below (S24). (c) Photograph of sample (S25), it is a fine grained orthogneiss in the centre of the shear zone. (d) Photograph of sample (S26), it is a coarse grained orthogneiss below the shear zone.

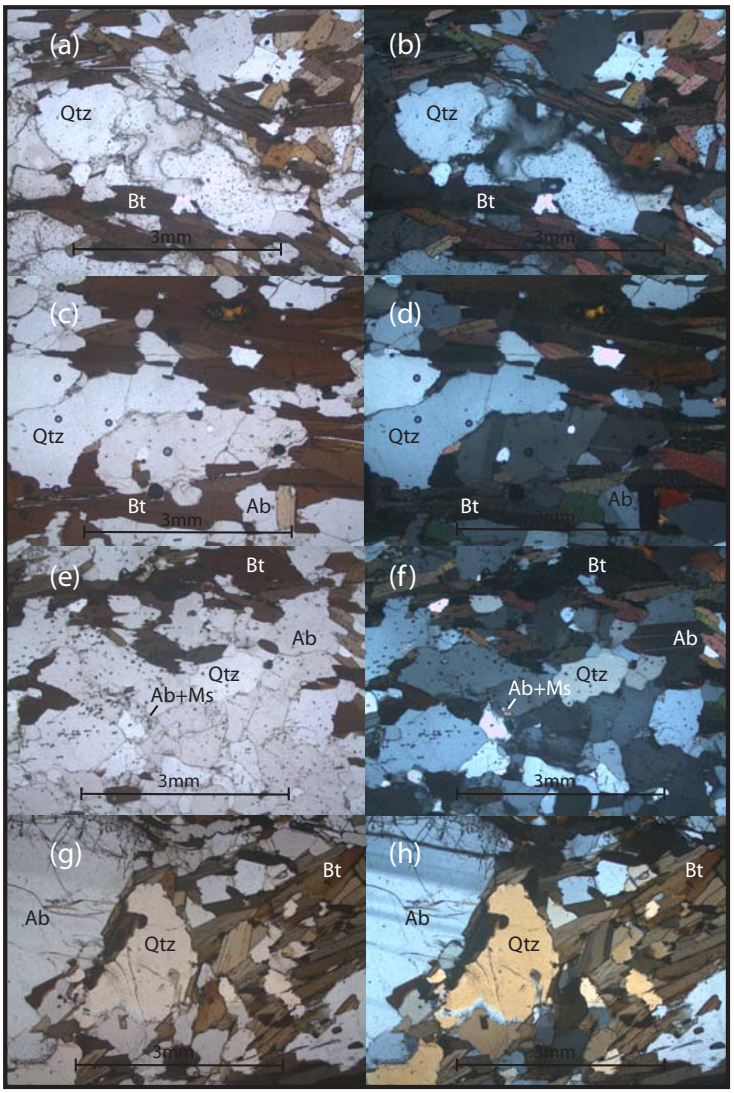

Figure 6.3: Photomicrographs taken from a shear zone within an orthogneiss unit, the sample numbers correspond to Figure 6.1. (a and b) are photomicrographs of sample (S24), it is a medium grained orthogneiss at the top of this sequence. (c and d) are photomicrographs of sample (S23), it is a medium to fine grained orthogneiss just below (S24). (e and f) are photomicrographs of sample (S25), it is a fine grained orthogneiss in the centre of the shear zone. (g and h) are photomicrographs of sample (S26), it is a coarse grained orthogneiss below the shear zone. (Ab-albite, Bt-biotite, Mc-microcline, Ms-muscovite, Qtz-quartz)

6.1.2 Lineation

As observed on the outcrop/meso-scale, quartz frequently defines a lineation and there is commonly two lineations present in the rocks, with 140° and 080 ° trends. The 140 ° trending lineation is dominant and more recent because in the field it is the stronger and it is the only lineation found in the shear zones, whereas outside the shear zones it is always found alongside the weaker 080° trending lineation. In the thin sections that have been cut along the 140° trending lineation there is a strong S-C fabric which shows top-to-the-NW transport direction, this agrees with the field observations (Figs. 6.4c and d).

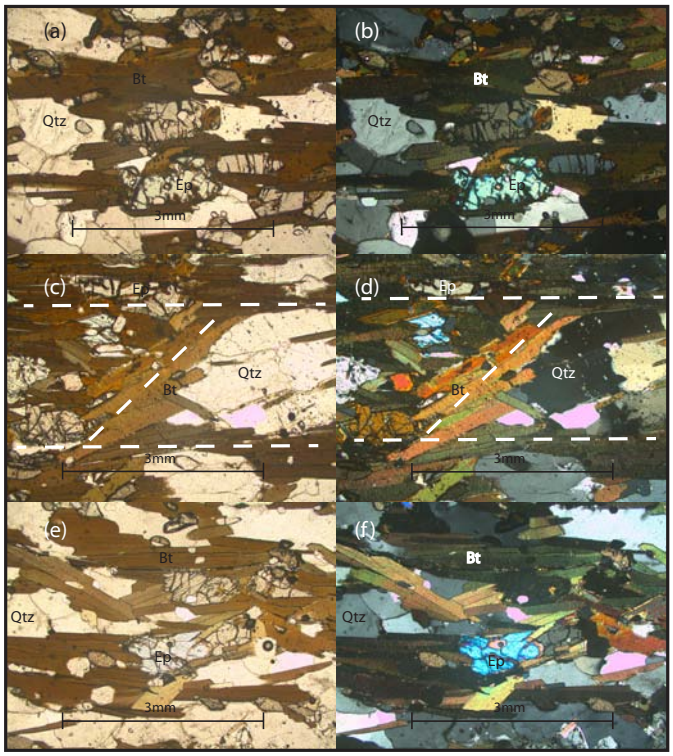

Figure 6.4: Fabrics from paragneiss samples taken from H.U. Sverdrupfjella: (a) Epidote grains elongated and aligned parallel to the fabric in a thin section cut along the 140° trending lineation (PPL). (b) The XPL of (a). (c) S-C fabric formed by biotite grains, grains run both horizontally and diagonally across the image. This images is taken of a thin section cut along the 140° trending lineation (PPL). (d) XPL of (c). (e) Image taken of a thin section cut along the 080° trending lineation. The epidote grains are orientated randomly and are euhedral in shape, they have not been elongated. The biotite grains are orientated more randomly, forming a weak S-C fabric (PPL). (f) XPL of (e). (Bt-biotite, Ep-epidote, Qtz-quartz)

Parallel to the 140° trending lineation, epidote grains are elongate parallel to the biotite foliation (Fig. 6.4 a). By comparison, along the 080° trending lineation, the epidote grains are more euhedral (Fig. 6.5 e). This implies that the shape of the epidote grains reflect the 140° trending lineation. The S-C fabric is well-defined in thin sections cut along the 140° trending lineation, whereas thin sections cut parallel to the 080° trending lineation only contain a weak S-C fabric (Fig. 6.4 c and e). This implies that the deformation event that caused the 140° trending lineation is the more recent event, because it has overprinted the deformation event that resulted in the 080° trending lineation. The angle between the S and C fabric in the sample taken from the 140° trending lineation is 45°.

6.1.3 Porphyroclasts

The rocks from H.U. Sverdrupfjella have a large spread of grain sizes ranging from large porphyroclasts of feldspar and quartz to small subgrains of quartz and feldspar. These subgrains are distributed throughout the larger parental grains, from the edges to the centre of the grain. Figure 6.5 a and b shows quartz and albite subgrains within and surrounding a larger parental grain. In the samples that contain myrmekite, it is not only small grains of albite forming around the microcline porphyroclast but also small subgrains of microcline. These subgrains form along the edges of parental porphyroclast and within them, the subgrains are rounded in shape and range in size from 40 μm to 250 μm with an average sub-grain size of 146 μm (n=97, Stdev=67 μm) on Alan Piggen and a range of 40 μm to 400 μm with an average sub-grain size of 248 μm (n=35, Stdev=124 μm) in the minor shear zone within a orthogneiss unit. Commonly grains of quartz exhibit undulose extinction. Plagioclase grains contain deformation twins (Fig. 6.5 a). Deformation twins look similar to albite twinning except that the twins peter out or extend into other grains. Most grains are not euhedral and have wavy grain boundaries.

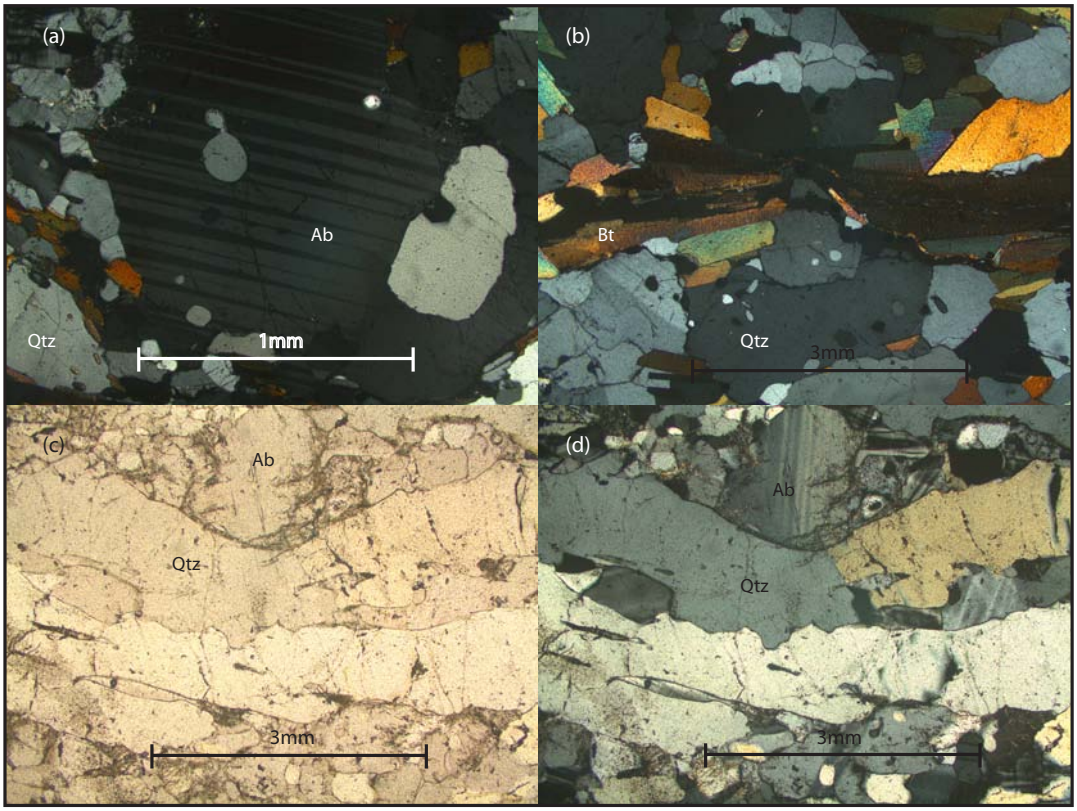

Figure 6.5: Images showing the various microstructures found in samples taken from H.U. Sverdrupfjella: (a) Deformation twins extending through two plagioclase grains. Photomicrograph taken under cross polar light. (b) Subgrains of quartz along the porphyroclasts grain boundaries and within grains. The grain boundaries themselves are also wavy. (c) Stretched quartz grains forming a fabric within an orthogneiss. The thin section was cut along the 140° trending lineation. (d) XPL of (c). (Ab-albite, Bt-biotite, Qtz-quartz)

6.2 Neumayerskarvet

6.2.1 Foliation

Para- and orthogneisses from Neumayerskarvet are very similar to H.U. Sverdrupfjella in that biotite defines the main foliation and quartz the lineation. In the paragneisses and mafic boudins, hornblende and epidote are found oriented parallel to the biotite foliation. In the orthogneisses K-feldspar is commonly elongated in the same orientation as the dominant quartz foliation. Samples were taken from a leucosome in the paragneiss that contains mafic inclusions. The leucosome is made up predominantly of quartz and microcline with a few grains of biotite. The mafic boundin consists mainly of quartz, hornblende and biotite with some grains of albite. The leucosome has a very weak fabric, with euhedral quartz grains, while in the mafic boudin the hornblende grains are very elongated, forming a fabric with biotite. The quartz grains within the mafic boudin are also very elongated, in contrast to the quartz grains within the leucosome (Fig. 6.6).

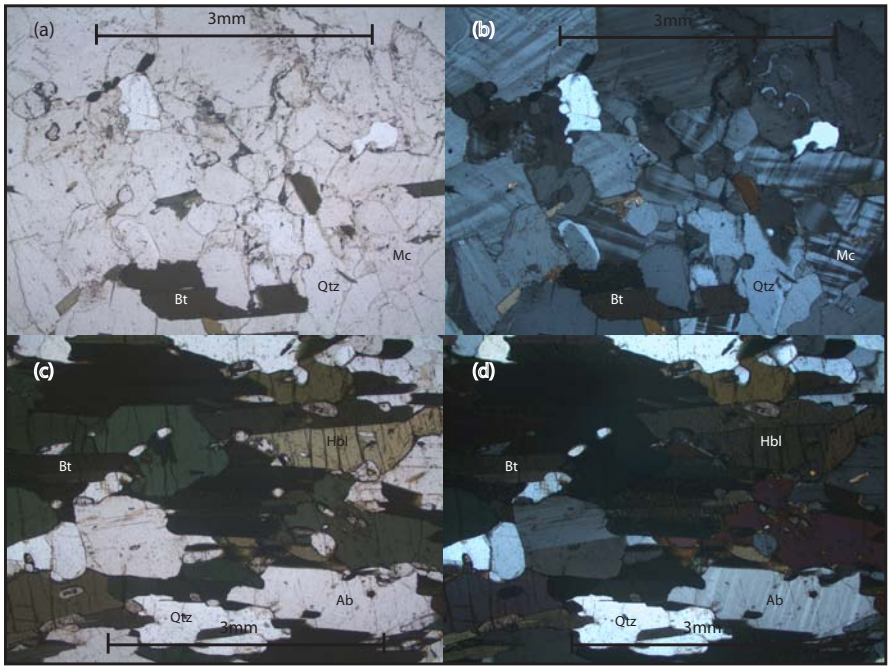

Figure 6.6: Thin sections of a leucosome with a mafic boudin within it taken from the mafic intrusion bearing paragneiss north of "The Corridor": (a) Leucosome mainly consisting of microcline and quartz, with a poorly developed fabric. (b) XPL version of (a). (c) Mafic boudin mainly consisting of hornblende which is elongated, quartz and albite are also elongated. (d) XPL of (c). (Ab-albite, Bt-biotite, Hbl-hornblende, Mc-microcline, Qtz-quartz)

Samples from the strike-slip shear zone south of "The Corridor" illustrate how strain varies closer to the shear zone (Fig. 6.7). The rock outside the shear zone is made up almost entirely of gedrite, the gedrite grains have a shape preferred orientation defining a foliation (Fig. 6.7 a and b). Below the shear zone the rocks no longer contain gedrite but instead are made up of quartz and hornblende. The grains are medium to coarse in size and the hornblende grains have been elongated, showing increasing aspect ratios near the shear zone (Fig. 6.7 c and d). Within the shear zone rocks are finer grained and consist of quartz, hornblende and some biotite (5%), all of these minerals are elongate in a preferred orientation, showing the direction of the main stretching (Fig. 6.7 e and f).

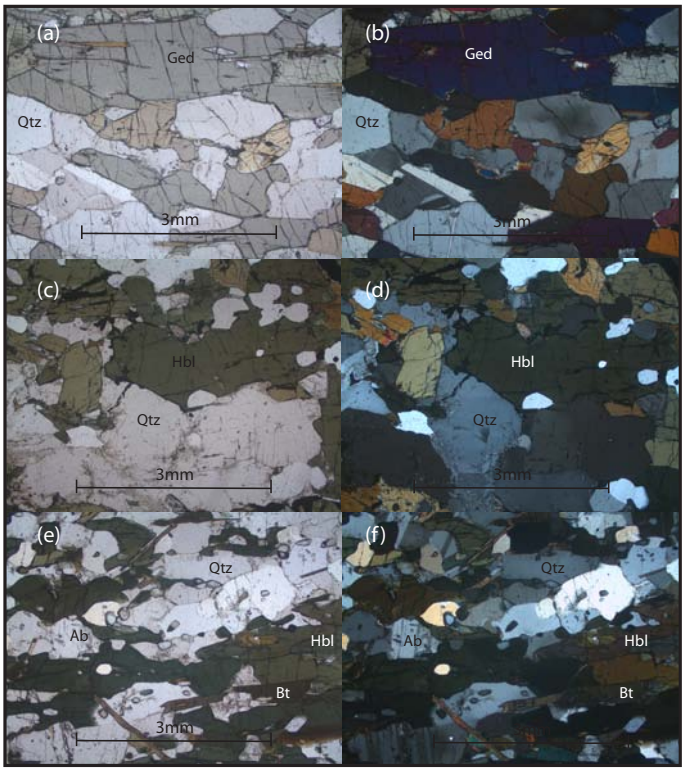

Figure 6.7: Thin sections starting from the host paragneiss and moving in towards the sub-vertical strike-slip shear zone: (a) Host paragneiss made up almost entirely of gedrite, this is inter-layered with calc-silicates (PPL). (b) XPL of (a). (c) Below the shear zone, coarse grained hornblende forming the foliation (PPL). (d) XPL of (c). (e) Within the shear zone, fine, highly strained grains of biotite and hornblende forming the foliation (PPL). (f) XPL of (e), shows elongated quartz grains parallel to the hornblende and biotite foliation. (Ab-albite, Bt-biotite, Ged-gedrite, Hbl-hornblende, Qtz-quartz)

6.2.2 Lineation

As observed on the outcrop-scale, quartz frequently defines a lineation and there is commonly two lineations present in the rocks, with southerly and easterly trends. The southerly trending lineation is dominant and more recent because in the field it is the stronger and it is the only lineation found in the shear zones. Outside the shear zones the southerly trending lineation is always found alongside the weaker easterly trending lineation, therefore hinting that it overprints the easterly trending lineation. Figure 6.8, illustrates two thin sections cut from the migmatitic paragneiss along a 189° trending lineation and a 089° trending lineation. Along the southerly, 189° trending lineation, the hornblende and garnet grains are elongated parallel to the biotite foliation (Fig. 6.8 a and b), whilst parallel to the easterly, 089° trending lineation, the hornblende and garnet grains are more euhedral (Fig. 6.8 c and d).

S-C fabric in biotite shows a transport direction of top-to-the-NW (Fig. 6.9e), which corresponds with the transport direction of the whole region and both study areas. The angle between the S and C fabrics is 68°. Throughout Neumayerskarvet biotite ribbons can be seen, this is biotite grains forming a fabric that wraps around the more competent, larger porphyroclasts of quartz and feldspar (Fig. 6.9 a and c).

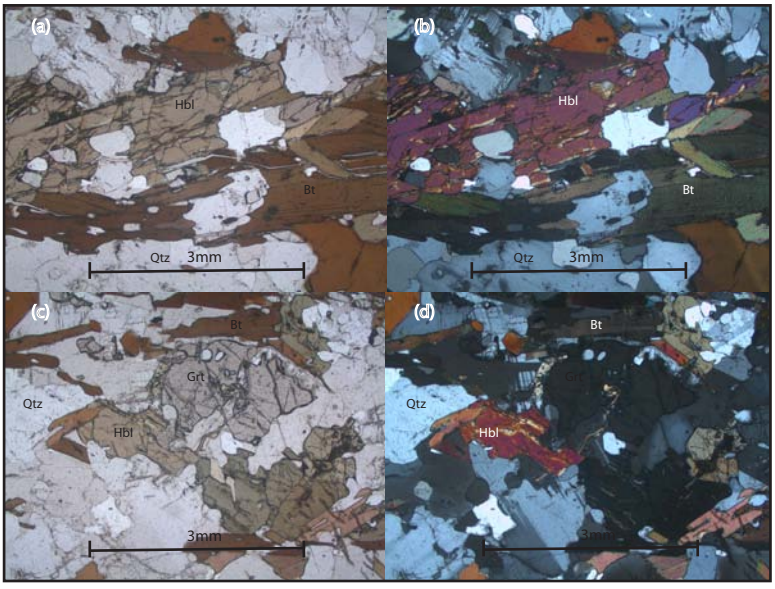

Figure 6.8: Thin sections were cut along two different lineations from the same paragneiss sample: (a) Thin section cut along a 189° lineation, the garnet and hornblende are stretched parallel to the biotite fabric. (b) XPL of (a). (c) Thin section cut along a 089° lineation, here the garnet and hornblende grains are more euhedral in shape. (d) XPL of (c). (Bt-biotite, Grt-garnet, Hbl-hornblende, Qtz-quartz)

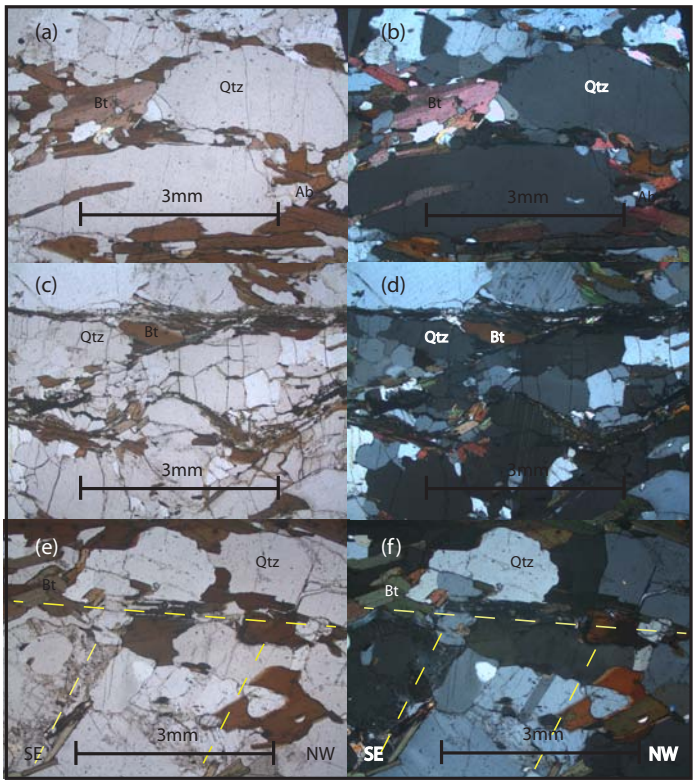

Figure 6.9: Fabrics from rock samples taken from Neumayerskarvet: (a) Quartz elongated, forming a lineation, with a biotite fabric wrapping around these large elongated quartz porphyroclasts. (b) XPL of (a). (c) Biotite forming a ribbon fabric around larger quartz and feldspar porphyroclasts. (d) XPL of (c). (e) S-C fabric forming in a banded paragneiss, the yellow dotted lines illustrating the orientation of the biotite grains, this also showing a top-to-the-NW transport direction. (f) XPL of (e). (Ab-albite, Bt-biotite, Qtz-quartz)

6.2.3 Porphyroclasts

The mineral grains have a wide range of grain sizes, with large porphyroclasts of microcline, quartz and garnet throughout all the rock types, surrounded by smaller grains making up the matrix. A portion of these small grains are subgrains, these are mainly quartz and albite and commonly microcline. The subgrains of albite form along the edges of larger microcline grains, resulting in a myrmekite texture. Quartz subgrains form on the margin of larger quartz porphyroclasts and also within the larger grains (Fig. 6.10 a, b and c). These sub-grains are rounded in shape and range in size from 50 μm to 380 μm with an average sub-grain size of 210 μm (n=30, Stdev=114 μm). Feldspar grains do not only contain subgrains but often also deformation twins (Fig. 6.10 d, e and f). Frequently the grains are not euhedral and instead have wavy grain boundaries (Fig. 6.10 c).

Figure 6.10: Photomicrographs of the various deformation mechanisms found in the thin sections from Neumayerskarvet: (a) Subgrains of quartz forming along the edges of larger quartz grains and within them (b) A fine grained matrix of biotite and quartz subgrains, with quartz and feldspar porphyroclasts (c) Subgrains of quartz forming along the edges of larger quartz grains and within them (d) Deformation twins within a plagioclase grain (e) Deformation twins in a plagioclase porphyroclast with a fine grained matrix of biotite and quartz and albite subgrains (f) Deformation twins within a plagioclase grain. (Ab-albite, Bt-biotite, Qtz-quartz)

6.3 Differences and Similarities

The microstructures that occur within the rocks of H.U. Sverdrupfjella and Neumayerskarvet are uniform, showing that they have experienced the same deformation history. In both study areas the same minerals define the major fabrics, with biotite forming the foliation and quartz the lineation and in places hornblende, silliminite, epidote and garnet aligning parallel to the biotite foliation. S-C fabrics are found at both locations but are more common at H.U. Sverdrupfjella. A comparison of two thin sections cut from two different lineations from one sample is used in both study areas to determine the timing and mineral compositions of the deformational events. The result from both, is that in the thin section cut along an 080° trending lineation mineral grains are fairly euhedral in shape, this showing that the deformation event that formed the 080° trending lineation has been overprinted by a younger event. The thin sections cut along 140° and 189° trending lineations have elongated and highly strained grains which implies that it is the most recent deformation event. Another observation that supports these findings is that all of the shear zones have a dominant 140° trending lineation, this agreeing with it been the most recent and that it would have overprinted any previous deformation traces within the shear zones.

The deformation mechanisms that have affected the two study areas are the same, mechanical twinning and dislocation creep. These mechanisms have resulted in deformation twinning, sub-grains and grain boundary migration occurring throughout the rocks of the study areas.

Chapter 7

Discussion

7.1 Relation of fabrics to deformation events

The Maud Belt of Western Dronning Maud Land, specifically the rocks exposed at H.U. Sverdrupfjella and Neumayerskarvet, have experienced polyphase deformation. This study defined two deformational events, D_1 and D_2, at both study areas. D_1 is defined by a biotite and quartz foliation (S_1) with a strike between 000° E and 050° SE. S_1 commonly dips shallowly apart from the eastern region of Neumayerskarvet where the foliation is sub-vertical. The D_1 lineation (L_1) is defined by quartz, feldspar and in places sillimanite and hornblende. L_1 generally plunges shallowly east, with a trend of ∼080°. D_2 is defined by a biotite and quartz foliation (S_2) also dipping shallowly E-SE. S_1 is generally transposed into S_2 and therefore they will be grouped as S_{1+2}. The D_2 lineation (L_2) is defined by quartz, feldspar and in places sillimanite, epidote and hornblende. At H.U. Sverdrupfjella L_2 has a dominant trend of 140°, and at Neumayerskarvet L_2 trends both 140° and 320°, plunging shallowly. The shear zones are interpreted as D_2 because they only contain one of the two lineations found in both study areas. The SE/NW-trending lineation is interpreted as D_2 because, in the host rocks, the 080° and 140°/320° trending lineations are found in the same rock, with the 080° trending lineation being the weaker. Within the shear zones only the 140°/320° trending lineation is found. If the 080° trending lineation was the youngest, then there would not only be traces of it in the host rock but probably also within the shear zones. Throughout both study areas, the 080° trending lineation has not been observed alone, it is always found together with the 140°/320° trending lineation. The shear zones have therefore experienced more deformation than the host rock in order to overprint L_1 within the shear

zones. D_2 was localized within the shear zones but it also partially affected the host rock, resulting in both L_1 and L_2 in the host rock and a S_{1+2} foliation.

7.2 Conditions of fabric formation

Thin sections cut along a 140° trending lineation contain a strong S-C fabric and the quartz, feldspar, garnet, hornblende and epidote grains are elongated in the 140° orientation. The presence of epidote and hornblende along the 140° trending lineation, means that it formed late. Thin sections cut along the 080° trending lineation contain a weak S-C fabric and the mineral grains are more euhedral in shape and not elongate as found within the 140° thin sections.

Along with S-C fabrics there are also other microstructures found in rocks from both study areas. Deformation twins are formed by the bending rather than breaking of crystal lattices. Deformation twins do not require high temperatures and confining pressures to form but do need relatively high differential stresses (>250 MPa) (Stünitz *et al.*, 2003). These twins are found in plagioclase grains throughout both study areas. Sub-grains are found along the edges of large porphyroclasts and within them. The sub-grains are rounded in shape and range in size from 40 μm to 400 μm with an average sub-grain size of 167 μm (n=158, Stdev=90 μm). Quartz, K-feldspar and plagioclase sub-grains are found in the rocks from the two study areas, this means that metamorphic conditions were at least middle to upper amphibolite facies (Tullis *et al.*, 1982; Passchier, 2005). Both D_1 and D_2 contain sub-grains of quartz, K-feldspar and plagioclase and therefore have similar metamorphic conditions of middle to upper amphibolite facies.

7.3 Kinematic history of the Maud Belt

Both study areas experienced a similar deformation and metamorphic history because both study areas consist of paragneisses and orthogneisses, consisting of similar minerals that represent amphibolite facies conditions. Both study areas also contain similar microstructures, both contain a S_{1+2} foliation and both contain a weak L_1 constrained to the host rocks and a strong L_2 that occurs throughout the host rocks and shear zones. In both study areas only a top-to-the-NW transport direction was observed, this differs to the findings of previous authors such as Grantham et. al (1995), who found a top-to-the-SE transport direction for

the Pan-African orogeny in western Sverdrupfjella. There are however some differences between the two study areas. H.U. Sverdrupfjella consists of a duplex structure of orthogneiss and paragneiss layers separated by sub-horizontal shear zones. Neumayerskarvet contains a larger variety of rocks types, which includes more intrusive rocks and contains both sub-horizontal and sub-vertical shear zones. H.U. Sverdrupfjella is similar to the rest of the Maud Belt (Grantham *et al.*, 1995; Groenewald, 1995; Board, 2001), with a shallow E/SE-dipping foliation and a dominant shallow SE-plunging lineation. Neumayerskarvet also contains a shallow SE-dipping foliation and a dominant shallow SE-plunging lineation but it also contains a steep NE-dipping foliation in its eastern region and a shallow NW-dipping foliation containing a shallow NW-plunging lineation in its western region.

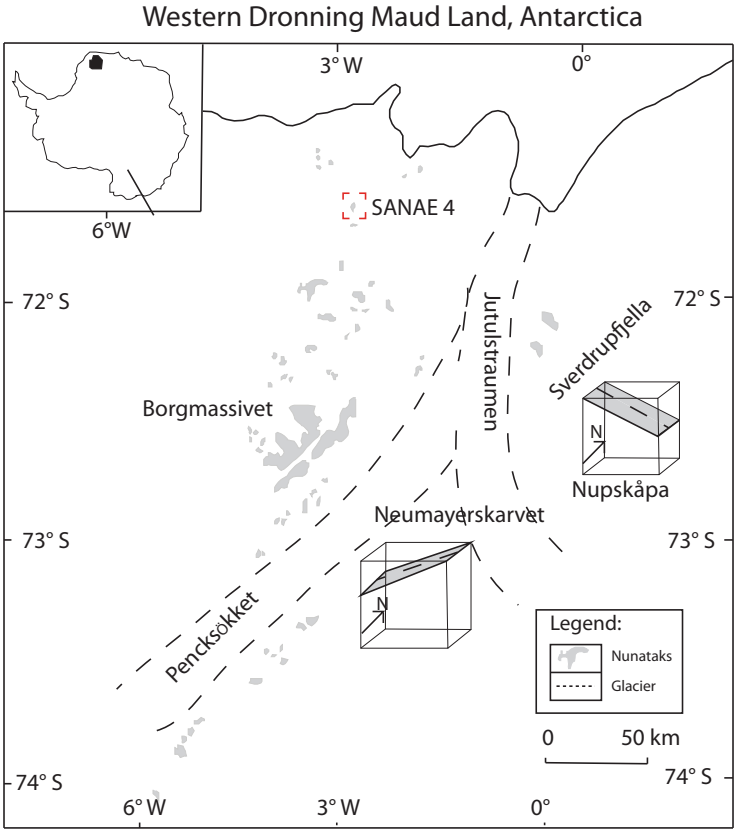

Figure 7.1: A block diagram of each of the study areas illustrating the dominant strike, dip and dip direction of the foliation and the plunge and trend of the lineations. The block diagrams are identical apart from been rotated by less than 40° around a horizontal NE/SW axis.

Figure 7.1 shows a regional map with block diagrams of the foliation and lineation of both study areas. It shows the norm of H.U. Sverdrupfjella with its shallow E or SE-dipping foliation containing its shallow SE-plunging lineations and the different Neumayerskarvet with

its shallow NW-dipping foliation and shallow NW-plunging lineation. There are a number of possible explanations for these differences in fabric orientation. The foliations and lineations are so shallow, that a rotation of less than 40° around a horizontal NE/SW axis will change the dip direction/trend of the foliation and lineation from SE to NW. There are two possible scenarios that could result in a rotation of up to 40°. One possibility is that because of the shallow nature of the foliation and lineation, large scale undulation of the foliation could result in it changing dip direction from SE to NW along with its lineation (Dumond *et al.*, 2010; Relf *et al.*, 2004). The second scenario takes into account the situation of Neumayerskarvet on a region scale, where it is separated from the rest of the Maud Belt by two major glaciers, Pencksökket and Jultulstraumen. Gravity and magnetic anomalies indicate that these glaciers cover a deep, major graben between the Grunehogna Province and the Maud Belt (Riedel *et al.*, 2012; Jacobs and Lister, 1999). Grantham (1991) proposed that this could be the site of initial thrusting that was then overprinted by normal faulting.

There are multiple combinations of normal and reverse faults, active and inactive faults, that could result in this rotation but Figure 7.2 illustrates two possible examples. It shows how a combination of two, either reverse or normal faults below the Pencksökket and Jultulstraumen glaciers could cause a rotation of Neumayerskarvet so that the foliation and lineation would change in orientation from SE to NW. For normal faults to be the cause of the rotation, the fault below the Pencksökket glacier would have to experience large displacement and the fault below the Jultulstraumen glacier would have to experience small displacement. This would result in the rotation of Neumayerskarvet's foliation and lineation on the NW side down the normal fault below the Pencksökket glacier, causing a change in orientation from SE to NW. For reverse faults to be the cause of the rotation, the fault below the Jultulstraumen glacier would have to experience large displacement and the fault below the Pencksökket glacier would have to experience small displacement. This would result in the rotation of Neumayerskarvet's foliation and lineation on the SE side up the reverse fault below the Jultulstraumen glacier, causing a change in orientation from SE to NW. This combination of two reverse faults however is unlikely to be the cause of the rotation because they would have occurred during one of the collisional orogenies that affected the region.

Observations presented in this study show that both of these collisional orogenies had a transport direction of top-to-the-NW which does not agree with the orientation of the reverse faults in Figure 7.2 which show a top-to-the-SE transport direction. A best fit scenario cannot be found between undulation and faulting because no accurate description of what lies below

the Pencksökket and Jultulstraumen glaciers is known, therefore the exhumation history is not known apart from deformation along localized structures such as faults related to the breakup of Gondwana.

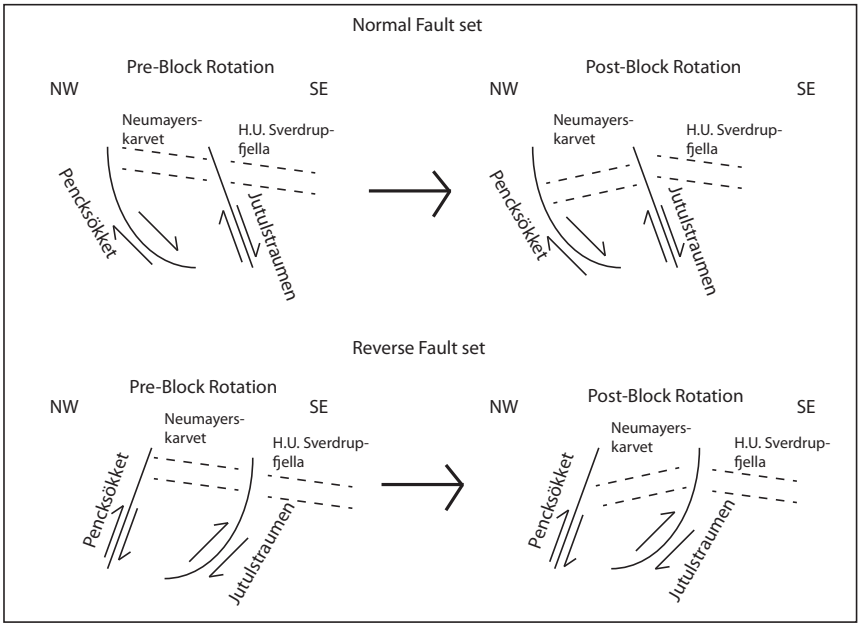

Figure 7.2: A diagram showing how two sets of thrust/normal faults below the Pencksökket and the Jultulstraumen glaciers could result in a rotation of the rocks at Neumayerskarvet.

7.4 Regional variations in geometry

The eastern section of Neumayerskarvet differs from the western section of Neumayerskarvet and H.U. Sverdrupfjella because it contains sub-vertical shear zones and steep NE-dipping foliations. H.U. Sverdrupfjella contains layers of orthogneiss but these have been transported to their current position in the duplex structure by the thrust faults. These orthogneiss layers within the duplex structure contain a sub-horizontal foliation. The strongly foliated orthogneisses in eastern Neumayerskarvet contain a strong magmatic sub-vertical foliation which suggests that they intruded pre- or syn-deformation. These granites intruded into paragneisses which mainly consist of interconnect biotite, feldspar and quartz. The granites are made up of quartz and feldspar with sporadic biotite grains. The granite is more coarse grained than the paragneiss, which is finer grained because its protolith could of been shale/mudstone. The stronger minerals and coarser grain size of the granites make it more competent than the fine grained paragneiss which is weak because of its interconnected biotite

grains (Holyoke and Tullis, 2006; Johnson *et al.*, 2004; Handy *et al.*, 1999). Therefore when stresses were applied during deformation the strain was probably partitioned more into the relatively incompetent paragneiss than the relatively competent granite. This caused the sub-horizontal shear zones to anastomose around the granite intrusions, causing the strain axes to rotate. The greatest shortening direction changed from sub-vertical in the sub-horizontal shear zone to sub-horizontal as it anastomosed around the granite intrusion causing the shear zone to become strike-slip and the foliation to steepen to sub-vertical on the boundaries of the granite intrusions (Fig. 7.3). The lineations remain sub-horizontal showing that the shear zones rotated sideways around the granite intrusions. This is the same as in a smaller scale, weak biotite grains anastomosing around competent feldspar porphyroclasts (Fig. 6.9 c). The steep domain found in eastern Neumayerskarvet is therefore not found elsewhere because it is the result of the multiple granite intrusions and these intrusions are only found in eastern Neumayerskarvet.

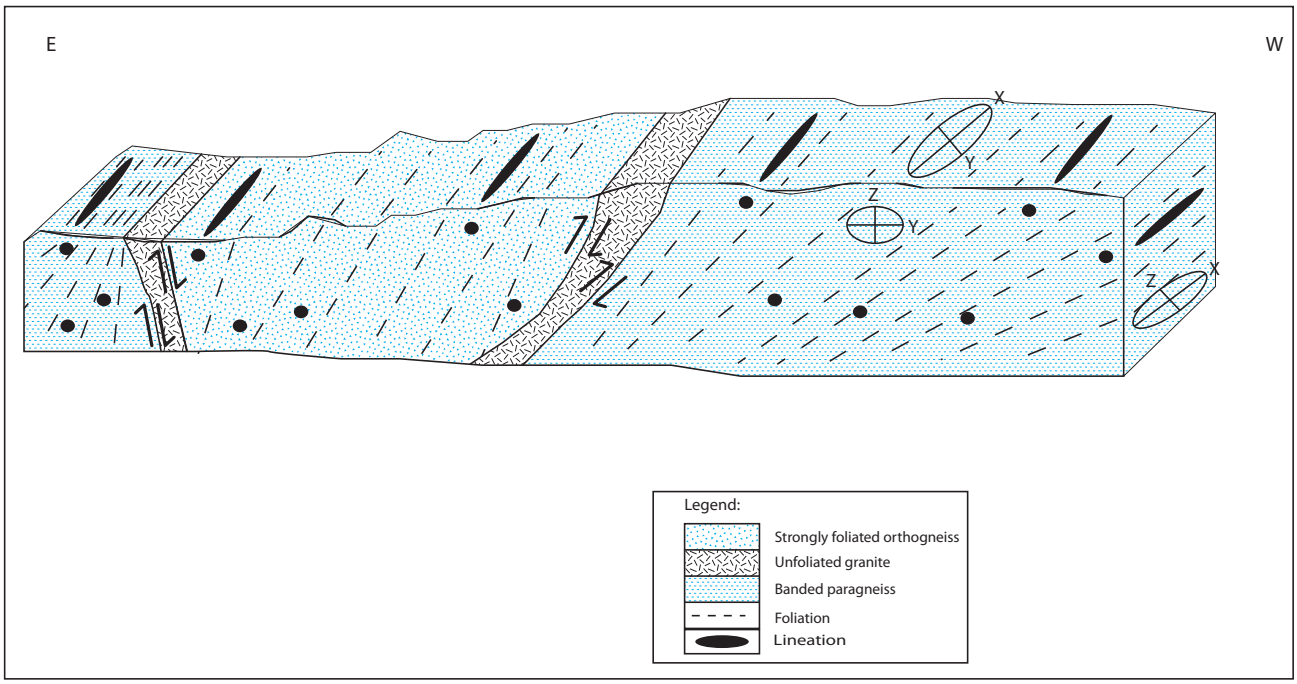

Figure 7.3: A simple sketch taken from a panorama photograph of eastern Neumayerskarvet. It illustrates how the sub-horizontal foliation steepens as it approaches the competent granite intrusion because of strain axes rotation due to strain partitioning. This results in a sub-vertical foliation, sub-horizontal lineation and a strike-slip shear zone. It also shows the two unfoliated granites intruding into the shear zones separating the strongly foliated orthogneiss from the banded paragneiss.

7.5 The possibility of an oblique crustal section

Another difference between the study areas is that Neumayerskarvet contains a larger amount of migmatite than H.U. Sverdrupfjella. This could be due to a P-T difference between the two areas. If this were the case, then Neumayerskarvet's peak metamorphism would have to be deeper and hotter than that of H.U. Sverdrupfjella's. The P-T estimates from Harris (1999), Grantham (1995), Groenewald (1995) and Board (2001) of H.U. Sverdrupfjella and Neumayerskarvet are plotted in Figure 3.5 and can be used to compare if there are any P-T differences. The estimates of previous authors do however not support the suggestion of Neumayerskarvet metamorphosing in deeper and hotter conditions than H.U. Sverdrupfjella. Further work is needed to explain the presence of more migmatite at Neumayerskarvet because it is out of the scope of this study.

Another difference between the study areas is that H.U. Sverdrupfjella has experienced more post-D_2 granite intrusions that cross-cut all structures and fabrics. The granite intrusions are post-D_2 because of their sub-vertical orientation, hinting at an extensional tectonic environment with a sub-horizontal σ_3 (least compressive stress). This extensional environment would be post-D_2 because it cross-cuts all the fabrics but not linked to the break-up of Gondwana because that was dominated by mafic intrusions (Segev, 2002). Neumayerskarvet has a local lack of these post-deformation granite intrusions.

7.6 Melt as a weakening mechanism

Neumayerskarvet does, however, have an unfoliated granite intrusion that is found within the strike-slip shear zone separating the strongly foliated orthogneiss from the paragneisses. The question is, did the strain partition into the melt or did the melt intrude into the shear zone? If the melt intruded into the contact between the orthogneiss and the paragneiss first and then the strain was partitioned into this weaker zone, then the granite would have some sort of magmatic foliation, but this is not the case. This means that the granite probably intruded post-tectonically into the weaker shear zone, separating the orthogneiss from the paragneiss, this agrees with the lack of foliation (solid or magmatic) in the granite.

Shear zones occur because of strain partitioning, this partitioning could be caused by heterogeneities in the rocks, such as weaker minerals, grain size differences, retrogression,

pre-existing fabrics and melts. The various shear zones throughout both study areas are finer grained than their host rocks and contain interconnected networks of biotite grains instead of load-bearing frameworks of quartz and feldspar. The interconnected biotite grains replacing the load-bearing frameworks of quartz and feldspar could be the result of retrogression. If fluids were present they could have caused reaction softening in the areas where they intruded. This could cause new biotite grains to form metamorphically, creating weaker zones.

In eastern Neumayerskarvet where the two unfoliated granites are found within the shear zones separating the strongly foliated orthogneiss from the banded paragneiss, the melts are not the cause of the partitioning because they intruded post-deformation and do not contain a magmatic foliation. In other areas throughout both study areas, migmatite is abundant, showing that melts could have acted as a weakening mechanism in the rocks and therefore caused strain localization. In the case of the strike-slip shear zones, heterogeneity between rocks types could be the cause, with the strain partitioning into the weaker paragneiss and anastomosing around the stronger, more competent granite. The pelitic layers within the paragneiss are weaker because they contain interconnected biotite grains which are weaker than a load-bearing framework of quartz and feldspar, this initiates weakening and strain localization.

After a yield is reached the interconnected biotite grains will begin to kink, causing portions of the grains to rotate out of the easy slip orientation, this strengthens them and causes strain hardening (Handy *et al.*, 1999; Holyoke and Tullis, 2006). In order to maintain the shear zone more weakening mechanisms need to continue strain localization and eliminate strain hardening. Subgrains of quartz, feldspars and biotite form by dynamic recrystallization to continue strain localization and maintain the weakness of the shear zone. Weakening continues by moving dislocations and kinks from the strain hardened grains by dislocation creep and then removing these dislocations and kinks by recovery and recrystallization. This results in shape changes and new grains forming that are finer grained which increases their surface area and therefore the amount of reactions that can take place with them, such as hydrolitic weakening. The new grains are also strain free compared to the wall rocks and therefore will deform more easily. This all results in strain concentrated into these weaker zones, as strain keeps being partitioned into the zones, they become weaker and weaker compared to the wall rocks.

7.7 Shear zone reactivation

Pre-existing shear zones result in zones of weakness because they are already fine grained and made up of interconnected biotite networks, these shear zones remain weaker than the surrounding country rock (Imber *et al.*, 1997). Strain from the next deformation event will partition into these initially weaker zones, if they have a favourable orientation, instead of dispersing throughout the rocks. In the two study areas no shear zones were found with the 080° trending lineation within them, this could mean that if D_1 shear zones existed, they could have acted as zones of weakness for strain to be partitioned into during D_2. This could result in sufficient strain in these initially weak zones that it totally overprints or transposes the initial fabric, therefore only leaving behind the most recently developed fabric (140° trending lineation). If this is the case then outside of the shear zones the amount of strain would be less and that is why L_1 is still found, because the D_2 fabric was not pervasive enough to totally overprint it. The other option is that the strain during D_1 was broadly distributed and not partitioned into shear zones, this would explain why no shear zones with a 080° trending lineation are found. If this is the case there could still be zones that are slightly weaker than the surrounding rock and during D_2 the strain may have partitioned into these weakened zones.

7.8 Estimates of strain rate

In order to estimate the strain rate that the rocks experienced in and around the shear zones, Shimizu's (2008) piezometer is used in combination with Hirth et al.'s (2001) quartz flow law. These methods were combined by Boutonnet et al. (2013) to use estimates of subgrain sizes, temperature and pressure to work out the differential stress and then strain rate that the rocks experienced. This method is used because of the lack of reliable deformation rate measurements in the deep crust (Boutonnet *et al.*, 2013). Piezometers use average subgrain sizes formed by dynamic recrystallization, temperature and some empirically determined constants to work out the differential stress in the rocks. The quartz flow law uses differential stress, temperature and water fugacity along with empirical constants to calculate strain rates (Boutonnet *et al.*, 2013; Shimizu, 2008; Hirth *et al.*, 2001). Board's (2001) P-T estimates (T=680°C, P=7.8kbar) were used because it is the most recent paper and it focuses on an area close to the study areas, the water fugacity (802MPa) was calculated using Tony Withers

Fugacity Calculator based on Sterner and Pitzer, (1994). Subgrains were measured in thin sections from Alan Piggen (Fig. 5.7) and from a minor shear zone within an orthogneiss unit in H.U. Sverdrupfjella (Fig. 6.1). Alan Piggen contains two major shear zones that separate ortho- and parageniss layers, the shear zones, named lower (average size = 103 μm, n=24, s.d.=38 μm) and upper (average size = 128 μm, n=24, s.d.=61 μm), contain finer-grained subgrains than the host rock (average size = 204 μm, n=24, s.d.=74 μm). Above the lower shear zone in the orthogneiss layer the subgrains have an average size of 149 μm (n=25, s.d.=50 μm), this is coarser than within the shear zones but still finer than the average host rock. Consequently, applying the piezometer to these subgrain sizes, the differential stress experienced in the shear zones (lower: σ=18 MPa, upper: σ=15 MPa) is greater than in the host rock (σ=10 MPa). The host rock close to the lower shear zone has experienced higher differential stress (σ=13MPa) than further away because of its close proximity to the shear zone. Using the quartz flow law the strain rates of the four samples are calculated, both shear zones (lower:$\dot{\varepsilon}$=2.1x10$^{-11}s^{-1}$, upper:$\dot{\varepsilon}$=1.0x10$^{-11}s^{-1}$) have experienced higher strain rates than the sample in the middle of the host rock ($\dot{\varepsilon}$=2.3x10$^{-12}s^{-1}$). The sample taken just above the lower shear zone ($\dot{\varepsilon}$=6.5x10$^{-12}s^{-1}$) reflects higher strain rates than the rest of the host rocks (Fig. 7.4).

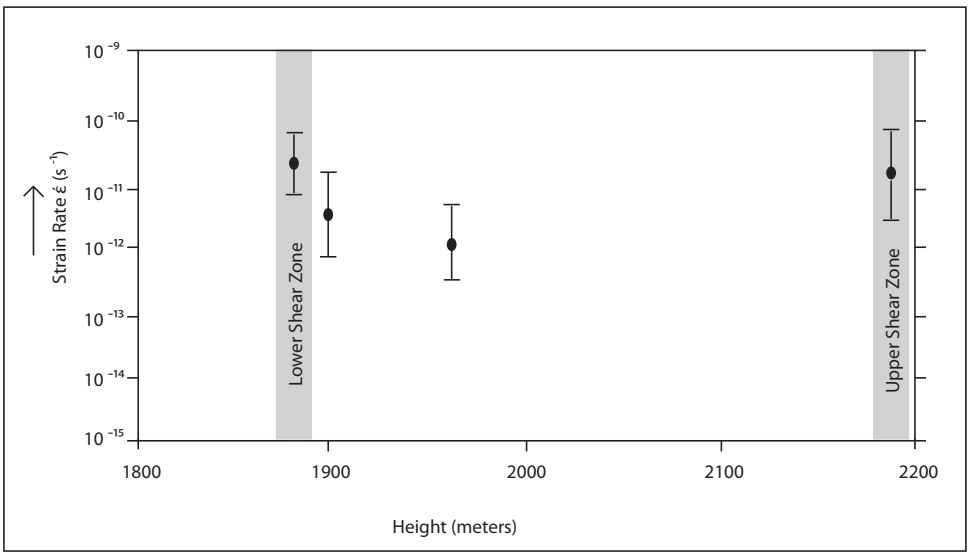

Figure 7.4: Graph comparing strain rates within shear zones and host rocks on Alan Piggen, H.U. Sverdrupfjella. The subgrains are finer within the shear zones because of the higher strain rates and more coarse grained in the host rock because of less strain. Standard deviation has been added to each sample to show its accuracy.

A minor shear zone within a orthogneiss layer at H.U. Sverdrupfjella (Fig. 6.1) shows a variation in grain size, with the centre of the shear zone containing fine grained minerals and further away from the centre the grains progressively become coarser. The subgrains replicate this with mylonite in the centre of the shear zone containing fine subgrains (average size = 124μm, n=11, s.d.=50μm), further away from the shear zone the subgrains become coarser, from an average size of 217μm (n=9, s.d.=62μm) to 318μm (n=6, s.d.=50μm) and the coarsest area having subgrains as large as 388μm (n=9, s.d.=97μm). These subgrain sizes are used to determine the variation in differential stress and strain rate within and around this minor shear zone. The differential stress varies from σ=29MPa in the centre of the shear zone to σ=12MPa on the outskirts. Figure 7.5 shows the variation in strain rate across the shear zone, with the standard deviation attached to each area, the central area of the shear zone has experienced the highest strain rates ($\dot{\varepsilon}$=1.2x10$^{-10}s^{-1}$). The strain rate lessens further away from the shear zone, corresponding with the change from mylonite to protomylonite rocks.

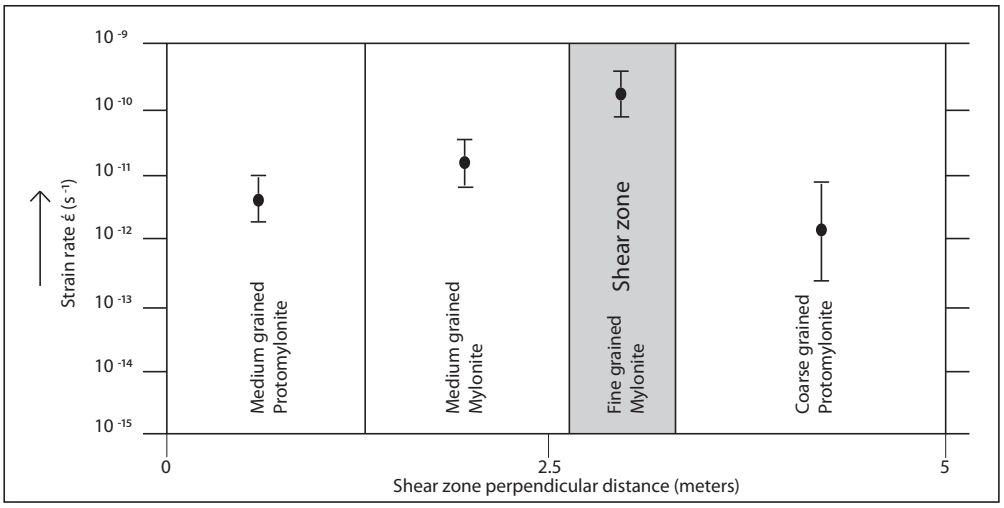

Figure 7.5: A graph showing strain rates from a minor shear zone within a orthogneiss layer. The coarser grained, protomylonite areas have experienced less strain than the finer grained, mylonite areas in the centre of the shear zone.

In both study areas the shear zones contain finer subgrains than the host rock. In close proximity to the shear zones the subgrains are finer than the average host rock size. This is due to the shear zones experiencing higher differential stress than the host rock and because of the close proximity of the sample to the lower shear zone, it too experienced more differential stress than the average host rock. Both graphs show that because of the finer subgrain size

and higher differential stress within the shear zones that they have experienced higher strain rates than the host rock. This shows that the rocks of the study areas have experienced strain partitioning, with thin shear zones experiencing higher strain rates than the surrounding host rock. The shear zones that experience the higher strain rate have finer grains and subgrains and frequently also contain a large portion of interconnected biotite grains. The feldspar grains within the shear zones also contain more deformation twins than in the host rock, deformation twins require relatively high differential stress. The field observations also agree with high strain within the shear zones because the foliation has been rotated to lie sub-parallel to the shear zone boundaries (Worley and Wilson, 1996).

However the graphs show that the minor shear zone experienced higher strain rates than the major shear zone, this is due to the methods used to calculate the strain rates. The methods use the size of quartz subgrains to work out the differential stress and strain rate, but most of the major shear zones contain a large portion of interconnected biotite grains which will take up more strain than the quartz grains. For the major shear zones where interconnected biotite grains take up most of the strain, the method will not be accurate because the method assumes quartz is taking up the strain. The minor shear zone appears within an orthogneiss layer, it therefore does not contain interconnected biotite grains and the quartz will take up the majority of the strain, the method will therefore be more accurate for it because quartz is taking the majority of the strain in the rock. The graphs do however still show a good trend of the shear zones having the highest strain rates and this progressively getting less away from the shear zone into the host rock. Deformation twins require >250MPa differential stress to form in plagioclase grains, the values calculated above are more in the region of 25MPa, yet the deformation twins are abundant throughout the study areas. The reason for this is that the differential stress values calculated are for quartz and the deformation twins are found in feldspars which can sustain higher stresses, the required high differential stress values could have been reached locally by colliding grains.

Figures 6.4 a and b, 6.5 c and d, 6.9 a and c, show that within the shear zones, along the 140° trending lineation, the grains are elongated and in the host rock the grains are flattened and more euhedral in shape (Figs. 6.4 e and f, 6.8 c and d). This plots the strain in the shear zones in the prolate region of the Flinn diagram (Fig. 2.7) and the strain in the host rock in the oblate region.

Within the shear zones the only lineation that is found has a trend of 140° or 320° and a shallow plunge of a few degrees. This along with the fact that all the shear sense indicators,

S-C fabrics, asymmetric folds and mantled porphyroclasts show a top-to-the-NW transport direction only, suggests that the shear zones only experienced shearing in one direction. If the shear zones had resulted from pure shear, then there would be an even spread of transport directions. The shear zones therefore resulted because of predominant simple shearing. The host rocks also only have a top-to-the-NW sense of shear but they contain a lineation and strong foliation which could be the result of a mixture of pure and simple shear or less strain from simple shear (Lister and Snoke, 1984; Lister and Williams, 1983).

7.9 Strain axes

Figure 7.6 displays stereoplots from within shear zones and the host rocks around them. The lineations from L_1 have been removed in order to determine the strain axes for each stereoplot for the most recent deformation event (L_2). The axes of the finite strain ellipse have been plotted on the stereoplots, X=the direction of greatest elongation, Y=intermediate direction and Z=the direction of greatest shortening. The shear zone lineation measurements are more tightly clustered compared to the host rock but they are all very uniform in SE- and NW-trends. Both H.U. Sverdrupfjella stereoplots have a SE-trending sub-horizontal X direction and a sub-vertical Z direction, the Y direction is also sub-horizontal and NE-trending (Fig. 7.6 e and f).

The stereoplots from the sub-horizontal shear zones and host rock at western Neumayerskarvet are similar to the stereoplots of H.U. Sverdrupfjella, also all having a shallow SE/NW-plunging lineation and a sub-horizontal foliation. Both stereoplots have sub-horizontal X direction and sub-horizontal Y directions with a sub-vertical Z direction (Fig. 7.6 a and c). The difference between the host rock and shear zone of western Neumayerskarvet is that the the shear zones have a SE-trending sub-horizontal X direction and a NE-trending sub-horizontal Y direction. The host rocks have a NW-trending sub-horizontal X direction and a SW-trending sub-horizontal Y direction. This makes the host rock of Neumayerskarvet different to the rocks of H.U. Sverdrupfjella. The eastern section of Neumayerskarvet differs from the rest of the rocks because it contains sub-vertical foliations. It has a SE-trending sub-horizontal X direction and a SW-trending sub-horizontal Z direction, with a NE-trending sub-vertical Y direction (Fig. 7.6 b and d). The shear zone in the eastern section of Neumayerskarvet is steeper than the host rocks and therefore its Z direction is shallower than in the

host rocks and its Y direction is steeper than the host rocks.

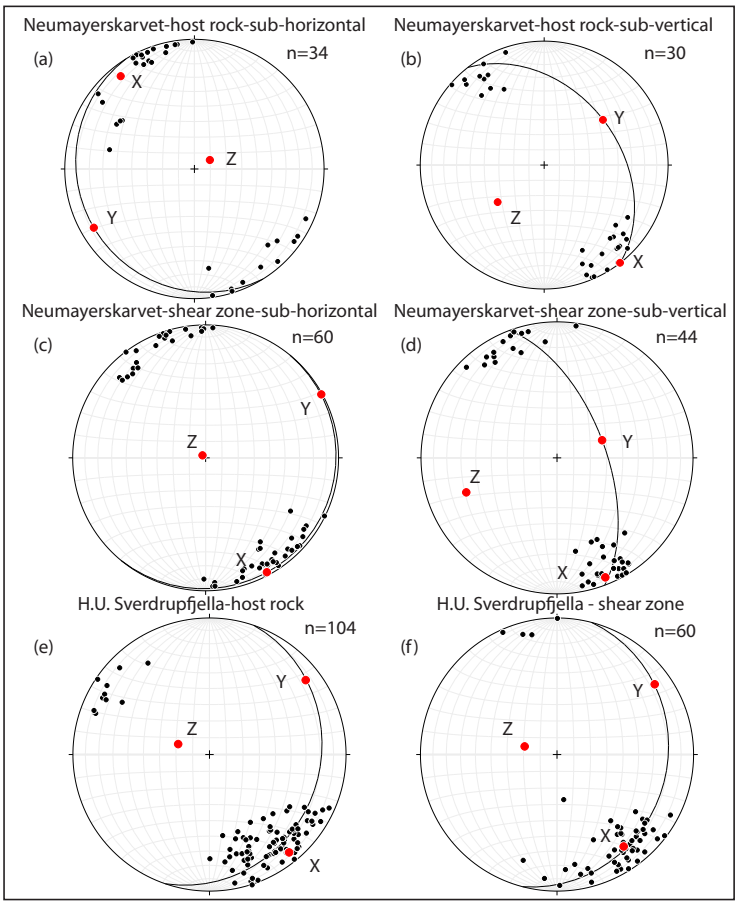

Figure 7.6: All L_2 lineations displayed on lower hemisphere, equal area stereoplots, for within shear zones and in host rocks. The average lineation is displayed as a red dot and was worked out using the conical best fit function in Stereonet 8. The average foliation plane, worked out using the mean vector function in Stereonet 8, is also displayed. The inferred strain axes have been added to the stereoplots, X=greatest extension direction, Y=intermediate direction, Z=greatest shortening direction.

Table 7.1: Table comparing the strain axes of all of the stereoplots in (Fig. 7.6).

	Strain Axes		
	X	Y	Z
Neumayerskarvet - host rock - sub-horizontal:	321°/09°	240°/11°	058°/78°
Neumayerskarvet - shear zone - sub-horizontal:	151°/03°	061°/01°	309°/87°
Neumayerskarvet - host rock - sub-vertical:	142°/00°	052°/40°	232°/50°
Neumayerskarvet - shear zone - sub-vertical:	158°/06°	068°/61°	249°/29°
H.U. Sverdrupfjella - host rock:	140°/08°	052°/12°	288°/70°
H.U. Sverdrupfjella -shear zone:	144°/18°	054°/13°	284°/69°

7.10 Synthesis of P-T-deformation history

In modern/active collisional orogens such as the Alpine Fault Zone , New Zealand, and the Himalayas, the average depth of the brittle-ductile transition is 6-13 km with temperatures ranging between 310 - 500°C and a geothermal gradient of 40 - 60°C/km (Holm *et al.*, 1989; Zeitler *et al.*, 2001; Henry *et al.*, 1997). The geothermal gradient of the Maud Belt was most likely similar to that of New Zealand and the Himalayas because they are all orogenic collisional zones. The depth of the brittle-ductile transitional zone will therefore be similar because of the similar geothermal gradient assuming similar composition, strain rate, fluid pressure etc.. This geothermal gradient of 40 - 60°C/km was warmer than the average stable continental crust geothermal gradient (25°C/km) because it was within an active collisional margin. Active collisional margins have warmer geothermal gradients because they have higher heat flows because of deep fault zones, magmatic intrusions or active tectonic forces (England and Thompson, 1984).

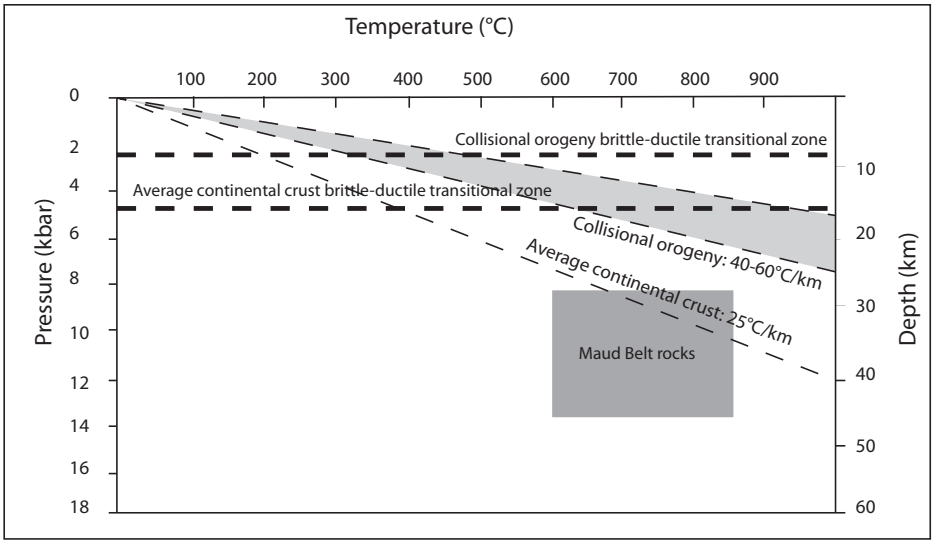

Figure 7.7: The figure shows the average continental crustal geothermal gradient of (25°C/km) and the warmer geothermal gradient (40 - 60°C/km) of a collisional orogeny such as New Zealand and the Himalayas. The brittle-ductile transitional zone for both of these geothermal gradients is plotted along with the P-T position of the Maud Belt rocks. This shows that actually the rocks of the Maud Belt plot on a cooler geothermal gradient than the collisional orogenies and the average continental crust. Even with this cooler geothermal gradient for the Maud Belt, the rocks are still situated well below any brittle-ductile transitional zone.

Figure 7.7 shows the average geothermal gradient of both continental crust and collisional

orogenies, along with position of the rocks from the Maud Belt. The P-T conditions calculated for the rocks of the Maud Belt (P = 8-14 kbar, T = 600°C - 850°C (Board, 2001; Grantham *et al.*, 1995; Groenewald *et al.*, 1995)) are situated below both of the geothermal gradients, this means that the rocks of the Maud Belt experienced a cooler geothermal gradient than collisional orogenies and the average continental crust. Even with the relatively cool geothermal gradient of the Maud Belt, the rocks are well below any brittle-ductile transition zone and will experience ductile deformation. This agrees with the field observations of the rocks and the microstructures that were studied in thin section.

The minerals (albite, epidote, quartz, feldspar, hornblende, silliminite and biotite) that define the fabrics in D_1 and D_2 in both study areas represent amphibolite facies metamorphic conditions (Powell, 1983). Previous authors describe the Grenvillian orogeny as experiencing initially high pressure eclogite facies conditions and then granulite to amphibolite facies conditions, and the Pan-African orogeny as experiencing amphibolite facies conditions (Tab. 3.1) (Grantham *et al.*, 1995; Groenewald *et al.*, 1995; Board, 2001). It is hard to separate D_1 and D_2 on metamorphic grade because this amphibolite facies grade corresponds to the grades inferred for both major orogenies that affected the region. Using the structural separation of D_1 and D_2 by their lineations and the presence of only L_2 in the shear zones, L_2 is assigned to D_2, the youngest deformation phase to affect the region. L_1 is then assigned to an older deformation phase, D_1. D_2 is the youngest and therefore most likely associated with the Pan-African orogeny($\sim$600 Ma to $\sim$450 Ma), D_1 is partially overprinted by D_2 and therefore older, it is most likely associated with the Grenvillian orogeny ($\sim$1300 Ma to $\sim$900 Ma).

This all shows that initial deformation is spread more widely through an area because there are usually no prior weakened areas, unless there is composition heterogeneity. This initial strain will cause areas to weaken, via the various mechanisms, compared to their surrounding rocks. During the next deformation event, strain will partition into these areas that were weakened during the earlier deformation event. Strain will localize into these weakened areas and be less influential in the surrounding rocks. In this way strain from an earlier deformation phase is widely spread throughout the rock and strain from a younger deformation phase is more localized. This is clearly seen in the Maud Belt and specifically H.U. Sverdrupfjella and Neumayerskarvet, where D_2 associated with the younger Pan-African orogeny is localized in the shear zones and D_1 associated with the older Grenvillian orogeny is found throughout the host rock along side D_2. This shows that most of the strain in D_2 was localized into the shear zones, overprinting D_1 and in the host rock D_2 was less influential and only partially

overprinted D_1. This will most likely also occur in other regions that experience multiple deformation phases and it shows that previous fabrics are effective at strain partitioning.

Chapter 8

Conclusions

Both field areas consist mainly of orthogneisses and paragneisses. The orthogniess is made up of the major minerals feldspar and quartz, with minor biotite, and in places hornblende, apatite and garnet. The paragneiss predominantly consists of biotite and quartz, with minor feldspar, and in places hornblende, epidote, gedrite, garnet, muscovite and sillimanite. The two study areas contain migmatite and granite intrusions but with Neumayerskarvet containing more migmatite than H.U. Sverdrupfjella and H.U. Sverdrupfjella more granite intrusions than Neumayerskarvet.

Shear zones are found throughout the two study areas. Major shear zones separate the orthogneiss and paragneiss rock types and minor shear zones occur within these rocks. In Sverdrupfjella and western Neumayerskarvet the shear zones are sub-horizontal, striking NE/SW. In eastern Neumayerskarvet the shear zones are sub-vertical strike-slip shear zones.

Both areas contain well-developed lineations and foliations. The foliation is commonly defined by biotite, and in places quartz. The lineation is commonly defined by elongated quartz grains and in places epidote, hornblende and sillimanite. The lineation often forms down dip in the biotite foliation. At least two deformation phases were found to have affected the study areas. This is inferred from the presence of two differently orientated lineations. The stronger, more prevalent lineation plunges shallowly SE and the weaker, less common lineation plunges shallowly E.

In Sverdrupfjella, the S_{1+2} foliation dips shallowly SE and the lineations also plunge shal-

lowly SE/E. In western Neumayerskarvet the S_{1+2} foliation dips shallowly SE or NW, with the lineation plunging SE or NW. Eastern Neumayerskarvet differs from the other study areas because the foliation steepens to sub-vertical. The lineation however remains sub-horizontal and plunging gently/shallowly SE, much the same as western Neumayerskarvet. The E-trending lineation is found only within the host rock and is always alongside the SE-trending lineation but only the SE-trending lineation is found within the shear zones. The shear zones have deformed the host rock which contains both the E- and SE-trending lineations and the shear zones only contain the SE-trending lineation. This implies that the SE-trending lineation could be linked to the more recent deformation event that affected the study areas. Therefore L_1 is defined as plunging shallowly east and L_2 as plunging shallowly SE.

All shear sense indicators in the study areas show a top-to-the-NW transport direction which shows a consistent component of simple shear. This does not agree with Grantham's (1995) findings of top-to-the-SE transport directions in western Sverdrupfjella for the Pan-African orogeny. This could be due to a variation in deformation across the region or that top-to-the-SE shear sense indicators were not found in the study areas.

Eastern Neumayerskarvet contains large orthogneiss units, which are made up mainly of coarse grains of quartz and feldspar. Surrounding the orthogneiss units is a finer grained paragneiss that has a higher proportion of biotite than the orthogniesses. The coarser grained orthogneiss is more competent than the finer, biotite rich, paragneiss alongside it and therefore strain would tend to localize in the less competent paragneiss units. As the paragneiss deforms to go around the competent orthogneiss, the thrust shear zones change to sub-vertical strike-slip shear zones. The shortening direction also changes orientation which causes the sub-horizontal foliation to become sub-vertical. The strain partitioning in eastern Neumayerskarvet is caused by the proportion of competent minerals in the rock types, the orthogniess containing higher proportions of quartz and feldspar than the paragneiss. Other controls on strain partitioning that were inferred in the study areas are grain size, retrogression, melt and pre-existing fabrics. Commonly within the shear zones the grain size is finer than within the host rock, indicating that strain could have been partitioned into the finer grains. In places in the minor shear zones, muscovite is found, which is the result of retrogression because the rocks peak T is above the muscovite stability field. The presence of muscovite in places only within the minor shear zones could indicate that strain was partitioned into retrogressed areas. Traces of leucosome are commonly found within shear zones, indicating that strain

could have been partitioned into these weakend zones.

Previous fabrics could have also contributed to strain partitioning. This is inferred by the presence of a transposed S_{1+2} foliation. The transposed S_{1+2} foliation could indicate that the strain of D_2 might have partitioned into the same orientation as S_1 because it has already experienced deformation softening.

The interpretation that the SE-trending lineation is associated with D_2 and that it is the only lineation found within the shear zones, infers that it could be the result of the most recent deformation phase to affect the region. D_2 is therefore interpreted to be associated to the Pan-African orogeny and the weaker L_1, associated to D_1, is interpreted as the Grenvillian orogeny.

The study areas illustrate how strain from multiple deformation phases can be partitioned differently. The strain from the earlier deformation is distributed broadly throughout the rocks of the study areas, resulting in a weak, L_1, lineation and foliation throughout the rocks. The strain from the more recent deformation is concentrated into narrow shear zones, resulting in a well-developed, L_2, lineation that appears alongside L_1 in the host rock but is alone within the shear zones and a transposed S_{1+2} foliation. This illustrating how strain from the more recent deformation is localized into already weakened zones by earlier deformation. Strain was partitioned into areas that had pre-existing fabrics, finer grain sizes, retrogressed minerals and areas with melt present because these are weaker than the surrounding rocks. Earlier strain distribution broadly throughout the rocks and then more recent strain concentrating into narrow shear zones could be typical of areas that have experienced multiple deformation phases such as the Wenchuan-Maowen Shear zone in the Tibetan Plateau (Worley and Wilson, 1996).

References

Arzi, A. (1978). Critical phenomena in the rheology of partially melt rocks. *Tectonophysics*, *44*, 173–184.

Barton, J., Klemd, R., Allsopp, H., Auret, S., and Copperthwaite, Y. (1987). The geology and geochronology of the Annandagstoppane granite, western Dronning Maud Land, Antarctica. *Contribution Mineral Petrology*, *97*, 488–496.

Bell, T. (1978). Progressive deformation and reorientation of fold axes in a ductile mylonite zone: the woodroffe thrust. *Tectonophysics*, *44*, 285–320.

Berthe, D., Choukroune, P., and Jegouzo, P. (1979). Orthogneiss, mylonite and non coaxial deformation of granites: The example of South Armorican shear zone. *Journal of Structural Geology*, *1*, 31–42.

Blenkinsop, T. and Treloar, P. (1995). Geometry, classification and kinematics of S-C and S-C' fabrics in the Mushandike area, Zimbabwe. *Journal of Structural Geology*, *17*, 397–408.

Board, W. (2001). *Tectonothermal evolution of the southern H.U. Sverdrupfjella, western Dronning Maud Land, Antarctica*. Ph. D. thesis, Cape Town: Department of Geological Sciences University of Cape Town.

Boutonnet, E., Leloup, P., Sassier, C., Gardien, V., and Ricard, Y. (2013). Ductile strain rate measurements document long-term strain localization in the continental crust. *Geology*, *41*, 819–822.

Burkhard, M. (1993). Calcite twins, their geometry, appearance and significance as stress-strain markers and indicators of tectonic regime. *Journal of Structural Geology*, *15*, 351–368.

Butler, R. (1982). The terminology of structures in thrust belts. *Journal of Structural Geology*, *4*, 239–245.

Carreras, J. (2001). Zooming on Northern Cap de Creus shear zones. *Journal of Structural Geology*, *23*, 1457–1486.

Coney, P., Edwards, A., Hine, R., Morrison, F., and Windrim, D. (1990). The regional tectonic of the Tasman orogenic system, east Australia. , *12*, 519–543.

Cosgrove, J. (2007). *The Antarctica zones and structures as kinematic indicators: a review.* Ph. D. thesis, London: Department of earth science and engineering, Royal School of Mines, Imperial College.

Craddock, J., Jackson, M., van der Pluijm, B., and Versical, R. (1993). Regional shortening fabrics in Eastern North America: Far-field stress transmission from the Appalachian-Ouachita Orogenic Belt. *Tectonics*, *12*, 257–264.

Davis, G., Reynolds, S., and Kluth, C. (2012). *Structural Geology of Rocks and Regions.* John Wiley & Sons.

Dumond, G., Goncalves, P., Williams, M., and Jercinovic, M. (2010). Subhorizontal fabric in exhumed continental lower crust and implications for lower crustal flow: Athabasca granulite terrane, western Canadian Shield. *Tectonics*, *29*, 1–32.

Durney, D. (1972). Solution-transfer, an Important Geological Deformation Mecahnism. *Nature*, *235*, 315–318.

England, P. and Thompson, A. (1984). Pressure-Temperature-Time Paths of Regional Metamorphism I. Heat Transfer during the Evolution of Regions of Thickened Continental Crust. *Journal of Petrology*, *25*, 894–928.

Fagereng, A. and Diener, J. (2011). San Andreas Fault tremor and retrograde metamorphism. Technical report, Geophysical Research Letters.

Ferrar, G. (1995). The metamorphic geology of the Armalsryggen, northern Kirwanweggen, western Dronning Maud Land, Antarctica. Master's thesis, Pietermaritzburg: University of Natal.

Fitzsimons, I. (2000). A review of tectonic events in the East Antarctic Shield and their implications for Gondwana and earlier supercontinents. *Journal of African Earth Science*, *31*, 3–23.

Flinn, D. (1962). On fold during three-dimensional progressive deformation. *Quarterly Journal of the Geological Society of London*, *118*, 385–428.

Goodwin, L. and Tikoff, B. (2002). Compentacy contrast, kinematic, and the development of foliations and lineations in the crust. *Journal of Structural Geology*, *24*, 1065–1085.

Grantham, G. (1992). *Geological evolution of western H.U. Sverdrupfjella, Dronning Maud Land, Antarctica*. Ph. D. thesis, Pietermaritzburg: University of Natal.

Grantham, G., Groenewald, P., and Hunter, D. (1988). Geology of the northern H.U. Sverdrupfjella, western Dronning Maud Land, and implications for Gondwana reconstructions. *South African Journal Ant. Res*, *18*, 2–10.

Grantham, G., Groenewald, P., and Moyes, A. (1995). The geology of the granitoids of the western Sverdrupfjella and Kirwanweggen, western Dronning Maud Land, Antarctica. In *Siena, Italy: VIIth International Symposium on Antarctic earth Sciences*.

Grantham, G., Moyes, A., and Hunter, D. (1991). The age, petrogenesis and emplacement of the Dalmatian Granite, H.U. Sverdrupfjella, Dronning Maud Land, Antarctica. *Antarctic Science*, *3*, 197–204.

Gratier, J., Dysthe, D., and Renard, F. (2013). The role of pressure solution creep in the ductility of the Earth's upper crust. *Advances in Geophysics*, *54*, 47–179.

Gratier, J., Guiguet, R., Renard, F., Jenatton, L., and Bernard, D. (2009). A pressure solution creep law of quartz from identation experiemnets. *Journal of Geophysical Research*, *114*, 1–16.

Groenewald, P. (1995). *The geology of northern H.U. Sverdrupfjella and its bearing on crustal evolution in Dronning Maud Land, Antarctica - unpublished*. Ph. D. thesis, Pietermaritzburg: University of Natal.

Groenewald, P., Moyes, A., Grantham, G., and Krynauw, J. (1995). East Antarctic crustal evolution: geological constraits and model in western Dronning Maud Land. *Precambrian Research*, *75*, 231–250.

Groshong, R. (1988). Low temperature deformation mechanisms and their interpretation. *Geological Society of America Bulletin*, *100*, 1329–1360.

Halpern, M. (1970). Rubidium-strontium date of possibly 3 billion years for a granitic rock from Antartctica. *Science*, *169*, 977–978.

Handy, M., Wissing, S., and Streit, L. (1999). Frictional-viscous flow in mylonite with varied bimineralic composition and its effect on lithospheric strength. *Tectonophysics*, *303*, 175–191.

Hanmer, S., Williams, M., and Kopf, C. (1995). Modest movements, spectacular fabrics in an intracontinental deep-crustal strike-slip fault: Striding-Athabasca mylonite zone, NW Canadian Shield. *Journal of Structural Geology*, *17*, 493–507.

Harris, C. and Grantham, G. (1993). Geology and petrogenesis of the Straumsvola nepheline syenite complex, Dronning Maud Land, Antarctica. *Geology Magazine*, *130*, 513–532.

Harris, P. (1999). *The geological evolution of Neumayerskarvet in the northern Kirwanveggen, western Dronning Maud Land, Antarctica*. Ph. D. thesis, Johannesburg: Rand Afrikaans University.

Henry, P., Pichon, X., and Goffe, B. (1997). Kinematics, thermal and petrological model of the Himalaya: constraints related to metamorphism within the underthrust Indian crust and topographic elevation. *Tectonophysics*, *273*, 31–56.

Hirth, G., Teyssier, C., and Dunlap, W. (2001). An evaluation of quartzite flow laws based on comparisons between experimentally and naturally deformed rocks. *International Journal Earth Science*, *90*, 77–87.

Hoffman, P. (1991). Did the breakout of Laurentia turn Gondwana inside-out? *Science*, *252*, 1409–1412.

Holm, D., Norris, R., and Craw, D. (1989). Brittle and ductile deformation in a zone of rapid uplift: Central Southern Alps, New Zealand. *Tectonics*, *8*, 153–168.

Holyoke, C. and Tullis, J. (2006). Formation and maintenance of shear zones. *Geology*, *34*, 105–108.

Hudleston, P. (1999). Strain compatibilty and shear zones: is there a problem. *Journal of Structural Geology*, *21*, 923–932.

Imber, J., Holdsworth, R., Butler, C., and Lloyd, G. (1997). Fault-zone weakening processes along the reactivated Outer Herbrides Fault Zone, Scotland. *Journal of the Geological Society*, *154*, 105–109.

Jackson, C. and Jacobs, J. (1995). Reconciliation of the kinematics and timing of deformation in concontrast structural domian within 1.1 Ga terrains of western Dronning Maud Land. In *VIIth International Symposium on Antarctic Earth Sciences*.

Jacobs, J. and Lister, F. (1999). Post-Permian tectono-thermal evolution of western Dronning Maud Land, E-Antarctica: an apatite fission-track approach. *Antarctic Science*, *11*, 451–460.

Jefferies, S., Holdsworth, R., Wibberley, C., Shimamoto, T., Spiers, C., Niemeijer, A., and Lloyd, G. (2006). The nature and importance of phyllonite development in crustal-scale fault cores: An example from the Median Tectonic Line, Japan. *Journal of Structural Geology*, *28*, 220–235.

Ji, S., Jiang, Z., Rybacki, E., Wirth, R., Prior, D., and Xia, B. (2004). Strain softening and microstructual evolution of anorthite aggregates and quartz-anorthite layered composites deformed in torsion. *Earth Planet Science Letter*, *222*, 377–390.

Johnson, S., Vernon, R., and Upton, P. (2004). Foliation development and progressive strain-rate partitioning in the crystallizing carapace of a tonalite pluton: microstructual evidence and numerical modeling. *Journal of Structural Geology*, *26*, 1845–1865.

Kronenberg, A. (1994). Hydrogen speciation and chemical weakening of quartz. In: Heaney PJ, Prewitt CT, Gibbs GV (eds) Silica: physical behavoir, geochemistry, and materials applications. *Mineral Soc Am Rev Mineral*, *29*, 123–176.

Krynauw, J. (1996). A review of geology of East Antarctica, with special reference to the c. 1000 Ma and c. 500 Ma events. *Terra Antarctica*, *3*, 77–89.

Krynauw, J., Behr, H., and van den Kerkhof, A. (1994). Sill emplacement in wet sediments: fluid inclusions and cathodoluminescence studies at Grunehogna, western Dronning Maud Land, Antarctica. *Journal of Geological Society*, *151*, 331–344.

Küster, M. and Stöckhert, B. (1999). High differential stress and sublithostatic pore fluid

pressure in the ductile regime - microstructural evidence for short-term post-seismic creep in the Sesia Zone, Western Alps. *Tectonophysics*, *303*, 263–277.

Lister, G. and Snoke, A. (1984). S-C Mylonites. *Journal of Structural Geology*, *6*, 617–638.

Lister, G. and Williams, P. (1983). The partioning of deformation in flowing rock masses. *Tectonophysics*, *92*, 1–33.

McClay, K. (1991). *Glossary of thrust tectonic terms.* Chapman & Hall.

Mitra, G. (1978). Ductile deformation zones and mylonites: the mechanical processes involved in the deformation of crystalline basement rocks. *Am J Sci*, *278*, 1057–1084.

Montesi, L. (2013). Fabric development as the key for forming ductile shear zones and enabling plate tectonics. *Journal of Structural Geology*, In press.

Moyes, A., Krynauw, J., and Barton, J. (1995). The age of the Ritschersflya Supergroup and Borgmassivet intrusions, Dronning Maud Land, Antarctica. *Antarctic Science*, *7*, 87–97.

Passchier, C. (1994). Mixing in flow Perturbations: a model for development of mantled porphyroclasts in mylonites. *Journal of Structural Geology*, *16*, 733–736.

Passchier, C. and Simpson, C. (1986). Porphyroclast system as kinematic indicators. *Journal of Structural Geology*, *8*, 831–843.

Passchier, C. and Sokoutis, D. (1993). Experimental model of mantled porphyroclasts. *Journal of Structural Geology*, *15*, 895–909.

Passchier, C.W. & Trouw, R. (2005). *Microtectonics.* Springer.

Platt, J. and Behr, V. (2011). Lithospheric shear zones as constant stress experiments. *Geology*, *39*, 127–130.

Post, A. and Tullis, J. (1998). The rate of water penetration in experimentally deformed quartzite: Implications for hydrolytic weakening. *Tectonophysics*, *295*, 117–137.

Powell, R. (1983). Fluids and melting under upper amphibolite facies conditions. *Journal of Geological Society*, *140*, 629–633.

Ramsay, J. (1980). Shear Zone Geology: a review. *Journal of Structural Geology*, *2(1/2)*, 83–99.

Relf, C., Patterson, M., Nykipilo, G., Krauss, C., McCollum, D., Weisbeck, G., and Smart, K. (2004). New insights into geology of the Lac du Sauvage area, NWT. Master's thesis, Geoscience Office, Yellowknife and Department of Earth and Atmospheric Sciences, University of Alberta.

Riedel, S., Jacobs, J., and Jokat, W. (2012). Interpretation of new regional aeromagnetic data over Dronning Maud Land (East Antarctica). *Tectonophysics*.

Rutter, E. (1976). The kinetics of rock deformation by pressure solution. *Phil Trans Soc Lond*, *A283*, 203–219.

Rutter, E. and Brodie, K. (1988). The role of tectonic grain size reduction in the rheological stratification of the lithosphere. *Geologische Rundschau*, *77*, 295–307.

Schelling, D. and Arita, K. (1991). Thrust tectonic, crustal shortening, and the structure of the far-eastern Nepal Himalaya. *Tectonics*, *10*, 851–862.

Segev, A. (2002). Flood basalts, continental breakup and the dispersal of Gondwana: evidence for periodic migration of upwelling mantle flow (plumes). *EGU Stephan Mueller Special Publication Series*, *2*, 171–191.

Shimizu, I. (2008). Theories and applicability of grain size piezometers: The role of dynamic recrystallization mechanisms. *Journal of Structural Geology*, *30*, 899–917.

Sibson, R. (1977). Fault Rocks and Fault Mechanics. *Journal of the Geological Society*, *133*, 191–213.

Sibson, R. (1982). Fault zone models, heat flow, and the depth distribution of earthquakes in the continental crust of the United States. *Seismological Society of America*, *72*, 151–163.

Stünitz, H., Gerald, J. F., and J.Tullis (2003). Dislocation generation, slip system, and dynamic recrystallization in experimentally deformed plagioclase single crystals. *Tectonophysics*, *372*, 215–233.

ten Grotenhuis, S., Trouw, R., and Passchier, C. (2003). Evolution of mica fish in mylonitic rocks. *Tectonophysics*, *372*, 1–21.

Torsvik, T., Smethurst, M., Meert, J., van der Voo, R., McKerrow, W., Brasier, M., Sturt, B., and Walderhaug, H. (1996). Continental break-up and collision in the Neoproterozoic and Paleozoic - A tale of Baltica and Laurentia. *Earth Science Reviews*, *40*, 229–258.

Toy, V., Norris, R., Proir, D., Walrond, M., and Cooper, A. (2013). How do lineations reflect the strain history of transpressive shear zones? The example of the active Alphine Fault zone, New Zealand. *Journal of Structural Geology*, *50*, 1878–1998.

Tsurumi, J., Hosonuma, H., and Kanagawa, K. (2003). Strain localization due to a positive feedback of deformation and myrmekite-formining reaction in granite and aplite mylonites along the Hatagawa Shear Zone of NE Japan. *Journal of Structural Geology*, *25*, 557–574.

Tullis, J., Snoke, A., and Todd, V. (1982). Significance and petrogenesis of mylonitic rocks. *Geology*, *10*, 227–230.

Unrug, R. (1997). Structure, evolution and paleogeography of the West African craton and bordering belts during the Neoproterozoic. *GSA Today*, *7*, 1–5.

White, S., Burrows, S., Carreras, J., Shaw, N., and Humphreys, F. (1980). On mylonites in ductile shear zones. *Journal of Structural Geology*, *2*, 175–187.

Wintsch, R., Christoffersen, R., and Kronrnberg, A. (1995). Fluid-rock reaction weakening of fault zones. *Journal of Geophysical Research*, *100*, 13021–13032.

Wolmarans, L. and Kent, L. (1982). Geological investigations in Western Dronning Maud Land, Antarctica - a synthesis. *South African Journal Ant. Res*, *2*, 93.

Worley, B. and Wilson, C. (1996). Deformation partitioning and foliation reactivation during transpressional orogenesis, an example from Central Longmen Shan, China. *Journal of Structural Geology*, *18*, 395–411.

Zeitler, P., Meltzer, A., Koons, P., Craw, D., Hallet, B., Chamberlain, C., Kidd, W., Park, S., Seeber, L., Bishop, M., Meltzer, J. S. A., Koons, P., Craw, D., Hallet, B., Chamberlain, C., Kidd, W., Park, S., Seeber, L., Bishop, M., and Shroder, J. (2001). Erosion, Himalayan Geodynamics, and the Geomorphology of Metamorphism. *Rock Geosociety*.